THESIS APPROVAL

GRADUATE SCHOOL, KASETSART UNIVERSITY

Master of Science (Chemistry)

DEGREE

Chemistry | Chemistry

FIELD | **DEPARTMENT**

TITLE: Improving Magnetic Properties of Rubber Ferrite Composites by Doping Barium Hexaferrite Synthesized by The Oxide One Pot Synthesis (OOPS) Process with Lanthanum (La)

NAME: Mr. Sitthisak Sorlateap

THIS THESIS HAS BEEN ACCEPTED BY

(Assistant Professor Wirunya Keawwattana, Ph.D.) **THESIS ADVISOR**

(Assistant Professor Nattamon Koonsang, Ph.D.) **THESIS CO-ADVISOR**

(Assistant Professor Pongsakorn Jantaratana, Ph.D.) **THESIS CO-ADVISOR**

(Professor Supa Hannongbua, Dr.rer.nat.) **DEPARTMENT HEAD**

APPROVED BY THE GRADUATE SCHOOL ON _____

(Associate Professor Gunjana Theeragool, D.Agr.) **DEAN**

THESIS

IMPROVING MAGNETIC PROPERTIES OF RUBBER FERRITE COMPOSITES BY DOPING BARIUM HEXAFERRITE SYNTHESIZED BY THE OXIDE ONE POT SYNTHESIS (OOPS) PROCESS WITH LANTHANUM (La)

SITTHISAK SORLATEAP

A Thesis Submitted in Partial Fulfillment of
the Requirements for the Degree of
Master of Science (Chemistry)
Graduate School, Kasetsart University
2013

Sitthisak Sorlateap 2013: Improving Magnetic Properties of Rubber Ferrite Composites by Doping Barium Hexaferrite Synthesized by The Oxide One Pot Synthesis (OOPS) Process with Lanthanum (La). Master of Science (Chemistry), Major Field: Chemistry, Department of Chemistry. Thesis Advisor: Assistant Professor Wirunya Keawwattana, Ph.D. 124 pages.

The Oxide One Pot Synthesis process (OOPS) has been used for barium hexaferrites ($BaFe_{12}O_{19}$, BaF) preparation. The improvement of magnetic properties of barium hexaferrites including the coercivity (*Hc*) and saturation magnetization (*Ms*) by La substituted and La-Zn co substituted was investigated. It was found that *Ms* and *Hc* increased by substitution of La ions on Ba sites at the content up to x=0.15 and then decreased. However in term of La-Zn substitution, *Ms* and *Hc* were dropped in due to the formation of $ZnFe_2O_4$ and the incomplete conversion to BaF. Magnetic properties (*Ms* and *Hc*) are dependent on amount of magnetic filler and their own magnetic properties. Moreover, EDX showed the spectrum of La. It was confirmed that La can be completely substituted in barium hexaferrite. The effect of BaF ($BaFe_{12}O_{19}$ and $Ba_{1-x}La_xFe_{12}O_{19}$) on the cure characteristics, mechanical and magnetic properties of rubber ferrite composites was also reported. The cure characteristic of RFCs is dependent on the particle size of fillers. It was found that RFC 1 (filled with commercial grade BaF) gave the lowest cure time and scorch time because the commercial grade BaF had a smaller particle size than synthesized BaF which gave the higher surface areas, then filler-rubber interaction was better than those of RFC 2 (filled with synthesized BaF) and RFC 3 (filled with La doped BaF). It was also found that tensile strength and elongation at break of RFC 1 were higher than those of both RFC 2 and RFC 3 due to the effect of particle size. Moreover, RFC 3 gave the highest magnetic properties as compared to RFC 1 and RFC 2.

_____ _____ __ / __ / __

Student's signature Thesis Advisor's signature

ACKNOWLEDGEMENTS

First and foremost, I would like to grateful thank and deeply indebted to Asst. Prof. Dr Wirunya Keawwattana my thesis advisor for advice, encouragement and valuable suggestion for completely writing of thesis.

I would like to thank Asst. Prof. Dr Nattamon Koonsaeng for suggestion of the material preparation method, comment and consults in the experimental and also Asst. Prof. Dr. Pongsakorn Jantaratana from Department of Physic, Faculty of science, Kasetsart University for providing the VSM facility, comment and guidance for experiment. I am sincerely grateful to the Department of Chemistry, Faculty of science, Kasetsart University and Department of Material Engineering, Faculty of Engineering, Kasetsart University for providing the devices.

This thesis could not be successfully complete without supported by Graduate school for publication in international journal and Postgraduate Education and Research Program in Physical Chemistry (ADB KU-Chem) for giving the scholarship.

Finally, my graduation would not be achieved without best wish from my parents, who help me for everything and always gives me greatest love, will power and financial support until this study completion. And the last gratefully special thanks to my relation and my friends for their help and encouragement.

Sitthisak Sorlateap

April 2013

TABLE OF CONTENTS

Page

LIST OF TABLES

LIST OF FIGURES

LIST OF FIGURES (Continued)

LIST OF FIGURES (Continued)

LIST OF FIGURES (Continued)

LIST OF FIGURES (Continued)

LIST OF ABBREVIATIONS

MDR	=	Moving-Die Rheometer
MPa	=	Mega Pascal
NR	=	Natural rubber
OOPS	=	Oxide One Pot Synthesized
phr	=	parts per hundred of rubber (resin)
RFC	=	Rubber Ferrite Composite
TMQ	=	2,2,4-trimethyl-1,2-dihydroquinoline
CBS	=	N- cyclohexyl-2-benzothiazole Sulphenamide
BaF	=	Barium hexaferrite
BaM	=	M-type barium hexaferrite
LaM	=	M-type lanthanum hexaferrite

IMPROVING MAGNETIC PROPERTIES OF RUBBER FERRITE COMPOSITES BY DOPING BARIUM HEXAFERRITE SYNTHESIZED BY THE OXIDE ONE POT SYNTHESIS (OOPS) PROCESS WITH LANTHANUM (La)

INTRODUCTION

Recently, rubber ferrite composite (RFCs) has been studied for their applications. They are important in that they are composite materials suitable for devices where flexibility is an important parameter. Moreover, these composites can be molded into complex shapes. They are also excellent materials as microwave absorbers (Sindhu *et al.,* 2002). The advantages of RFCs over their metallic and ceramic counterparts include low weight and cost, resistance to corrosion, ease of machining and forming, and capability of high production rates (Otaigbe *et al.*, 1999).

Natural rubber (NR) is an immediate choice because of its low cost and easy availability in this part of the world. Moreover, NR is an unsaturated elastomeric characterized by its crystalline and has some good properties, such as high strength, hot tear resistance, retention of strength at break, excellent dynamic properties and general fatigue resistance. However, NR is very sensitive to heat and oxidation because of the double bonds in its chain (Erbil HY 1986). Furthermore, NR can be vulcanized with sulfur compounds, which can crosslink the chain because of the presence of the reactive double bonds, so it has accounted for its use in many applications. Normally, NR is inherently non-magnetic. The impregnation of magnetic filler in polymer matrix imparts magnetic natures, and considerably modifies the physical properties of the matrix as well (Makled and Matsui, 2009).

Ferrites are one of the most useful magnetic materials ever discovered and due to its ease of synthesis and low cost, it cannot easily be replaced by any other magnetic materials. So, they are still widely used wherever the product cost is a

major consideration over magnetic performance although they have less magnetic strength than rare earth magnets.

Barium hexaferrites, $BaFe_{12}O_{19}$, is one of the most importance magnetic materials because of their low price combined with reasonable magnetic performance. They have been intensively investigated and used in permanent magnet. They have high saturation magnetization, high coercivity, high chemical stability which can be adjusted for a wide range of application. The hexagonal structure had 64 ions per unit cell on 11 different symmetry sites ($P6_3/mmc$ space group). The 24 Fe^{3+} ions are distributed on five different crystallographic sites: three octahedral sites (12*k*, 2*a*, and $4f_2$), one tetrahedral site ($4f_1$) and one trigonal bipyramidal site (2*b*). The ferromagnetic structure given by the Gorter model shows three parallel (12*k*, 2*a*, and 2*b*) and two anti-parallel ($4f_1$ and $4f_2$) sites (Ounnunkad, 2006). The barium hexaferrite structure is shown in Figure 1.

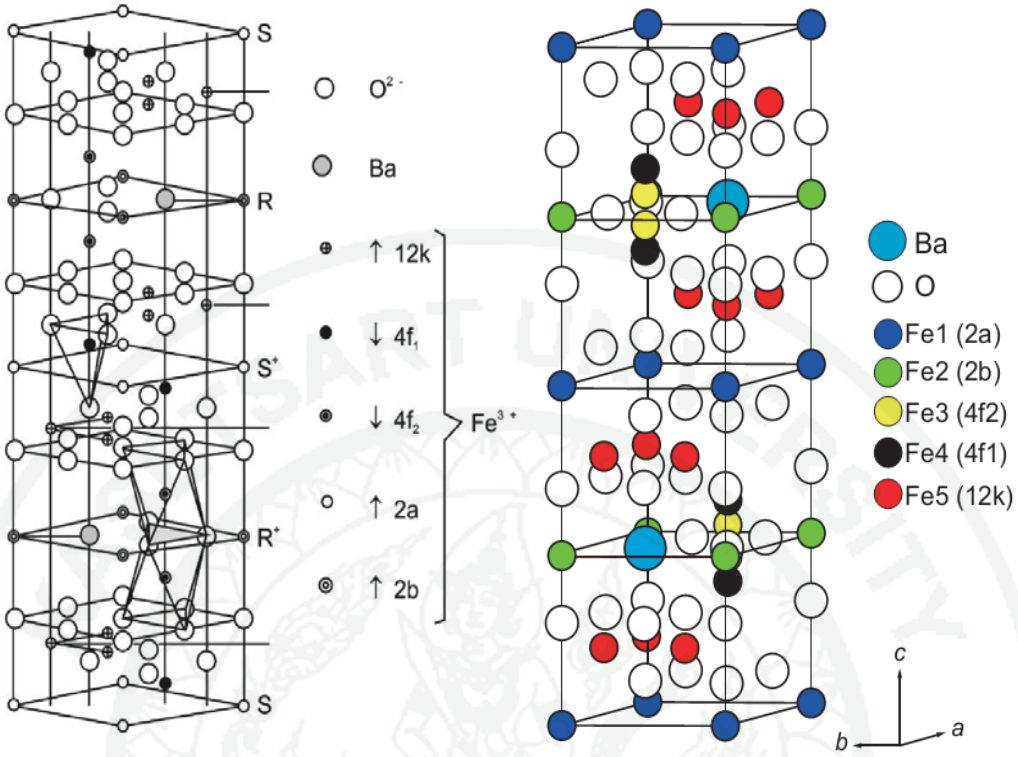

Figure 1 Crystal structure of $BaFe_{12}O_{19}$ (unit cell of barium hexaferrite based on two cells. (a) the spin orientations of the Fe^{3+}ions at the different sites. (b) the different position of atom.

Source: (Tsutaoka and Koga, 2013).

Barium hexaferrite can be synthesized from many synthetic routes such as standard ceramic techniques, coprecipitation, sol–gel process, citrate synthesis (Pullar, 2012). However, some of synthetic methods have been developed to a wide variety of inexpensive preceramic polymers directly from the corresponding metal oxide or hydroxides. One of them is called the "oxide one pot synthesis (OOPS)" process. Recently, OOPS process was successfully used to prepare the barium ferrite (Lalita *et al.,* 2009). This process is very simple and straight forward. It provides many advantages, as compare to other chemical techniques, while retaining purity homogeneous and permitting low processing temperature (Laobuthee *et al.,* 2000).

Lalita *et al.,* (2009) studied the effect of barium ferrite loading on the magnetic properties of RFCs. It was found that barium ferrite loading has significantly effect on the magnetic properties, including coercivity (*Hc*), saturation magnetization (*Ms*) and magnetic remanence (*Mr*) of the RFCs, as a result of the magnetic properties of RFCs increased with increasing barium ferrite content incorporated in NR matrix. However, the more barium ferrite loading, the greater chance to deteriorate the physical properties of RFCs. Therefore, instead of using high barium ferrite loading at 100 phr, it is of interest for our study to emphasize on the 60 phr loading and improve the magnetic properties of RFCs without ruin the physical properties. In addition to the magnetic properties of RFCs, the magnetic properties of barium ferrite powder has to be improved before incorporating into NR matrix.

An improvement of the intrinsic magnetic properties of barium hexaferrites (BaM) can be obtained by the partial substitution of Ba or Fe, or both. A variety of different cation substitutions are possible in $BaFe_{12}O_{19}$ such as (Ounnunkad, 2006) studied effect of La^{3+} and Pr^{3+} on magnetic properties of BaM, (Lixi *et al.*, 2007) investigated the influence of Sm^{3+}on microwave magnetic performance of BaM, (Litsardakis *et al.,* 2007) reported the structure and magnetic properties of BaM with Gd^{3+} substitution which partly or entirely replaced the Ba site. In addition (Winotai *et al.*, 2000) doping Bi into BaM, (Chang *et al.*, 2012) studied microwave absorber with Ce substituted BaM, (Lisjak and Drofenik, 2004) investigated Sn doping into BaM introduced directly as substituent's Fe sites. Moreover, the co substituted of ions on Ba and Fe sites such as La-Zn (Grusková *et al.,* 2005), Gd-Co (Litsardakis *et al.*, 2007) Sm-Zn (Yanbing *et al.,* 2009) substituted on BaM was investigated.

In fact radius of La^{3+} (1.22Å) is close to Ba^{2+} (1.43Å) radii as compared with other rare earth. Therefore, it is of interest for our study to choose La ion for substituting into barium hexaferrite (BaM) because it is possible to substitutes into BaM structure. Many researches that reported substitutions of La ion can enhance the magnetic properties of barium ferrite, such as saturation magnetization (*Ms*) and coercive field (*Hc*) (Li *et al.*, 2012; Ounnunkad, 2006; Ounnunkad *et al.*, 2006; Sözeri

et al., 2011). Moreover, from theoretical the magnetic saturation can be increased with the substitution by non-magnetic ions such as Zn^{2+}(Pullar, 2012). This is because the zinc ions greatly prefer tetrahedral positions, and in M type ferrite the tetrahedral sites oppose the spin of most of the octahedral sites, which produce the net moment. Therefore, substitution with Zn^{2+} reduced this negative contribution, increasing the net magnetic moment (Pullar, 2012). Many reports have recently shown co- substituted of rare earth and Zn^{2+}into barium hexaferrites structure have improved magnetic properties (Bai *et al.,* 2000; Corral-Huacuz and Mendoza-Suárez, 2002; Grusková *et al.*, 2005; Lee *et al.*, 2005; You *et al.*, 2008).

In this study, we proposed to use the oxide one pot synthesis (OOPS) process for synthesizing barium hexaferrite. The major aim in the proposed method is to study the effect of La substituted barium hexaferrites, ($Ba_{1-x}La_xFe_{12}O_{19}$, x=0.00-0.20) and effect of co-substituted of La-Zn into barium hexaferrite, $Ba_{1-x}La_xZn_xFe_{12-x}O_{19}$ (x =0-0.20) on their magnetic properties and also investigate the magnetic and mechanical properties of $BaFe_{12}O_{19}$ and $Ba_{1-x}La_xFe_{12}O_{19}$ filled natural rubber at 60 phr loading.

OBJECTIVES

1. To prepare barium hexaferrite ferrite by using the oxide one pot synthesis (OOPS) process.

2. To study the effect of La and La-Zn substituted barium hexaferrite on the structure and magnetic properties of barium hexaferrite powder.

3. To compare the cure characteristic, mechanical properties and magnetic properties of composite filled with different types of barium ferrite ($BaFe_{12}O_{19}$ and $Ba_{1-x}La_xFe_{12}O_{19}$).

LITERATURE REVIEW

1. Natural Rubber (NR)

1.1 Introduction of natural rubber

Natural rubber (NR) is a polymer of isoprene. About 95% of isoprene production is used to produce cis-1,4-polyisoprene with a molecular weight of 100,000 to 1,000,000 as shown in Figure 2. Typically, a few percent of other materials, such as proteins, fatty acids, resins and inorganic materials are found in high quality natural rubber. Some NR sources called gutta percha are composed of trans-1,4-polyisoprene, a structural isomer which has similar, but not identical properties. However, NR is very sensitive to heat and oxidation because of the double bonds in its chain as shown in Figure 2 (Jame *et al*., 1994). Furthermore, NR is vulcanized with sulfur compounds, which can crosslink the chain because of the presence of the reactive double bonds. It has strain induced crystallization at low temperature that behave high strength, resistance, retention of strength at elevated temperature, excellent dynamic properties and general fatigue resistance (Morton., 1987). It is suitable for wide range of application.

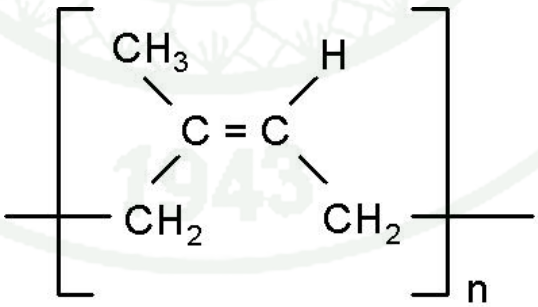

Figure 2 The structure of natural rubber (cis- 1,4 polyisoprene)

1.2 Properties of natural rubber

Strength

The strength of a material refers to the material's ability to resist an applied force. Strength is considered in terms of compressive strength, tensile strength, and shear strength. The effects of dynamic loading is probably the most important practical part of the strength of materials. NR is well-known for the strength properties of its vulcanizates. The tensile strength of gum vulcanizates ranges from 17 to 24 MPa while that of black filled vulcanizates ranges from 24 to 32 MPa. Strength can also be characterized as tear resistance, in both of which NR is excellent. This high strength of NR is certainly due to its ability to undergo strain-induced crystallization. The strength drops rapidly with increase in temperature but is still better than other elastomers.

Elongation at break

The elongation recorded at the moment of rupture of the specimen, often expressed as a percentage of the original length. It corresponds to the breaking or maximum load. The ultimate elongation depends, naturally, on the nature and amount of fillers in the compound, and on the degree of vulcanization. In general, it is about 500 to 1,000% or even greater.

2. Vulcanization

Vulcanization is generally applied to rubber or elastic materials. These materials forcibly retract to their approximately original shape after a rather large mechanically imposed deformation. Vulcanization can be defined as a process which increases the retractile force and reduces the amount of permanent deformation remaining after removal of the deforming force. Thus, vulcanization increases elasticity while it decreases plasticity. It is generally accomplished by the formation of a crosslinked molecular network (Jame *et al.,* 1994**)**.

According to the theory of rubber elasticity, the retractile force to resist a deformation is proportional to the number of network-supporting polymer chains per unit volume of elastomer. A supporting polymer chain is a linear polymer molecular segment between network junctures. An increase in the number of junctures or crosslinks give an increases in the number of supporting chains. In an unvulcanizate linear high polymer (above its melting point) only molecular chain entanglements constitute junctures.

Vulcanization is a process of chemically producing network junctures by the insertion of crosslinks between polymer chains (Akiba *et al*., 1997). The crosslink may be a group of sulfur atoms in a short chain, a single sulfur atom, carbon to carbon bond, a polyvalent organic radical, an inorganic cluster, or a polyvalent metal ion. The process is usually carried out by heating the rubber (mixed with vulcanizing agents) in a mold under pressure.

Usually, the actual chemical cross-linking is done with sulfur, but there are other technologies, including peroxide-based systems. The combined cure package in a typical rubber compound comprises the cure agent itself, (sulfur or peroxide), together with accelerators, activators like zinc oxide and stearic acid and antidegradants. Prevention of vulcanization starting too early is done by addition of retarding agents. Antidegradants are used to prevent degradation by heat, oxygen and ozone.

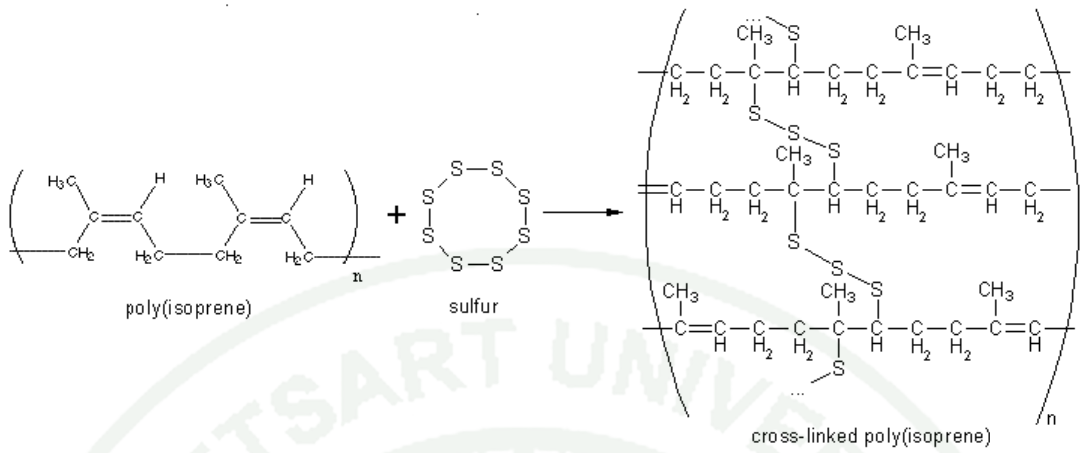

Figure 3 Sulfur vulcanization of polyisoprene

Along the rubber molecule, there are a number of sites which are attractive to sulfur atoms. These are called cure sites, and are generally sites with an unsaturated carbon-carbon bond, like in polyisoprene (Figure 3), the basic material of natural rubber. The active sites are allylic hydrogen atoms; that means they are hydrogen atoms connected to the first saturated carbon atom connected to the carbon-carbon double bond. During vulcanization the eight-membered ring of sulfur breaks down in smaller parts with one to eight sulfur atoms. These small sulfur chains are quite reactive. At each cure site on the rubber molecule, such short sulfur chain can attach itself, and eventually reacts with a cure site of another rubber molecule, and so forming a bond between two chains. These sulfur bridges are typically between two and eight atoms long. The number of sulfur atoms in a sulfur crosslink has a strong influence on the physical properties of the final rubber article. Short sulfur crosslinks, with just one or two sulfur atoms in the crosslink, give the rubber a very good heat resistance. Crosslinks with higher number of sulfur atoms, up to six or seven, give the rubber very good dynamic properties but with lesser heat resistance. Dynamic properties are important for flexing movements of the rubber article, e.g., the movement of a side-wall of a running tire. Without good flexing properties these movements will rapidly lead to formation of cracks and, ultimately, to failure of the rubber article.

2.1 Effects of vulcanization on properties of vulcanizates.

At the molecular level, vulcanization causes profound chemical changes. The long rubber molecules usually between 100,000 to 500,000 which become linked together with crosslinks spaced along the polymeric chains. As a result of this network information, the rubber becomes essentially insoluble in any solvent and it cannot be processed by any means which requires it to flow in a mixer, an extruder, a mill, calender or during shaping, forming or molding. Thus, it is essential that vulcanization occur only after the rubber article is in its final form.

Uncured NR is sticky and can easily deform when warm, and is brittle when cold. In this state it cannot be used to make article with a good level of elasticity. The reason of unvulcanized rubber can be found in the chemical nature which made of long polymer chains. These polymer chains can move independently relative to each other, and this will result in a change of shape. Vulcanization is a chemical process performed on rubber to strengthen it by causing polymer molecules to interlink with other polymer molecules. The vulcanized rubber is harder, more durable, and more resistant to chemicals and other damage. The surface becomes smoother and less likely to stick to metal or plastic. Rubber being vulcanized is usually exposed to sulfur or peroxide for curing; the sulfur atoms are released, and grow "bridges" from rubber molecule to rubber molecule, creating a tight network throughout the rubber structure. The resulting chemical reaction is irreversible, and the compounds created are thermoset, they do not melt on heating, unlike other thermoplastics (Hoffman *et al.,* 1965).

In order for a rubbery polymer to attain an effectively high elastic state, it is necessary to lightly crosslink the highly flexible polymer molecules to prevent them from slipping past each other on application of a stress. In the rubber industry this process is known as ‘vulcanization’. Vulcanization increases the retractile force and reduces the amount of permanent deformation remaining after removal of the deforming force by the insertion of crosslinks between polymer chains forming a crosslinked molecular network. The crosslink may be a group of sulfur atoms in a

short chain, a single sulfur atom, carbon-to-carbon bond, a polyvalent organic radical, an ionic cluster, or a polyvalent metal ion. The process is usually carried out by heating the rubber (mixed with vulcanizing agents) in a mold under pressure.

More effect of vulcanization on use related properties are studied on the idealization. The dynamic modulus is a composite of viscous and elastic behavior, whereas modulus is largely a measure of only the elastic component of rheological behavior. Hysteresis is reduced with increasing crosslink formation. Hysteresis is the ratio of the rate-independent or viscous component to the elastic component of deformation resistance. It is also a measure of deformation energy which is not stored or borne by the elastic network but which is converted to heat. Vulcanization then cause the trade-off of elasticity for viscous or plastic behavior. Tear strength, fatigue life and toughness are related to the breaking energy. Values of these properties increase with small amounts of crosslinking but they are reduced by further crosslink formation. Properties related to the energy-to-break increase with increasing in both the number of network chain and hysteresis. When the hysteresis decreases as more network chains are developed, the energy-to-break related properties are maximized at some intermediate crosslink density.

Reversion is a general term that applied to the loss network structures by thermal aging. It is usually associated with isoprene rubbers vulcanized by sulfur. It can be the result of too long vulcanized time (post cure) or hot aging of thick section. It is almost severe at temperatures above about 155 $^{\circ}$ C. It occurs in vulcanizates containing a large number of polysulfidic crosslinks. Though its mechanism is complex, a good deal about the chemical changes which occur during the reversion of natural rubber has been deduced.

2.2 Vulcanization by sulfur without accelerator

Generally, vulcanization was accomplished by using sulfur at 8 part per hundred parts of rubber (phr). It requires 5 hours at 140 $^{\circ}$ C. The addition of zinc oxide reduced the time to 3 hours. The use of accelerators in concentration as low as

0.5 phr has since reduced the time to as short as 1 – 3 minutes. As a result, elastomer vulcanization by sulfur without accelerator is no longer of much commercial significance. The chemistry of unaccelerated vulcanization is controversial. Many slow reactions occur over the long period of vulcanization. A proposed mechanism involving free radicals is given in Figure 4.

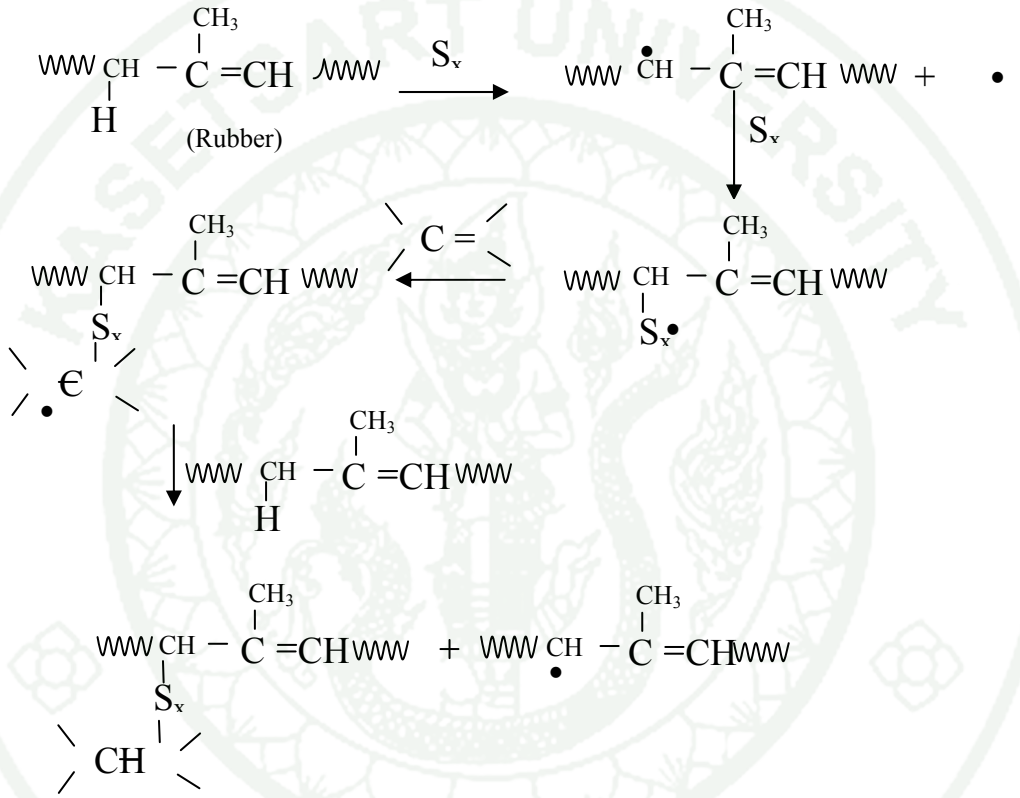

Figure 4 Unaccelerated vulcanization by sulfur, free radical mechanism

2.2.1 Metal Oxides

Carboxylated nitrile, butadiene, and styrene - butadiene rubbers may be crosslinked by the reaction of zinc oxide with the carboxylated groups on the polymer chains. This involves the formation of zinc salts. Other metal oxides are also capable of reacting in the same manner

In case of neoprenes, the double bond is 'hindered' by the neighbouring chlorine atoms, and so vulcanization with sulfur is not possible.

Neoprenes are generally vulcanized by reaction with metal oxides; zinc oxide is generally used along with magnesium oxide. Neoprenes can be vulcanized in the presence of zinc oxide alone; however, magnesium oxide is necessary to give scorch resistance. The reaction is supposed to involve the allylic chlorine atom (active chlorine) which is the result of the allylic shift of chlorine atom occurring during small amount of 1,2 polymerization. Figure 5 is given for the vulcanization of neoprene rubber by the action of zinc oxide and magnesium oxide.

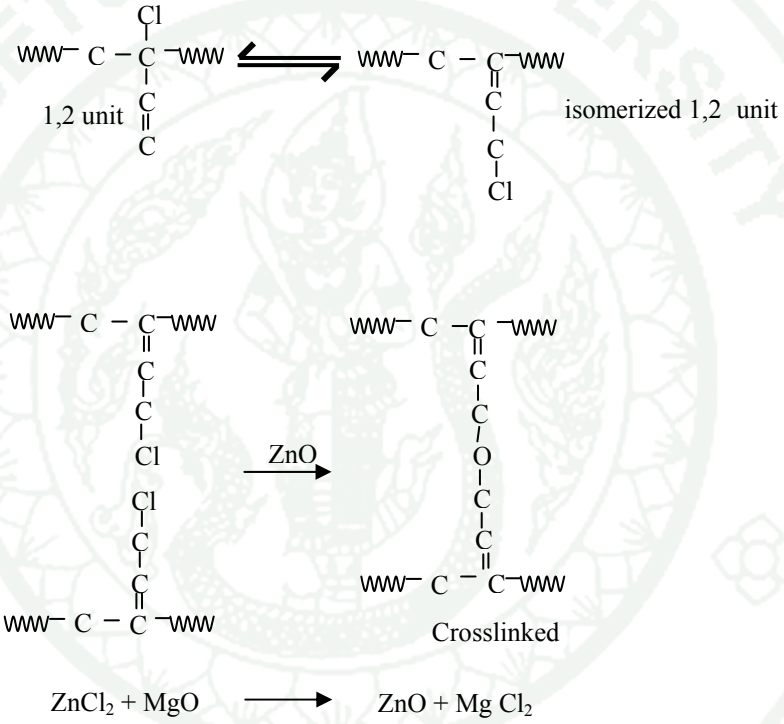

Figure 5 Mechanism of crosslinking of neoprenes by the action of metal oxide

2.3 Accelerated – sulfur vulcanization

Accelerated- sulfur formulation is the most common vulcanization system used in commercial and industrial application. Elemental sulfur is the predominant vulcanizing agent for general-purpose rubbers. It is used in combination with one or more accelerators and an activator system comprising zinc oxide and stearic acid. The most popular accelerators are delayed-action sulfenamides, thiazoles, thiuram

sulfides, dithocarbamates and guanidines which shown in Table 1. The accelerator determines the rate of vulcanization, whereas the accelerator to sulfur ratio dictates the efficiency of vulcanization.

Accelerator are grouped as follows:

1. Inorganic compounds (mainly metal oxides): Include zinc oxide, hydrated lime, litharge, red lead, white lead, magnesium oxide. Zinc oxide is the most common and is generally used in combination with a fatty acid to form a rubber soluble soap in the rubber matrix. The majority of metal oxide is used in coated or treated forms in order to disperse more readily in the rubber mixtures. Normal use level is 2 to 5 phr.

2. Organic acids: Normally used in combination with metal oxides such as zinc oxide; they are generally monobasic fatty acids or mixtures of the types, stearic, oleic, lauric, palmitic and myristic acids, and hydrogeneated oils from palm, castor, fish, and linseed oils. The usage of each particular type depends on the accelerator used and the amounts of compounding ingredients present. Normal use level is 1 to 3 phr.

It is believed that fatty acids with zinc oxide (or other metal oxides) give a salt that form intermediate complexes with the accelerators. The complex thus formed is more effective in activating the sulfur present in the mixture, thus increasing the reaction rate.

The reduction in the amount of time required for vulcanization is generally accomplished by changing the amounts and types of accelerators used. There are some common practice used by rubber compounders to arrive at suitable recipes for specific applications:

1. Single accelerator systems (primary accelerators) which are of sufficient activity to produce satisfactory cures within specified time.

2. Combinations of two or more accelerators, consisting of the primary accelerator which is used in the largest amount, and the secondary accelerator which is used in smaller amounts (10-20 % of the total) in order to activate and improve the properties of the vulcanizate. Combinations of this type usually produce a synergistic effect as the final properties are somewhat better than those produced by either accelerator separately. For example, when a mixture of a benzothiazole with smaller amounts of a dithiocarbamate or thiuram or amine is used, each accelerator activates the other and high crosslinking rates can be obtained.

3. Delayed action accelerators, not affected by processing temperatures (thus providing some protection against scorching) but produce satisfactory cures at ordinary vulcanization temperatures.

Table 1 Several common accelerators used in sulfur vulcanization

Compound	Abbreviation	Structure
Benzothiazoles		
2-Mercaptobenzothiazole	MBT	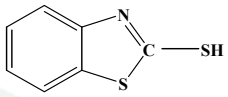
2-2'-Dithiobisbenzothiazole	MBTS	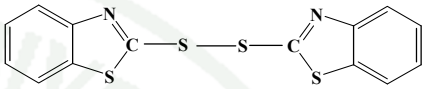
Benzothiazolesulfenamides		
N-Cyclohexylbenzothiazole-2-sulfenamide	CBS	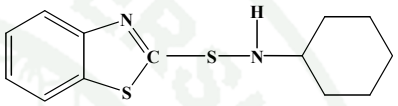
N-t-Butylbenzothiazole-2-sulfenamide	TBBS	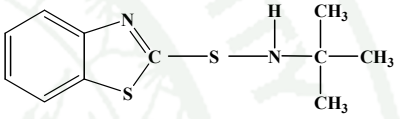
2- Morpholinothiobenzothiazole	MBS	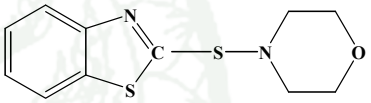
N-Dicyclohexabenzothiazole-2-sulfenamide	DCBS	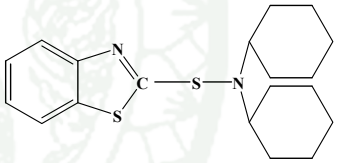
Dithiocarbamates		
Tetramethylthiuram monosulfide	TMTM	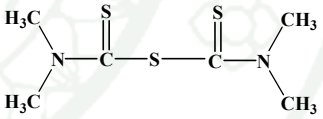
Tetramethylthiuram disulfide	TMTD	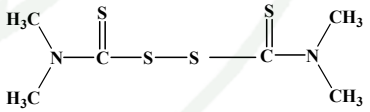
Zinc diethyldithiocarbamate	ZDEC	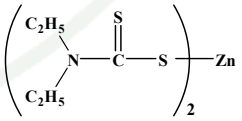
Amines		
Diphenylguanidine	DPG	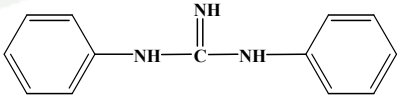
Di-o-tolylguanidine	DOTG	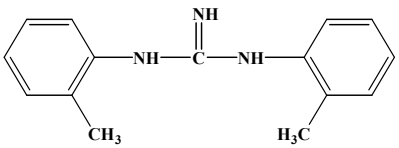

Source: Jame *et al*. (1994)

Table 2 Classes of accelerators used in sulfur vulcanization

Classes of accelerators	Compound	Speed of vulcanization
Guanidines	DPG, DOTG	Medium
Thiazoles	MBT, MBTS	Semi-fast
Sulfenamides	CBS, TBBS, MBS	Fast, delayed action
Thiurams	TMTD, TETD, TMTM	Very fast
Dithiocarbamates	ZDMC, ZDEC	Super fast

2.3.1 The sulfur vulcanization system can be classified into three types (Hoffman *et al.,* 1965).

Conventional vulcanization (CV)

In rubber an accelerator to sulfur ratio typically of 1: 5 is called a conventional vulcanizing system and it gives a network in which about 20 sulfur atoms are combined with the rubber for each inserted chemical crosslink. Most of the crosslinks are polysulfidic (ie. with a bridge of not less than three sulfur atoms) and a high proportion of the sulfur is in the form of cyclic sulfide main chain modifications. This combination provides good mechanical properties and excellent low temperature resistance, but polysulfidic crosslinks are thermally unstable and reversion can occur at high vulcanizing temperatures and high service temperatures.

Efficient vulcanization (EV)

An accelerator to sulfur ratio of 5: 1 is typical of an efficient vulcanizing (EV) system where no more than 4 - 5 sulfur atoms are combined with the rubber for each chemical crosslink. Most of the crosslinks at optimum cure are monosulfidic or disulfidic and only a relatively small proportion of the sulfur is wasted in main chain modifications. This combination provides very much enhanced

heat stability and oxidation resistance, however, have a poor resistance to fatigue because of the presence of predominantly monosulfidic and disulfidic crosslinks.

Semi-efficient vulcanization (semi-EV)

An intermediate accelerator to sulphur ratio of 1: 1 is typical of a semi-efficient vulcanizing (semi-EV) system and provides properties between those of conventional and EV systems that are comprised between resistance to oxidation and required product fatigue performance because of the presence of predominantly disulfidic crosslinks.

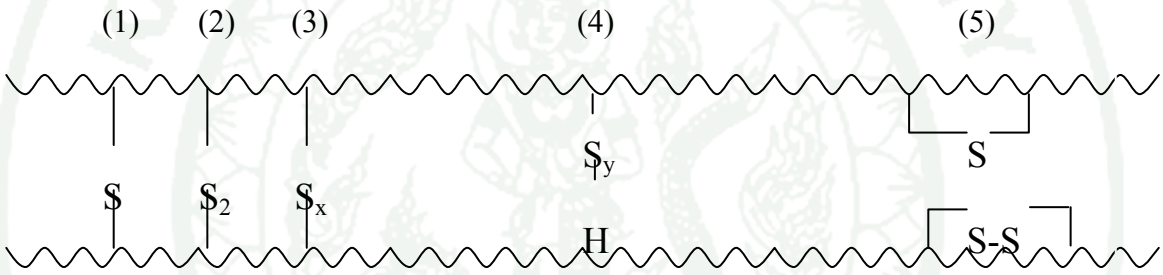

Figure 6 Different crosslink structures: (1) monosulfidic, (2) disulfidic, (3) polysulfidic, when $_X \geq 3$, (4) thiol gruops, (5) cyclic sulfur structures

2.4 Cure time

Many of these substances, particularly rubbers and some high viscosity polymeric elastomers, are difficult to measure in conventional rheometers because of their high viscosity and the promotion of cross-linking, often through vulcanization, during processing at higher temperatures. After vulcanization, the viscoelastic mixture is converted to an elastic material, whose properties include high resistance to deformation and strength. These substances must be properly characteristic to ensure that they are not over-or under-processed.

The main equipment for assessing these properties in the rubber sector are the Mooney viscometer, the Oscillating Disc Rheometer (ODR) and the Moving Die Rheometer (MDR).

The ODR is an oscillatory rheometer, consisting of an oscillating disc, enclosed in an unsealed, stationary cavity. The disc oscillates at a fixed frequency and amplitude (generally determined by international testing standards) and operates in the same range of temperatures and pressure as the Mooney viscometer.

Vulcanization is measured by the increase in the torque required to maintain given amplitude (e.g. degree of arc) of oscillation at a given temperature. The torque is proportional to a low-strain modulus of elasticity. Since this torque is measured at the elevated temperature of vulcanization, the portion of it due to viscous effects is minimal. Thus, it has been assumed that the increase in torque unit volume of rubber, while the torque is automatically plotted against time to give a so-called rheometer chart, rheograph, or cure curve as shown in Figure 8.

The MDR which is a current generation cure-meter and is suitable for the rubber and elastomer industries. It helps overcome problems of thermal inertia, which has dogged the ODR. The MDR may be automated if necessary and continued use of volumetrically consistent samples, and good handling procedures, ensure repeatability.

MDR has a cavity rather than an internally oscillating fixture, which is filled with sample and enclosed by a biconical die. The sample is much smaller and heat transfer is faster. Also, because there is no rotor, the temperature of the cavity and sample can be changed more rapidly.

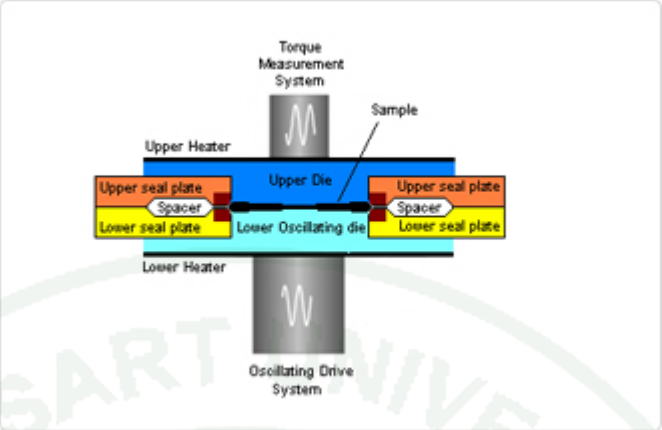

Figure 7 Moving die rheometer

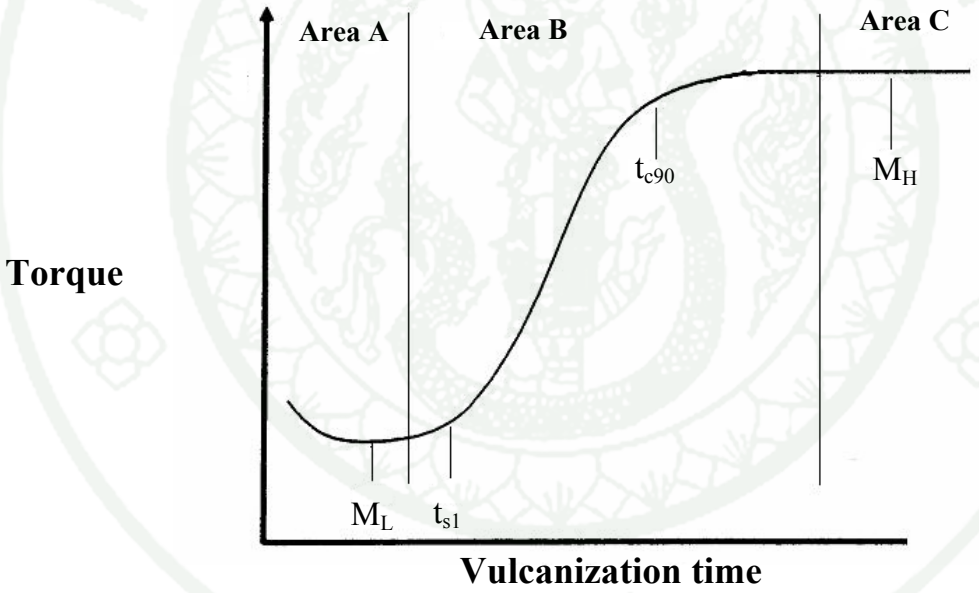

Figure 8 Rheometer cure curve

The measurements which can be made from this curve and the term used to describe them are:

Table 3 The measurement parameter of Rheometer cure curve

Parameter	**Explanation**
Area A **Area B** **Area C**	This gives an indication of compound viscosity before curing. This indicates the rate of cure of the compound. This indicates the state of cure of the vulcanizate.
$\mathbf{t_{s1}}$	Time for torque to increase 1 dn.m (0.1 N.m) or 1 lb_f-in above M_L - a measure of scorch time or processing safety, some laboratories use t_{s2} (i.e., time for torque to increase 2 dN.m or 2 lb_f-in above M_L) instead of t_{s1}.
$\mathbf{t_{c90}}$	Time needed for rubber compounds to reach maximum viscosity or elastic modulus at a given temperature. Cure time is conventionally considered complete at 90 percent of maximum torque.
$\mathbf{M_L}$	Minimum torque - A measure of the viscosity of the uncured compound
$\mathbf{M_H}$	Maximum torque - A measure of cure state during the specific period of time where no returning of cure, maximum torque can be related to vulcanizate modulus and hardness.
$\mathbf{M_H}$-$\mathbf{M_L}$	The difference between the maximum and the minimum torque, related to the crosslink density of the material although further detail for the evaluation will be given.

Note: t_{c50}, t_{c90} - Time for torque to reach $M_L + 0.5 (M_H-M_L)$ or $M_L + 0.9 (M_H-M_L)$

3. Fillers

Fillers are used for improved materials that satisfy increasingly stringent requirement such as higher strength, modulus, thermal, electrical and magnetic properties, flame retardant, etc. For the manufacturers, fillers have been used for cheap diluents or additives. The fillers are classified as reinforcing filler and non-reinforcing (Harry *et al*,. 1987).

In spite of the fact that filler characteristic might be best in filler if one could control its properties completely is worthy of consideration. For the good ideal of filler should include in the following.

1. Low cost
2. Availability
3. Low oil absorption
4. Good surface wetting bonding
5. Good chemical resistance
6. High strength

The use of fillers in rubber is almost as old as the use of rubber itself. It has been observed since long that incorporation of particulate fillers such as carbon black increases the strength of vulcanized rubbers significantly, even more than tenfold by reinforcing it. Thus it is hardly surprising that relatively few applications of elastomers use the polymer in the unfilled state.

Reinforcement has been defined as the incorporation of small particles of materials, known as fillers, into rubber which improves the modulus and failure properties (tensile strength, tear resistance and abrasion resistance) of the final vulcanizate. In general, when a reinforcing agent is added to a base pure gum recipe, that agent imparts greater stiffness and higher ultimate tensile strength than would be obtained by using an equal volume of a common filler, e.g. coarse particle size

whiting. The usual quantities of these materials are 10-50 parts per 100 parts by volume of rubber (Lee *et al.,* 2000).

The degree of reinforcement provided by a filler depends on a number of variables, the most important of which is the development of a large polymer-filler interface which can be furnished only by the particles of colloidal dimensions. Spherical particles 1 μm in diameter have a specific surface area of 6 m^2 /cm^3. This constitutes roughly the lower limit of significant reinforcement. The upper limit of useful specific surface area is of the order of 300-400 m^2/cm^3, and is set by the considerations of dispersibility, processability of the unvulcanized mix, and serious loss of rubbery characteristics of the composites. In general, the finer reinforcing agents require more energy for their dispersion into rubber and the plasticity of the resultant mix is lower. Therefore, it is more difficult to process in operations following mixing. This effect of reinforcing agents on the properties of the rubber - filler mixture is of great practical significance and, for the manufacture of some products, it may be a more important factor in the selection of reinforcing agents than their effect on the vulcanizate properties.

3.1 Principles of filler selection and use

Parameters affecting the performance of polymer or rubber composites functional filler are related to: the characteristics of the filler itself, including its geometry (particle shape, particle size and particle distribution, aspect ratio) its surface area and porosity affect to physical, mechanical, chemical, thermal, optical, electrical and magnetic properties or the other properties that dealing with specific fillers and surface modifiers, Harry *et al*., (1987) and Lee *et al*., (2000).

3.1.1 particle size and particle shape

Filler selection is primarily determined by the particle size distribution and the particle shapes which the particles pack together. This is fundamentally true whether or not a particular class of filler is indicated because of a

systemic requirement such as electrical properties. A general classification of filler particles is presented in Figure 9. The classes are some what arbitrary, being based on the primary properties of particle size and surface area, both of which are directly measurable and serve as a basis for systematizing filler functions. There are many types of fillers that contain variously shaped particles having greater surface area to equivalent spherical diameter (esd) ratios than those indicated in Figure 10. An example of heterogeneity is shown in Figure 11, where is the smallest (thickness) to largest (diameter) dimensions of kaolinite were obtained by microscopic methods. It may be seen that at about 13 μm esd, the particles are stacks of bound platelets equal in two dimensions. In effect then, the shapes of most real particles are too variable to be dealt with directly. Taken together, particle size and surface area provide the only means for classification of particles and their effects in composites (Xanthos *et al*., 2005).

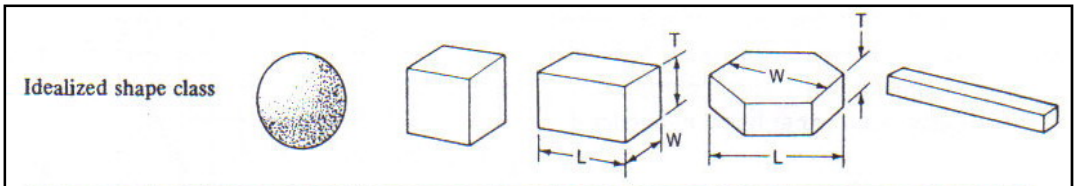

Particle Class	Sphere	Cube	Block	Flake	Fiber
Descriptor[a]	spheroidal[b]	cubic[c] prismatic rhombohedral	tabular prismatic pinacoid irregular	platy flaky[d]	acicular elongated fibrous
Shape ratios;					
length (L)	1	~1	1.4–4	1	1
width (W)	1	~1	1	<1	<1/10
thickness (T)	1	~1	1–<1	$\frac{1}{4}$–1/100	<1/10
Sedimentation diameter[e]	1	esd	esd	esd[f]	esd[f]
Surface area equivalence[g]	1	1.24[h]	1.26–1.5[i]	1.5–9.9[j]	1.87 for 1/10 2.3 for 1/20[k]
Examples	glass spheres microspheres	calcite[l] feldspar	calcite feldspar silica barite nephelite	kaolin mica talc graphite hydrous alumina	wollastonite tremolite wood flour

Figure 9 Particle characteristics

[a]Preferred to particle class since this is based on relative surface area. First descriptor

[b]In the sense that a spheroid approaches a true sphere.

[c]Generally distorted cubes; more nearly prismatic.

[d]Generally having the nature of hexagonal platelets, as illustrated.

[e]According to Stokes' law, esd = equivalent spherical diameter or the diameter of a sphere having the same volume as that of the particle.

[f]Must be modified for dissymmetry of greater than 4-1, maximum to minimum particle dimensions

[g]Equivalent to a spherical diameter of 1; an approximation of the area when the particle has a volume equivalent to an esd of 1

[h]About the same for cubic and prismatic shapes.

[i]For lengths of 1.4-4, respectively.

[j]Based on hexagonal platelets as follows:

length/thickness	area factor
4/1	1.47
6/1	1.78
8/1	2.09
10/1	2.34
100/1	9.88

[k]For a square cross-section

[l]There are more than 300 crystal shapes for calcite alone, but generally it is an irregular, low surface area particle

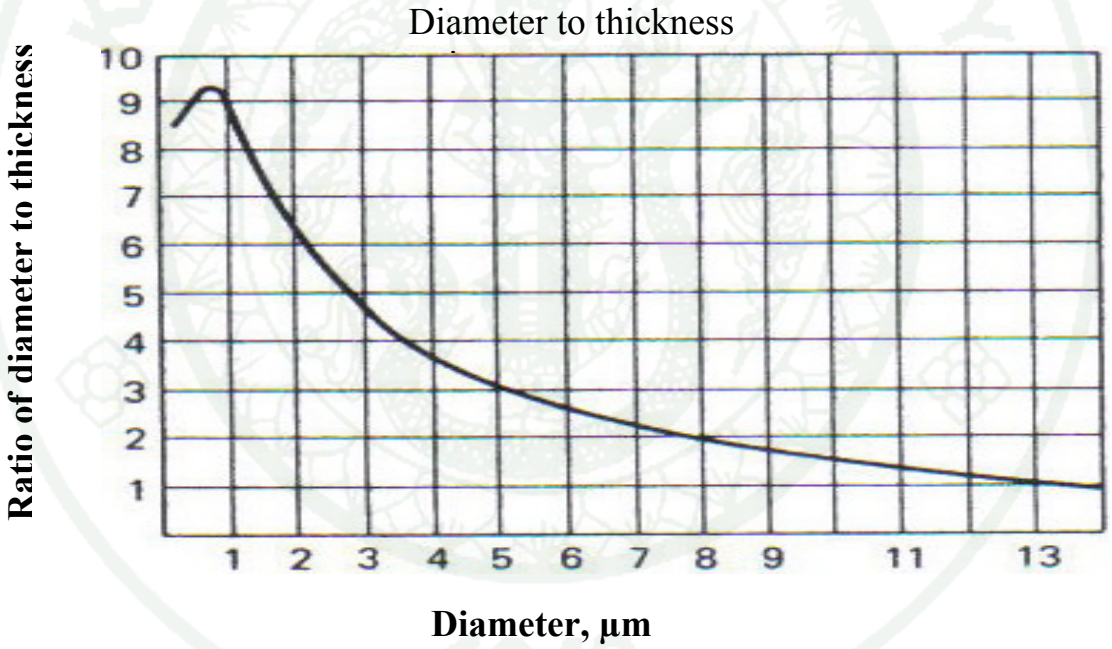

Figure 10 Comparison of diameter (largest dimension) to thickness (smallest dimension) of Kaolinite particle

3.1.2 Particle size distribution

Figure 11 illustrates the most common method of particle size graphing that describes a single species, because all particles have essentially the same density, the percent finer by weight and redundant volume are equal. Although

a filler of very broad distribution was chosen and values approach zero, it is a common failing of supplier's literature that the entire distribution is not reported. It will be emphasized later that these missing data do not allow adequate assessment of the particle size distribution for surface area, packing values, and the true nature of the distribution.

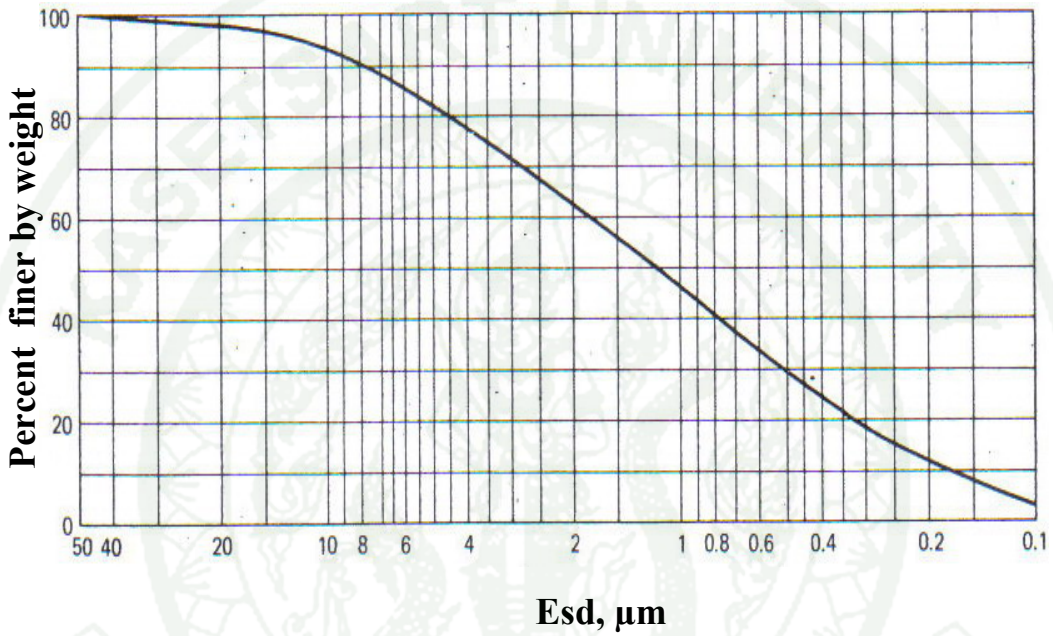

Figure 11 Particle size distribution of Huber 65A kaolin, semilog graph

3.1.3 Surface area

Surface area is one of the most important of filler properties. Surface area is generally the inverse of particle size. Many effects of fillers are surface-area-dependent, particularly where surfactants, dispersants, surfier, polar polymers, and so forth, are adsorbed or reacted with the filler surfaces. Fillers that have a high surface area have more contact area available, and therefore have a higher potential to reinforce the rubber chains. The chemistry and physics of solid surfaces are highly complex. Similar esd particle size distribution gives no indication of filler surface without considering shape factors.

3.1.4 Surface activity

A filler can offer high surface area and high structure, but still provide relatively poor reinforcement if it has low specific surface activity. The specific activity of the filler surface per cm^2 of filler-elastomer interface is determined by the physical and chemical nature of the filler surface in relation to that of the elastomer. Nonpolar fillers are best suited to nonpolar; polar fillers work best in polar elastomer. Beyond this general chemical compatibility is the potential for reaction between the elastomer and active sites on the filler surfaces.

3.1.5 Structure

The shape of an individual particle of reinforcing filler (e.g. carbon black or precipitated silica) is of less importance than the filler's effective shape once dispersed in elastomer. The blacks and precipitated inorganics used for reinforcement have generally round primary particles but function as anisometric acicular aggregates. The round particles clump together into chains or bundles that can be very dense or open and latticelike. These aggregate properties (shape, density, size) define their structure. High structure filler has aggregates favoring high particle count, with those particles jointed in chain-like clusters from which random branching of additional particle chains may occur. The more an aggregate deviates from a solid spherical shape and the larger its size, the higher is its structure. The higher its structure, in turn, the greater its reinforce potential. For reinforcing fillers which exist as aggregates rather than discreet particles, a certain amount of structure that existed at manufacture is lost after compounding. The high shear forces encountered in rubber milling will break down the weaker aggregates and agglomerates of aggregates. The structure that exists in the rubber compound, the persistent structure, is what affects processability and properties.

3.2 Chemical composition

Chemical composition, a primary property of fillers, is an essential consideration for their use in many systems. As all reactivities proceed from the surface of the filler, it is easy to be misled by apparent equivalence. For example, all silicates contain silica and might be considered to have equivalent good acid and poor alkali resistance. This is not the case, as chemical composition does not indicate the relative positions of modifying elements in the crystal lattice or at the surface of the particle. Crystal structure and bond strength relationship are dealt with by Pauling.

3.3 Reinforcing fillers

The most common reinforcing fillers are carbon blacks and silicates. Silicates, clays, whiting (calcium carbonate) and other mineral fillers are used extensively where a high degree of reinforcement is not required. Carbon blacks represent the most important class of reinforcing fillers, both in tonnage and in variety of properties.

3.4 Non reinforceing filler property

3.4.1 Optical

Color is an obvious property of fillers, but it is frequently misunderstood. The color of a dry powder is usually evaluated by pressing a disc shaped compact and obtained a reflectance value at a particular wavelength of light on the flat surface. When the full spectrum of visible light is used for the evaluation, subtle differences in the true color of the particles can be determined by calculation or by inspection of the reflectance graph, although such data are influenced by particle. Particles reflect, refract, or bend light according to their sizes.

3.4.2 Thermal

Thermochemical effects are of particular importance to fillers. Flammability of fillers is limited to organic types, with graphite again an exception for having oxidative stability to 1000 ^{o} C. Hydrated alumina, which is actually aluminum hydroxide, begins to lose significant amounts of hydroxide, water at 230 ^{o} C, continuing to do so endothermically until a total 35 % water loss at 900 ^{o} C. Hydrous silicate filler also release hydroxyls as water, but at much higher temperatures. Limestone fillers liberate carbon dioxide beginning at about 900 ^{o} C, and continuing at that temperature to leave a residue of calcium oxide or lime. Aluminum pigments will burn, and other metallic fillers are effective thermal conductors to promote heating and decomposition of plastics.

3.4.3 Physical

Density is the most important physical property of fillers because it affects the economics of composites. Densities for solid fillers vary from organics to metals in ascending order. Porous or cellular fillers fall into the lowest density range, depending on the voids contained in the fabricated part.

3.4.4 Electrical

It is necessary to consider the fundamental nature of filler particles in the absence of water when electrical properties are concerned. Virtually every surface at ambient conditions has a condensed layer of water molecules upon it, which are more or less tightly bonded depending on the nature of the surface. For the reason, the electrical properties of fillers may differ considerably on a fundamental versus a practical basis. As a generally valid statement, all metallic bonds produce excellent electrical conductivity, whereas ionic and covalent bonds produce nonconductors. Some materials have mixed bonds, ionic and metallic, and are semiconductors. Fillers having hydroxyl surfaces, adsorbed free ions, mixed

contaminants of polyvalent metal compounds, free salts, water, and water soluble matter all provide surface conductive paths for electricity.

3.3 Filler effects

Main effects of filler characterized on vulcanizate properties. Although rubber properties are interconnected and relate to the combination of all filler properties, a brief summary of the main influence of each of the four filler characteristics is given below:

1. Smaller particle size (larger external surface area) results in higher tensile strength, higher hysteresis, higher abrasion resistance, higher electrical conductivity and higher mooney viscosity, with minor effects on extrusion shrinkage and modulus (Lee *et al*., 2000).

2. An increase in surface activity (physical adsorption) results in modulus at the higher strain (≥ 300%), higher abrasion resistance, higher adsorption properties, higher 'bound rubber' (discussed later) and lower hysteresis.

3. An increase in persistent structure (bulkiness) results in lower extrusion shrinkage, higher modulus at low and medium strains (upto 300%), higher mooney viscosity, higher hysteresis and longer incorporation time. Higher electrical conductivity and heat conductivity are found for higher structure blacks. This property is interrelated with surface activity, structure changes on fillers without surface activity (graphitized black) showing the effects indicated above only rather faintly. At constant high activity, the structure effects are most pronounced.

4. Porosity results in higher viscosity and higher electrical conductivity in the case of carbon blacks.

4. Magnetic Material

Magnetic materials encompass a wide variety of materials, which are used in a diverse range of applications. Magnetic materials are utilized in the creation and distribution of electricity, and, in most cases, in the appliances that use electricity. They are used for storage of data on audiotape and videotape and on computer disks. In the world of medicine, they are used in body scanners and in a range of applications where they are attached to or implanted into the body. The home entertainment market relies on magnetic materials in applications such as PCs, CD players, televisions, games consoles, and loudspeakers.

It is difficult to imagine a world without magnetic materials, and they are becoming more important in the development of modern society. The need for efficient generation and use of electricity is dependent on improved magnetic materials and designs. Nonpolluting electric vehicles will rely on efficient motors utilizing advanced magnetic materials. The telecommunications industry is always striving for faster data transmission and miniaturization of devices, both of which require development of improved magnetic materials.

Magnetic materials are classified in terms of their magnetic properties and their uses. If a material is easily magnetized and demagnetized then it is referred to as a soft magnetic material, whereas if it is difficult to demagnetize then it is referred to as a hard (or permanent) magnetic material. Materials in between hard and soft are almost exclusively used as recording media and have no other general term to describe them. Other classifications for types of magnetic materials are subsets of soft or hard materials, such as magnetostrictive and magnetoresistive materials

4.1 The origin of magnetism

Almost everyone is familiar with what a magnetic material can do but very few know how a magnet works. To understand this phenomenon one must first grasp the inextricable connection that exists between magnetism and electricity.

A simple electromagnet can be produced by wrapping copper wire into the form of a coil and connecting the wire to a battery. A magnetic field is created in the coil, but it remains there only while electricity flows through the wire.

An ordinary bar magnet does not have an obvious connection with electricity, so howdoes it work? The field created by the magnet is associated with the motions and interactions of its electrons, the minute charged particles which orbit the nucleus of each atom.

Electricity is the movement of electrons, whether in a wire or in an atom, so each atom represents a tiny permanent magnet in its own right. The circulating electron produces its own orbital magnetic moment, and there is also a spin magnetic moment because the electron itself spins, like the earth, on its own axis (illustrated in Figure 12). In most materials these magnetic moments, measured in Bohr magnetons (μ_B), cancel each other out with each electronic magnet negating the field produced by another.

In certain magnetic materials the magnetic moments of a large proportion of the electrons align, producing a unified magnetic field. The field produced in the material (or by an electromagnet) has a direction of flow, and any magnet will experience a force trying to align it with an externally applied field, just like a compass needle. These forces are used to drive electric motors, produce sounds in a speaker system, and control the voice coil in a CD player, and so on.

The interactions between magnetism and electricity are therefore an essential aspect of many devices every day.

Figure 12. The orbit of a spinning electron about the nucleus of an atom

4.2 Types of magnetism

All magnetic materials contain *magnetic moments,* which behave in a way similar to microscopic bar magnetism. In order to define a ferromagnetism as a class of magnetism, it is easiest to compare the various properties of different possible types of magnetic material (Jung, n.d.). These are principally: dimagnetism, paramagnetism, ferromagnetism, antiferromagnetism and ferrimagnetism.

4.2.1 Diamangnetism

Diamagnetism is a very weak form of magnetism that is only exhibited in the presence of an external magnetic field. It is the result of changes in the orbital motion of electrons due to the external magnetic field. The induced magnetic moment is very small and in a direction opposite to that of the applied field. When placed between the poles of a strong electromagnet, diamagnetic materials are attracted towards regions where the magnetic field is weak. Diamagnetism is found in all materials; however, because it is so weak it can only be observed in materials that do not exhibit other forms of magnetism. Also, diamagnetism is found in elements with paired electrons. Oxygen was once thought to be diamagnetic, but a new revised molecular orbital (MO) model confirmed oxygen's paramagnetic nature.

4.2.2 Paramagnetism

In a paramagnet, the magnetic moments tend to be randomly orientated due to thermal fluctuations when there is no magnetic field. In an applied magnetic field these moments start to align parallel to the field such that the magnetization of the material is proportional to the applied field.

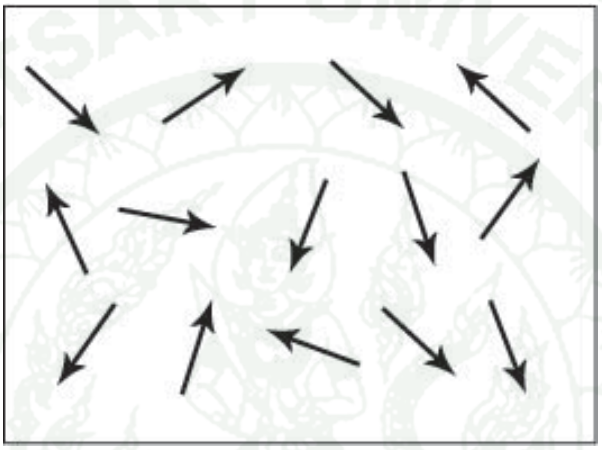

Figure 13 Schematic showing the magnetic dipole moments randomly aligned in a paramagnetic sample.

Paramagnetism is a type of magnetism that occurs in substances with a positive magnetic susceptibility. It results in these substances being weakly attracted by a strong magnet. Paramagnetism is caused by the presence of at least one unpaired electron orbital (i.e., an unpaired spin) in the atoms, molecules, or ions of the paramagnetic material, which results in these particles having a dipole moment. An applied magnetic field tends to align these dipoles in such a way that for small field and high temperatures the induced field is proportional to the applied field; the magnetization is in the same direction as the applied field. Paramagnetism is normally stronger than diamagnetism, and the effect varies inversely with temperature. Below the Curie temperature, certain paramagnetic materials exhibit ferromagnetism. Examples of paramagnetic materials at room temperature include aluminum (Al), manganese (Mn), platinum (Pt), oxygen (gas and liquid), and rare earth ions.

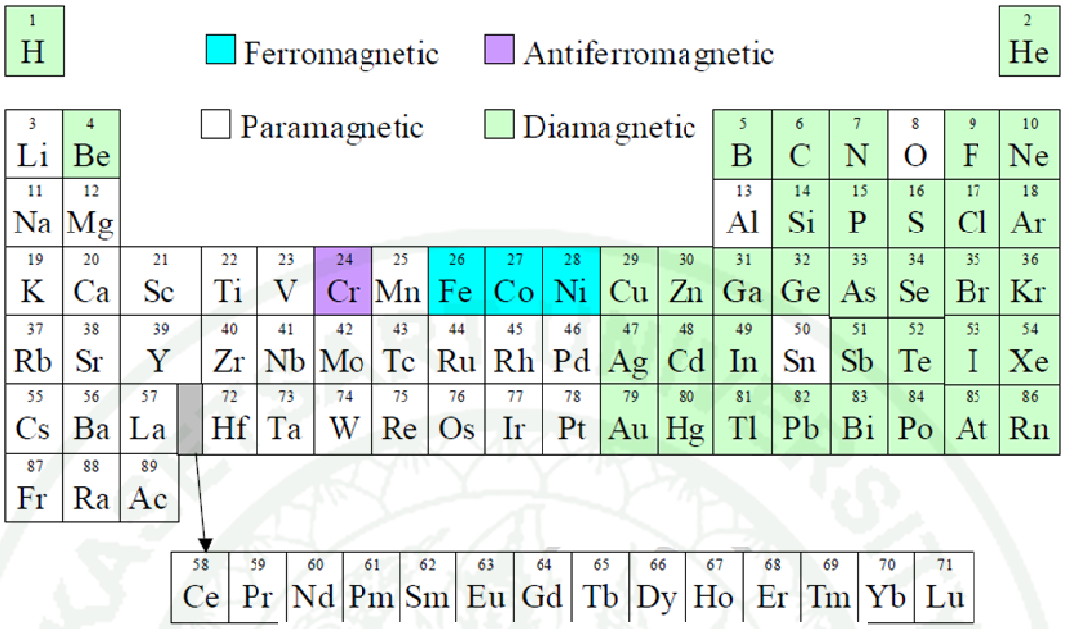

Figure 14 A periodic table showing the type of magnetic behavior of each element at room temperature

4.2.3 Ferromagnetism

The magnetic moments in a ferromagnet have the tendency to become aligned parallel to each other under the influence of a magnetic field. However, unlike the moments in a paramagnet, these moments will then remain parallel when a magnetic field is not applied (this will be discussed later). In a ferromagnet, they tend to align in the same direction because of the Pauli principle: two electrons with the same spin state cannot lie at the same position, and thus feel an effective additional repulsion that lowers their electrostatic energy. This difference in energy is called the exchange energy and induces nearby electrons to align. At long distances (after many thousands of ions), the exchange energy advantage is overtaken by the classical tendency of dipoles to anti-align (Brannen *et al*., 2006).

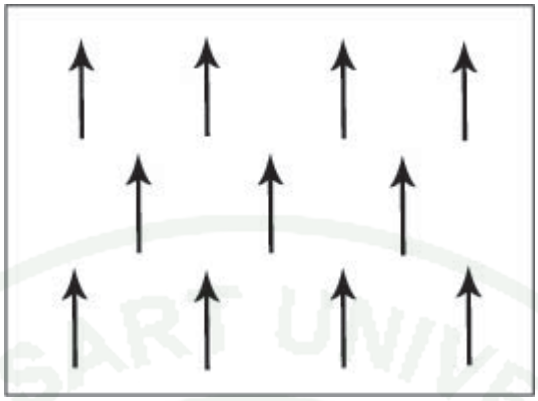

Figure 15 Schematic showing the magnetic dipole moments aligned parallel in a ferromagnetic material.

The net magnetization can be destroyed by heating and then cooling (annealing) the material without an external field. As the temperature increases, thermal oscillation, or entropy, competes with the ferromagnetic tendency for dipoles to align. When the temperature rises beyond a certain point, called the Curie temperature, there is a second-order phase transition and the system can no longer maintain a spontaneous magnetization, although it still responds paramagnetically to an external field. Below that temperature, there is a spontaneous symmetry breaking and random domains form (in the absence of an external field). The Curie temperature itself is a critical point, where the magnetic susceptibility is theoretically infinite and, although there is no net magnetization, domain-like spin correlations fluctuate at all lengthscales.

4.2.4 Antiferromagnetism

Adjacent magnetic moments from the magnetic ions tend to align anti-parallel to each other without an applied field. In the simplest case, adjacent magnetic moments are equal in magnitude and opposite therefore there is no overall magnetisation.

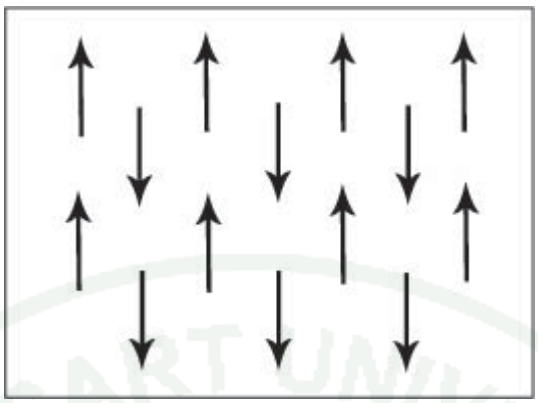

Figure 16 Schematic showing adjacent magnetic dipole moments with equal magnitude aligned anti-parallel in an antiferromagnetic material. This is only one of many possible antiferromagnetic arrangements of magnetic moments.

In materials that exhibit antiferromagnetism, the spins of magnetic electrons align in a regular pattern with neighboring spins pointing in opposite directions. This is the opposite of ferromagnetism. Generally, antiferromagnetic materials exhibit antiferromagnetism at a low temperature, and become disordered above a certain temperature; the transition temperature is called the Neel temperature. Above the Neel temperature, the material is typically paramagnetic. The antiferromagnetic behaviour at low temperature usually results in diamagnetic properties, but can sometimes display ferrimagnetic behaviour, which in many physically observable properties is more similar to ferromagnetic interactions. The magnetic susceptibility of an antiferromagnetic material will appear to go through a maximum as the temperature is lowered, in contrast, that of a paramagnet will continually increase with decreasing temperature. Antiferromagnetic materials are relatively uncommon. An example is the heavy-fermion superconductor URu_2Si_2. More everyday examples include metals such as chromium, alloys such as Iron Manganese (FeMn), and oxides such as Nickel Oxide (El-Nashr *et al*., 2006). Antiferromagnets can also couple to ferromagnetic materials through a mechanism known as exchange anisotropy, in which the ferromagnetic film is either grown upon

the antiferromagnet or annealed in an aligning magnetic field, causing the surface atoms of the ferromagnet to align with the surface atoms of the antiferromagnet.

4.2.5 Ferrimagnetism

The aligned magnetic moments are not of the same size; that is to say there is more than one type of magnetic ion. An overall magnetisation is produced but not all the magnetic moments may give a positive contribution to the overall magnetisation.

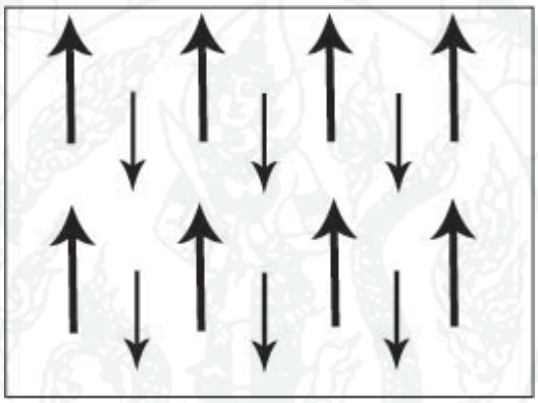

Figure 17 Schematic showing adjacent magnetic moments of different magnitudes aligned anti-parallel.

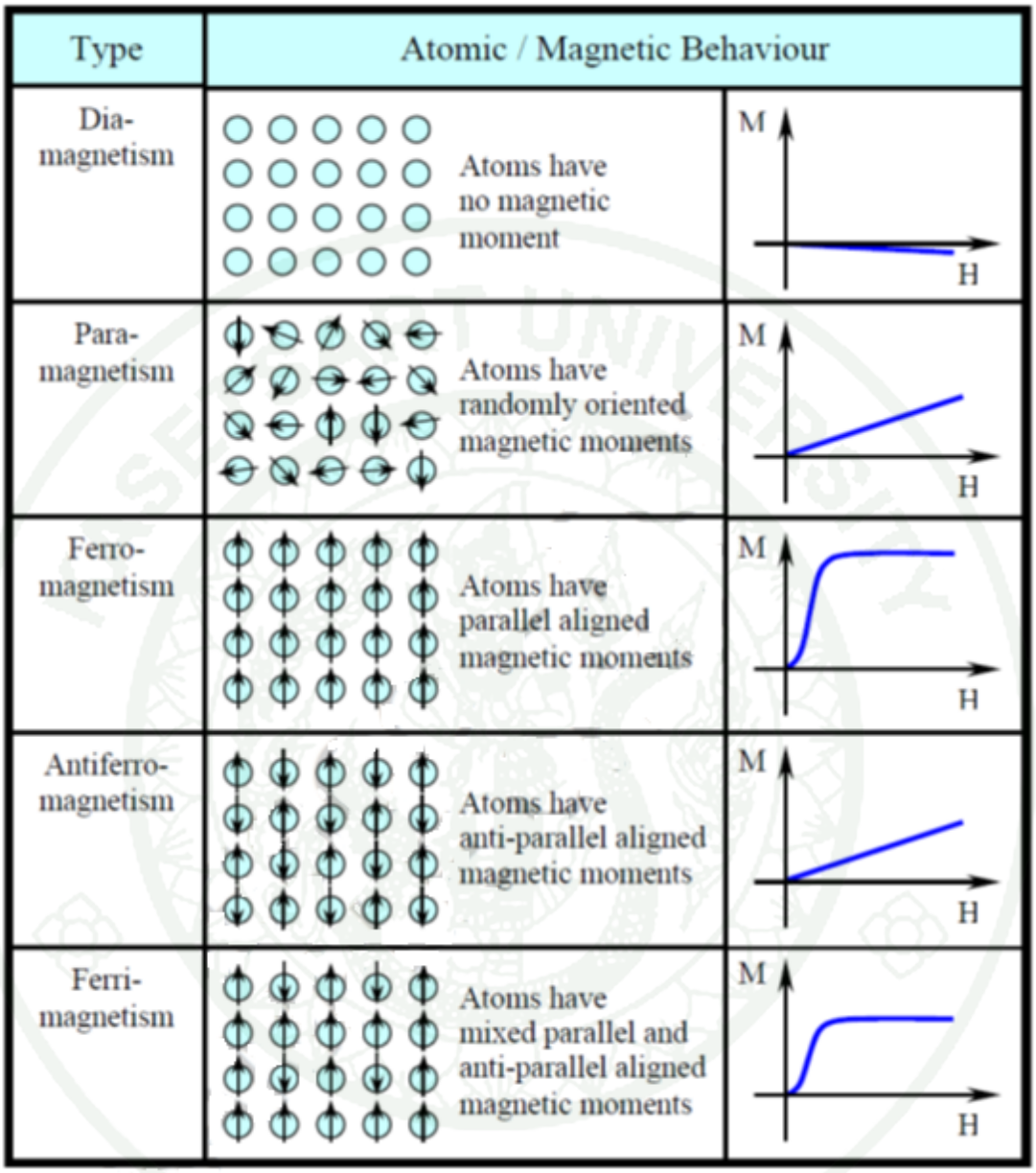

Figure 18 A summary of the different types of magnetic behavior

4.2.6 Intrinsic Properties of Magnetic Materials

The intrinsic properties of a magnetic material are those properties that are characteristic of the material and are unaffected by the microstructure (e.g., grain size, crystal orientation of grains). These properties include the Curie temperature, the saturation magnetization, and the magnetocrystalline anisotropy.

In physics, a ferrimagnetic material is one in which the magnetic moment of the atoms on different sublattices are opposed, as in antiferromagnetism; however, in ferrimagnetic materials, the opposing moments are unequal and a spontaneous magnetization remains. This happens when the sublattices consist of different materials or ions (such as Fe^{2+} and Fe^{3+}). Ferrimagnetic materials are like ferromagnets in that they hold a spontaneous magnetization below the Curie temperature, and show no magnetic order (are paramagnetic) above this temperature. However, there is sometimes a temperature below the Curie temperature at which the two sublattices have equal moments, resulting in a net magnetic moment of zero; this is called the magnetization compensation point. This compensation point is observed easily in garnets and rare earth - transition metal alloys (RE-TM). Furthermore, ferrimagnets may also exhibit an angular momentum compensation point at which the angular momentum of the magnetic sublattices is compensated. This compensation point is a crucial point for achieving high speed magnetization reversal in magnetic memory devices. Ferrimagnetism is exhibited by ferrites and magnetic garnets. The oldest-known magnetic substance, magnetite (iron(II,III) oxide; Fe_3O_4), is a ferrimagnet. Some ferrimagnetic materials are YIG (yttrium iron garnet) and ferrites composed of iron oxides and other elements such as aluminum, cobalt, nickel, manganese and zinc.

Ferrimagnetic materials have high resistivity and have anisotropic properties. The anisotropy is actually induced by an external applied field. When this applied field aligns with the magnetic dipoles it causes a net magnetic dipole moment and causes the magnetic dipoles to precess at a frequency controlled by the applied field, called Larmor or precession frequency. As a particular example, a microwave signal circularly polarized in the same direction as this precession strongly interacts with the magnetic dipole moments; when it is polarized in the opposite direction theinteraction is very low. When the interaction is strong the microwave signal can pass through the material. This directional property is used in the construction of microwave devices like isolators, circulators and gyrators. Ferrimagnetic materials are also used to produce optical isolators and circulator.

The most important category for magnetic applications are ceramic hard ferrite, $BaO_6(Fe_2O_3)$ or $SrO_6(Fe_2O_3)$, and ceramic soft ferrite, $MOFe_2O_3$, where M is a metal such as Ni, Fe, Mn, Mg or Zn (Kingery *et al*., 1975).

4.2.7 Hysteresis Loop

Hysteresis is well known in ferromagnetic materials (Sung *et al*., n.d.). When an external magnetic field is applied to a ferromagnet, the atomic dipoles align themselves with the external field. Even when the external field is removed. A part of the alignment will be retained, so the material has become magnetized. The relationship between magnetic field strength (H) and magnetic flux density (B) is not linear in such materials that shows in Figure 19 (b). The relationship between the two is plotted for increasing levels of field strength, it will follow a curve up to a point where further increases in magnetic field strength will result in no further change in flux density. This condition is called magnetic saturation.

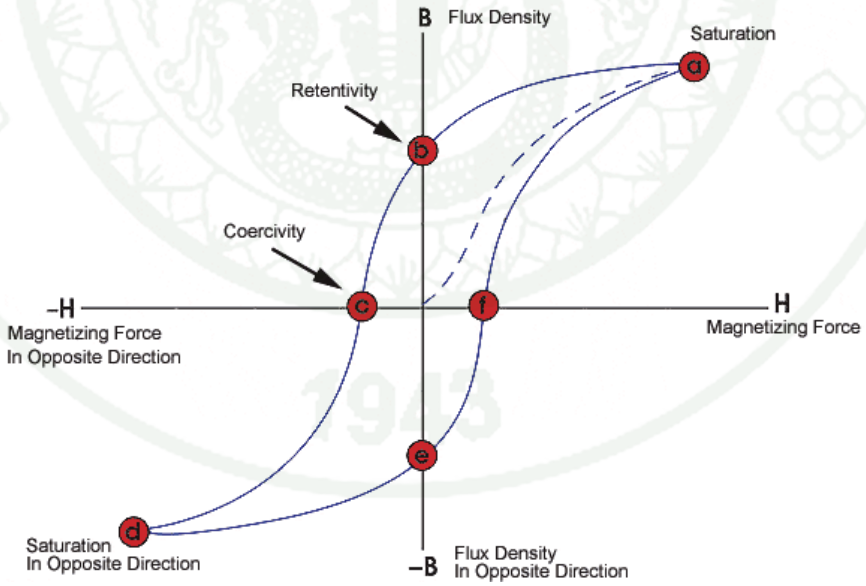

(a)

Figure 19 (a) and (b) show hysteresis loop for a solenoid's ferromagnetic core

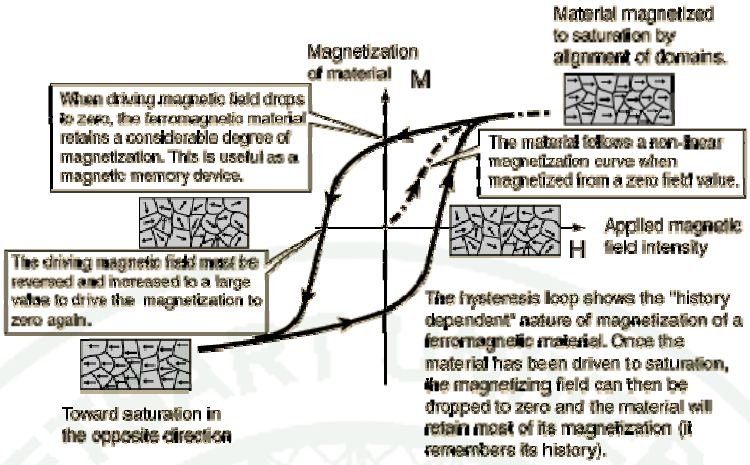

(b)

Figure 19 (Continued) (a) and (b) show hysteresis loop for a solenoid's ferromagnetic core

From Figure 19 (a) represent the hysteresis loop of magnetism material the point magnetizing force (H =0), that a magnetic material is not magnetized. As the current in the coil is increases, magnetizing force (H) also increases until the material is saturated at point (a) that material has reached saturation and Magnetic flux density can not increase any more. When the material start to reduce the current in the coil so that we can demagnetise the material, as stated before the graph will not following the same path it did when the current increased but instead goes from point a, through point b then down to point (c).

At point (b), H=0, therefore the current has reached zero but there is still some remanant flux density so that the material is still partially magnetised. The current is now reversed so that H is in the opposite direction. When the current is increased, the value of H reduces and then H has a negative value at point (c). At point c the material is finally demagnetized and the value of H at this point is called the coercive force.

The hysteresis loop that was shown in Figure 19 (a) The material saturates so that the magnetic poles of the domains face in the opposite direction to those at point

(b). The reversed current is now reduced and reaches zero at the point (f) however, once again, some flux remains. If the current is now increased in the original direction all the flux has gone at point (g) and saturation is reached once more at point (b).

4.2.8 Permanent magnets

The general classification of ferromagnetic materials, according to IEC standards, is based on the coercivity force. Magnetic materials are classified as: soft material, when coercivity is lower than 1000 A/m and hard material, when coercivity is higher than 1000 A/m. The coercive force is of fundamental importance in the technical applications. In soft magnetic materials, the coercivity is due mostly to structural defects (impurity atoms, elastic tensions, dislocations) that hinder the walls motions.

Hysteresis loses will always be a problem in AC transformers where the current is constantly changing direction and thus the magnetic poles in the core will cause losses because they constantly reverse direction. Rotating coils in DC machines will also incur hysteresis losses as they are alternately passing north the south magnetic poles. If you wish to create a permanent magnet you should use a material with a very fat hysteresis loop (Figure 20 a). Such as materials, once magnetised, are very difficult to demagnetise and when the magnetising force is removed a substantial magnetic flux density remains. These materials are known as hard magnetic materials. Since the coercive force must be applied to overcome the remanent magnetism, work is done in completing the hysteresis loop and the energy concerned appears as heat in the magnetic material. This heat is known as hysteresis loss, the amount of loss depends on the material's value of coercive force. By adding silicon to iron a material with a very small coercive force can be made, such materials typically contain 5% silicon and have very narrow hysteresis loop (Figure 20 b). Materials with narrow hysteresis loops are easily magnetised and demagnetised and known as soft magnetic materials (Saito, 1988).

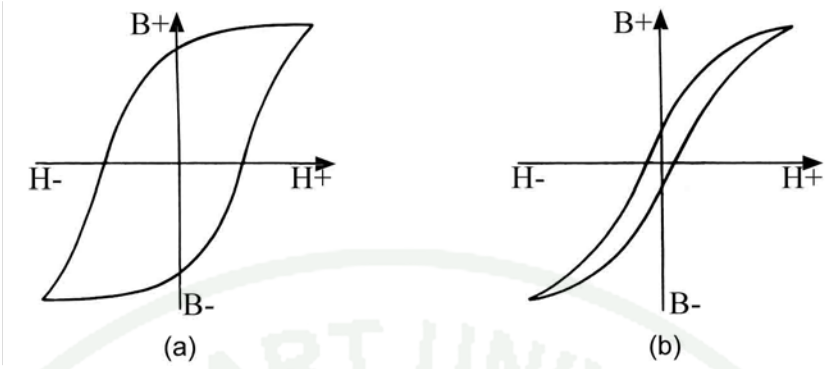

Figure 20 (a) the hysteresis loop for hard magnetic material
(b) the hysteresis loop for soft magnetic material

4.2.9 The high coercive fields of permanent magnets are obtained with other principles:

1. Crystalline anisotropy of the material, that makes difficult the rotating of the magnetization in directions different than the anisotropic one

2. Monodomain grains, which change their magnetization only when all the dipoles inside the grain rotate at the H_c field (for example, ferrite)

3. Shape anisotropy that makes difficult the rotation of the magnetization in directions other than the extended one. It is the case of alnico magnets, formed by of a magnetic monodomain phase (Fe-Co) with elongated shape, blocked in a non-magnetic phase (Fe-Ni-Al). In rare earth materials, that are all crystalline anisotropic, the mechanism of coercive force is of two types.

4. Nucleation mechanism in single phase magnets (NdFeB), the domain walls are locked at the grain boundaries, so the coercivity is the field at which a reverse domain nucleate inside a grain (Flavio et al., n.d.).

5. Pinning mechanism in multi phase magnets, such as the precipitation

hardened alloy (Sm_2Co_{17} family) the domain wall are locked in a lot of pinning sites inside the grain. So, the coercivity is the field at which the walls are released from the pinning sites.

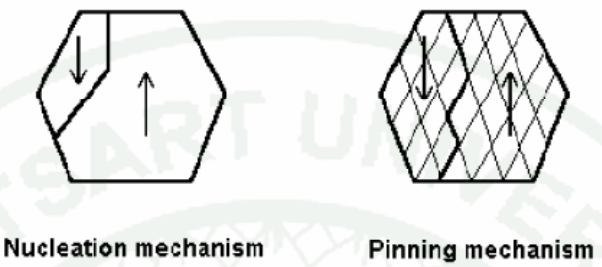

Figure 21 (a) Nucleation mechanism and (b) Pinning mechanism

4.5 Temperature behaviour

The change of the magnetic characteristics related to the temperature has a primary position in the evaluation of a permanent magnet. The characteristics of the magnets generally decay with the increase of temperature, except for coercive force of ferrite magnets (Olkhovik *et al*., 2000). We can distinguish the temperature losses in reversible and irreversible, according to the necessity to remagnetize or not the sample after the temperature decay. If the magnet overcomes the irreversible temperature limit it must be remagnetized. Being the working point of a magnet the intercepts between the demagnetization curve and the load line (that depends on geometry of the magnetic circuit only), it is clear that it hanges regard to the variation of the demagnetization curve. If the intercept at temperature T is in the linear region of the demagnetization curve, the value of Hc will be fully recovered returning the temperature to the room temperature value T_0. If the intercept is under the knee, only a partial recover is possible.

The temperature variations of Br and Hc are defined by two coefficients, αB_r and αH_{cJ}, given in % / ° C

$$\alpha B_r = \frac{1}{B_r(T_0)} \bullet \frac{B_r(T) - B_r(T_0)}{T - T_0} \quad \frac{1}{B_r(T_0)} \bullet \frac{B_r(T) - B_r(T_0)}{T - T_0}$$

Where: (T_0 is room temperature) IEC standards state that the measurements on hard materials (as well as soft materials) should be performed at 23 ± 5 °

Note on magnetic units, conversion factors and hysteresis loops

There exists a real confusion in the literature, with several different systems of units being used even today. The most common system in the literature is CGS (centimetre-gram-second system), and this is still used by many authors today, even though the accepted international standard has been the SI system for decades now. All values in this text have been converted to SI units, but some figures used may have CGS units.

Table 4 The unit and conversion factor.

Quantity	Symbol	CGS unit	Conversion factor to SI	SI unit
Magnetic induction/flux density	B	G	10^{-4}	T
Magnetic field strength/force	H	Oe	$10^3/4\pi$	A m^{-1}
Magnetic moment	m	emu	10^{-3}	A m^2
		erg G^{-1}	10^{-3}	JT^{-1}
Magnetisation (mass)	M, σ	emu g^{-1}	1	Am^2Kg^{-1}
Volume magnetisation	M	emu cm^{-3}	10	A m^{-1}
	4πM	G	$10^3/4\pi$	A m^{-1}
Energy product/anisotropy const.	W, K	erg cm^{-3}	0.1	J m^{-3}
Magnetic flux	Φ	Mx	10^{-8}	Wb
		Gcm^2	10^{-8}	Vs

5. Ferrite

5.1 The M ferrites

The compound BaM, $BaFe_{12}O_{19}$, was known to exist for many years, with a melting point of 1390 °C confirmed in 1936. However, the structure was not confirmed as being isomorphous with the hexagonal magnetoplumbite until it was first studied and characterised magnetically in the early 1950s by Philips. BaM was initially named ferroxdure, to distinguish it from the spinel ferrite which was named ferroxcube. At the time it was considered an unusual ferrite because it contained no cobalt or nickel, yet it was magnetically hard, with a coercivity of 160–255 kA m^{-1}. Although it had a lower saturation magnetisation than the existing alloy magnets, it was much cheaper to produce, had a high electrical resistivity of 108 Ω cm and the high magnetic uniaxial anisotropy along the c-axis. The molecular mass of BaM is 1112 g and the maximum density is 5.295 g cm^{-3}, although in reality the ceramic

material often has a density as low as 90% of theoretical density. The hardness of BaM in the c-axis has been calculated to be 5.9 GPa, and measured as 6.0 GPa. SrM, in which the barium has been replaced by the smaller strontium atom, has a density of 5.101 g cm^{-3} and molecular mass of 1062 g, but resembles BaM in most other physical properties. The Pb^{2+} ion is sized in between Ba and Sr, but lead is a much heavier atom than barium, and so PbM has a molecular mass of 1181 g and a density of 5.708 g cm^{-3}. Undoped CaM has never been seen as a pure phase, but it has been formed in glass by the glass crystallisation method. A detailed study of the thermal properties of polycrystalline M ferrites has been made, and the values are shown in Table 5. The Tc values are lower than those published for single crystal ferrites, and were taken from peaks in the standard molar heat capacity plots (Pullar, 2012).

Table 5 Some physical and thermal values and properties for polycrystalline M ferrites. δ = density in g cm^{-3} . Tm = melting point in K, α_a, α_c and α_v = average thermal expansion coefficients for a axis, c axis and volume, in 106 K^{-1} a and c = lattice parameters in Å, and □ = cell volume in $Å^{-3}$, from RT XRD. Tc = Curie temperature, in K, from standard molar heat capacity plots.

	δ	**T_m**	**α_a**	**α_c**	**α_v**	**a**	**c**	**□**	**T_c**
SrM	5.101	1692	8.62	16.08	33.50	5.8844	23.0632	691.6	732
BaM	5.295	1611	10.74	16.29	38.16	5.8876	23.1885	696.2	725
PbM	5.708	1538	10.80	18.34	40.46	5.8941	23.0984	694.9	718

5.2 The structure of the hexagonal ferrites

All of the hexagonal ferrites have closely related, highly complex crystal structures, At a simple level, they can all be seen as molecular combinations of the three ferrite compounds S (spinel, $MeFe_2O_4$), M ($BaFe_{12}O_{19}$) and Y ($Ba_2Me_2Fe_{12}O_{22}$).

W ferrite, $BaMe_2Fe_{16}O_{27}$, can be considered as M + 2S, X ferrite ($Ba_2Me_2Fe_{28}O_{46}$) = W+ M = 2M + 2S, Z ferrite ($Ba_3Me_2Fe_{24}O_{41}$) = M + Y, and U ferrite ($Ba_4Me_2Fe_{36}O_{60}$) = Z + M = 2M + Y. HRTEM images of the stacking of these layers have been published by Sudakar et al. The other larger hexagonal ferrites are similarly composed. The Ba^{2+} ion is large, as is the O^{2-} ion, and the barium always replaces an oxygen atom somewhere in the oxygen lattice. As the barium ion is slightly smaller than the oxygen ion, it distorts the lattice in its immediate vicinity. The barium ion can be substituted by another divalent metal provided it is of sufficient size, such as strontium or lead, to maintain the structure without too much distortion. Fe^{3+} and Me^{2+} are much smaller ions and insert themselves in interstices between the oxygen positions, and as in inverse spinels, both divalent and trivalent ions inhabit both octahedral and tetrahedral sites in the oxygen framework, as well as the trigonal bipyramidal site that exists in hexaferrites that contain the R block. To describe a hexagonal crystal four Miller indices h, j, k and l are needed. The principal axis is in the (0001) direction along the length of the crystal, and the three other axes are across the basal (0001) plane of the hexagonal polyhedron at angles of 120 to each other. The principal axis is named the c-axis and its length is the c lattice parameter. In the ferrites the three axes of the hexagonal plane are all equal, and so only one other parameter, a, is required to describe a regular hexagonal crystal, which is the length of one of the sides of this plane. Therefore, only two lattice parameters, c and a, are needed to give the dimensions of the crystal.

The molecular unit of M ferrite is made of one S and one R block, with an overlap of hexagonally and cubically packed layers. The basal plane containing the barium atom is a mirror plane, and the two S blocks above and below the R block are therefore 180 rotations around the c-axis of each other. A mirror R block, R⁄, is then required to continue the structure, and it is for this reason that the unit cell requires two molecular M units, giving the unit cell formula SRS⁄R⁄, where ⁄ = a rotation of the block through 180∘ around the c-axis (Fig. 22a) The lattice parameters of BaM are 23.17 Å for the c-axis lengthand 5.89 Å for a, the width of the basal plane, and this a-parameter is constant for all the barium hexagonal ferrites. The ratio of height to width is 3.94, so BaM has a large crystalline anisotropy,which becomes even higher

for the other hexagonal ferrites. Perspective views of the structure are also shown in Fig. 7b and c, while the polyhedra of the M structure, including the bipyramidal site of the R block, are shown in Fig. 7d. Fig. 7e depicts the stacking of the R and S blocks in theMstructure. SrM has smaller lattice constants due to the smaller size of the Sr^{2+} ion, giving the parameters c = 23.03 Å and a = 5.86 Å. Otherwise it has the same structure and unit cell ordering as BaM. The Pb^{2+} ion is also smaller than Ba^{2+}, and the lattice parameters for PbM are c = 23.02 Å, a = 5.88 Å.

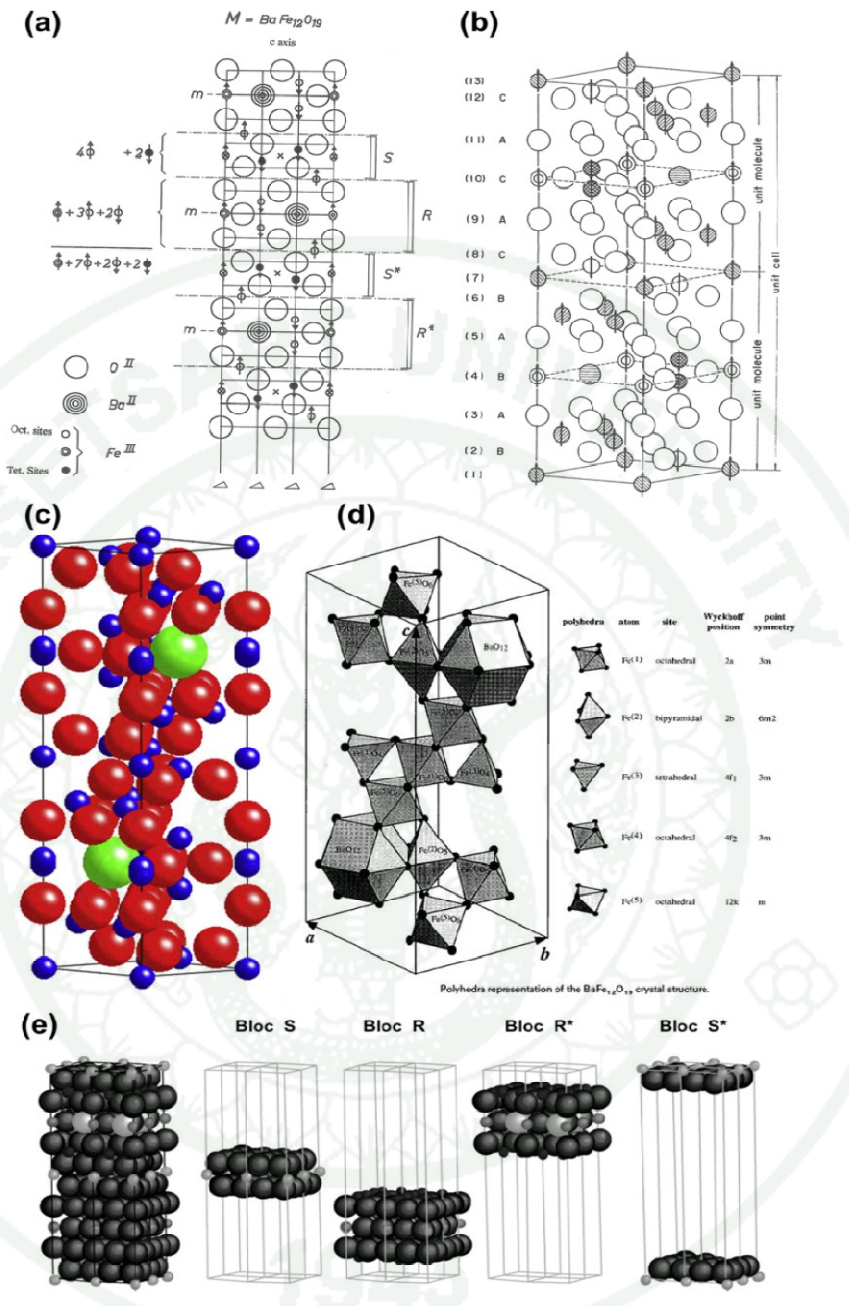

Figure. 22 (a) Cross section view of the M ferrite ($BaFe_{12}O_{19}$) structure in which the vertical lines are axes of threefold symmetry[8]. (b) and (c) Perspective views of the M unit cell. (d) The polyhedra of the M unit cell [29]. (e) The RSR⁄S⁄ stacking sequence . The arrows indicate the orientations of the magnetic moments of the cations relative to the c-axis, ⁄ = 180° rotation of the block around the c-axis, m = mirror plane.

6. Rubber Ferrite Composite

All of standard permanent magnet materials can be utilized to produce bonded type magnets when fine particles are embedded in elastomer matrices (Lopez *et al.,* 2007). The major permanent magnet materials in use are hard ferrite, alnico and rare earths. Most of the bonded magnet products use a flexible matrix, but rigid-type bonded magnet are also made. The flexible type can be manufactured in cut pieces or continuous lengths. They can be drilled, cut, bent and machined into complex shapes. These unique features offer the designer a wide range of design possibility and opportunities for cost saving. The rigid boned magnets offer close magnetic and dimension tolerances. They can be produced with a variety of magnetic orientations in sample and intricated shapes (Flavio *et al*., n.d.).

Saito *et al.,* (1988) studied hard ferrites characterized by the general formula $MFe_{12}O_{19}$ (Figure 23), where M is a divalent metal ion or combination of divalent metal ions such as barium or strontium. The crystal structure is hexagonal and is the same as the mineral magnetoplumbite.

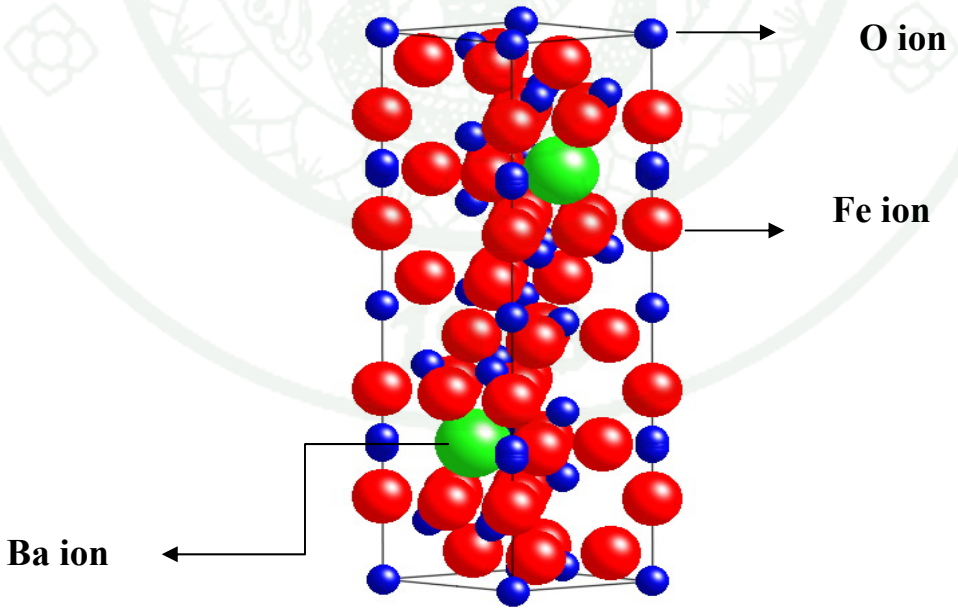

Figure 23 Hexagonal barium ferrite structure

A hard ferrite has a hexagonal crystal structure with the uni axial c axis being the one along which the magnetization prefers to align (Nowoseielski *et al*., 2007). Technical requirements for ferrite magnets are high residue flux density and high corecive force. Representative hard ferrite such as strontium ferrite and barium ferrite (Figure 23). Barium ferrite is lower in cost than strontium ferrite that contain plate-shaped particle having two relatively parallel surfaces and either the regular or and irregular edge parameter, depending on the method of manufacture. There are several methods for producing hard ferrite powders: solid state reaction, co-precipitation (Mallick *et al*., 2001), for example. The solid-state method is the most widely used Mali *et al*., (2005) and Mozaffari *et al*., (2009). A typical solid state process uses starting materials of barium or strontium carbonate and iron oxide. A high degree of consistency in the raw material is critical natural or amount of impurities or the particle size of raw materials can result in the considerable variation in the end product (Brannen *et al*., 2006). Ball mill or ribbon blenders are among the many different types of equipment used for mixing raw materials. The homogeneous mixture is formed into pellets or large slabs and reacted at temperature ranging from 1000 ° C to 1300 ° C. Milling, which is the next step in the process, determines the final magnetic and physical properties of a hard powder of a hard ferrite powder, ideally would produce single crystals as close to the critical magnetic domain size as possible. Vibratory, attrition and ball mills, either wet or dry are used to produce the required particle size. Particle size distribution has a major effect, not only on the magnetic properties but also on the loading characteristics when the powder is embedded in a polymer for bonded magnets.

Apirat *et al.,* (1999) developed synthetic routes for wide variety of inexpensive preceramic polymers directly from the corresponding metal oxides or hydroxides. One of them, called the ``oxide one pot synthesis (OOPS)'' process, is very simple and straight-forward. It provides many advantages, as compared to other chemical techniques, while retaining purity, homogeneity and permitting low processing temperatures. Additionally, this process may provide new chemicals, polymers and ceramics, in one or two steps directly from mineral sources. They

successfully used the oxide one pot synthesis (OOPS) process to prepare $MgAl_2O_4$ spinel powders.

Lalita *et al.,* (2009) studied the magnetic and mechanical properties of rubber ferrite composites (RFC). They successfully used the oxide one pot synthesis (OOPS) process to prepare the barium ferrite used as magnetic fillers in preparation of RFCs.

Jianxun *et al.,* (2005) synthesized barium ferrite at low temperatures by using the combination of two techniques, namely gel self-propagating combustion (GSPC) and high-energy ball milling (HEBM) process. The resultants of the self-propagating combustion of barium ferrite precursor gel are $BaCO_3$and γ-Fe_2O_3. The phase structure of Fe_2O_3 was important for the preparation of barium ferrite. It was discovered that γ-Fe_2O_3 was easier than α-Fe_2O_3 to be converted into barium hexaferrite.

Ogasawara *et al.,* (2000) investigated the microstructure and hysteresis curves of the barium hexaferrite from co-precipitation by organic agent. The temperature of sintering was varied. It was found that γ-Fe_2O_3 was formed at low temperature and showed the decrease in magnetic properties but γ-Fe_2O_3 can be converted to barium ferrite. The temperature of 1350 °C has been revealed as being the best for sintering of the barium hexaferrite in the range explored in their work.

Mohsen (2010) studied the effect of calcination temperatures on the synthesized $BaFe_{12}O_{19}$ powders. Barium ferrite was synthesized by oxalate precursor route. The hematite Fe_2O_3 phase appeared as a major phase at low temperature of annealing. However, the concentration of the hematite phase was decreased, while the formation of barium hexaferrite phase was enhanced with the increase in annealing temperature. The results can be summarized as follows :

(i) At the calcination temperature of 1200°C, single phase of barium hexaferrite ($BaFe_{12}O_{19}$) was formed evidently.

(ii) Regarding the particles size, it can be seen that, the minimum particle size appeared at 1000 ˚C, and the maximum size was found at 1200 ˚C, which most likely explained by the formation of the single phase of barium hexaferrite ($BaFe_{12}O_{19}$).

(iii) The morphologies of the particles at 1000 and 1100˚C were hexagonal platelet crystal. While, at 1200˚C grains have coalesced to form larger grains.

(iv) The oxalate precursor route has been proven to produce pure barium ferrite powders with good magnetic properties with maximum saturation magnetization value of 66.36 emu/g, and coercivity force value of 6400 Oe.

(v) Annealing temperature has great effect on the magnetic properties of barium hexaferrite.

Wang *et al.,* (2010) found that $BaFe_{12}O_{19}$ was fabricated by three kinds of procedures, respectively: (1) sintering mixture of α-Fe_2O_3 and $BaCO_3$, (2) ball milling of the mixture followed by heat treatment, and (3) glycin–nitrate method and subsequent heat treatment. The formation mechanism of the $BaFe_{12}O_{19}$ was different in the three kinds of procedures. In the first procedure, the α-Fe_2O_3 reacts with $BaCO_3$ to form an inter-mediate phase of $BaFe_2O_4$ firstly, and then the $BaFe_2O_4$ reacts with α-Fe_2O_3 to form $BaFe_{12}O_{19}$ in a sintering temperature ranging from 770 to 920˚C. In the second procedure, the α-Fe_2O_3 reacted with $BaCO_3$ to form $Ba_xFe_{3-x}O_4$ with spinel structure when the mixtures were milled for 8h, the $BaFe_{12}O_{19}$ was obtained by annealing the $Ba_xFe_{3-x}O_4$ at 700–1000˚C. And in the last procedure, the precursor powders containing α-Fe_2O_3, Fe_3O_4 and $BaFe_2O_4$ were fabricated by self-propagating reaction firstly, and then the single phase of $BaFe_{12}O_{19}$ was produced by sintering the precursor powders at1000˚C. The saturation magnetization and the coercivity of the $BaFe_{12}O_{19}$ fabricated by the second procedure were 47.24 emu/g and 5086.34 Oe, respectively. The coercivity of the $BaFe_{12}O_{19}$ fabricated by the second procedure was larger than that of the $BaFe_{12}O_{19}$ produced by other two procedures, which was not related to grain size and phase composition but should be due to remaining Ba^{2+} ions in the octahedral 2a site, leading to significant reduction in saturation magnetization and increase in coercivity.

Suriya (2006) attempted to improve the magnetic properties of barium hexaferrites by doping with La or Pr. He successfully prepared La or Pr substituted barium hexaferrites, $Ba_{1-x(}$La or Pr$)_xFe_{12}O_{19}$,(x= 0.00–0.20) by a citrate combustion process. The magnetic properties of the prepared La or Pr substituted barium hexaferrites, $Ba_{1-x(}$La or Pr$)_xFe_{12}O_{19}$ with x = 0.00–0.20, could be enhanced by partial substitution of the rare earths at the Ba sites. Substitution of La or Pr ions into the barium hexaferrite system can be utilized for improvement of both saturation magnetization (M_S) and coercive field (H_C). All of the magnets with La or Pr additions exhibited higher coercivities than that of pure barium ferrite magnet due to higher magnetocrystalline anisotropy. Enhancement of MS can be achieved with respect to La or Pr ion substitution content. The magnetization behavior could be contributed by increase in hyperfine field on some Fe lattice sites, magnetic dilution and disruption of collinear structure (spin canting).

Suriya *et al.,* (2006) studied the effect of La doping on structural, magnetic and microstructural properties of $Ba_{1-x}La_xFe_{12}O_{19}$ ceramics prepared by citrate combustion process. They were successfully prepared La-substituted M-type barium ferrites, $Ba_{1-x}La_xFe_{12}O_{19}$. It was found that increasing La substituted content, the saturation magnetization (M_S) was increased and reached to a maximum at x=0.15 and then decreased but coercivity (H_C) was increased. As of the magnetic property result, the disruption of La^{3+} ions on Fe^{3+}-O-Fe^{3+}superexchange interaction contributed to the behavior of magnetization. With increasing La^{3+} ions, the grain morphology could be changed from hexagonal platelet-like shape to irregular or spherical shape without changing in the crystalline structure.

Grusková prepared La–Zn substituted M-type Ba hexaferrite powders by sol-gel (Mx) and organometallic precursor (Sk) methods. The La^{3+} ions substituted the large Ba^{2+} ions at 2*a* site and for x ≥ 0.4 also at 4f_2 site. The nearly all Zn^{2+} ions were placed at the 4*f1* sites. The coercivity (Hc) did not show significant change at x = 0.2 for (Mx) samples and further decreased up to x = 0.6. For (Sk) samples at substitution x = 0.2 the values of Hc decreased, while they appeared to be stable at higher x. The Curie points, Tc , slowly decrease with x for both (Mx) and (Sk) samples.

Malini *et al.*, (2001) prepared rubber ferrite composites (RFC) containing Ni_{1-x} Zn_x Fe_2O_4 in natural rubber. The cure characteristics revealed that the processability and flexibility of the matrix was not much affected even up to a maximum loading of 120. Magnetic properties including the saturation magnetization (M_s) and magnetic field strength (H_c) were studied. The study also suggested that there was no possible interaction between the filler and the matrix at least at the macroscopic level.

Mohammed *et al.*, (2001) found that composite materials of manganese zinc ferrite with natural rubber can modify the electrical properties of ferrite. Mixed ferrites belonging to the series $Mn_{(1-x)}Zn_xFe_2O_4$ (MZF) were synthesized for different 'x' values in step of 0.2. These pre-characterized ceramic ferrites were incorporated in a natural rubber matrix. The samples were prepared for the different loadings of magnetic filler up to 120 phr in step of 30 phr. The tensile study indicated that the serviceability of the elastomer was not affected even for 120 phr loading of filler. The initial decrease in tensile strength was due to the reduction in the stress-induced crystallization of natural rubber matrix. The tensile was decreased then increased with the filler loading. Rubber ferrite composites with the filler composition 'x' being 0.6 showed the maximum tensile strength.

Makled *et al.*, (2004) studied barium ferrite powders having the particle size in a range 45–200 μm. Barium ferrite powder was incorporated into a natural rubber with different loading levels up to 120 phr. The dynamic properties were more strongly dependent on the particles and particle–matrix characteristics than the magnetic and the mechanical properties. For further improvement detailed future works were needed to study the effects of size, shape and surface roughness of fillers on the magnetic and dynamic properties of barium ferrite–rubber composites. The results showed that the coercivity was improved and the saturation magnetization was linearly dependent on the mass fraction of the filler, while the tensile strength, strain at break and modulus were highly influenced by the size, shape and volume fraction of ferrite particles. The BH_{max} was 1.18 MGOe and flexibility resilience of RFC was 0.844 at 120 phr.

Soloman *et al.,* (2004) investigated rubber ferrite composites (RFC) containing strontium ferrite ($SrFe_{12}O_{19}$) which synthesized by the ceramic techniques and then incorporated in natural rubber matrix according to a specific recipe. The rubber ferrite composites were prepared for various loadings of strontium ferrite, ranging from 40 to 120 phr in steps of 20. Hence, the 80 phr loading of strontium ferrite was taken as the control compound for further loadings of carbon black. RFCs containing carbon black were prepared for various loadings, namely 10 to 50 phr, in steps of 10. The mechanical properties of the RFCs studied showed that the ferrites behave as semi-reinforcing and the reinforcement was maximum in the presence of carbon black. The magnetization values increased with the loading of ferrite filler, but with the addition of carbon black, even though the values decreased, the RFCs containing carbon black still possessed appreciable magnetization values.

Soloman *et al.,* (2004) attempted to incorporate pre-characterized hexagonal ferrites, namely barium ferrite ($BaFe_{12}O_{19}$) into natural rubber matrix. It was found that the processability was not much affected by filler incorporation. The physical properties indicated that the addition of magnetic fillers increased the modulus and hardness, with marginal decreased in the tensile strength. Study of the magnetic properties indicated the formation of elastomer magnets with suitable value of saturation magnetization and retentivity. The magnetic properties of RFC can be controlled by the addition of appropriate amount of the ferrite filler.

Nontapat *et al.,* (2005) studied the effect of paticle sizes of ferrite on the physical properties of rubber ferrite composites (RFCs). The physical properties indicated that the addition of magnetic fillers increased the hardness, but decreased the tensile strength. The rubber ferrite composites at 60 phr was better shielding.

El-Nashar *et al.,* (2006) investigated the mechanical, electrical and magnetic properties of natural rubber composites containing iron or nickel nanoparticles at different percentage varying from 0-120 phr. It was found that the optimum concentration of magnetic fillers in NR was 30 phr, which improved the rheometric characteristics and mechanical properties. Magnetic measurements showed

characteristics and mechanical properties. Magnetic measurements showed superparamagnetic behavior for all Ni and Fe nanoparticles percentage. The electrical measurements showed a strong dependency of the conductivity on the percentage of magnetic nanoparticles.

El-Sabbagh *et al.,* (2006) studied rubber composites based on natural rubber vulcanizates loaded with iron oxide aluminium oxide ($Fe_2O_3Al_2O_3$) fillers and investigated physical and magnetic properties. The prepared fillers were evalutated as reinforcing fillers with some magnetic properties, these properties were dependent on the ratio of iron oxide to aluminum oxide in each prepared ratio of these fillers. Rheological properties of rubber mixes containing ($1Fe_2O_3{\cdot}3Al_2O_3$) and ($1Fe_2O_3{:}1Al_2O_3$) fillers exhibited better properties than mixes containing ($3Fe_2O_3{\cdot}3Al_2O_3$) and (α-Fe_2O_3). Physical properties such as tensile strength, 100, 200% modulus, hardness increased with increasing the volume fraction of the investigated fillers concentration in the mixed vulcanizates.

MATERIALS AND METHODS

Materials

Materials preparation

1. Barium nitrate ($Ba(No_3)_2$), Caro erba.
2. Ferric nitrate hexahydrate ($Fe(NO_3)_3.6H_2O$), Loba chemie.
3. Lanthanum nitrate hexahydrate ($La(NO_3)_3.6H_2O$), Loba chemie.
4. Zinc nitrate hexahydrate, Loba chemie.
5. Ethylene glycol (EG), Unilab.
6. Tetraethylammonium (TEA), Merck

Composites preparation

1. Natural Rubber (NR); STR5L, S.M.P. RUBBER, Thailand.
2. ZnO, an activator, Global Chemistry, Thailand.
3. Stearic acid, an activator, Imperial Industrial, Thailand.
4. Sulfur, crosslink agent, Sahapaisal Industry, Thailand.
5. 2,2,4- Trimethyl-1,2-dihydroquinoline polymer (TMQ), an antioxidant, Eliokem, USA.
6. N- cyclohexyl-2-benzothiazole Sulphenamide (CBS), an accelerator, Flexsys, Germany.

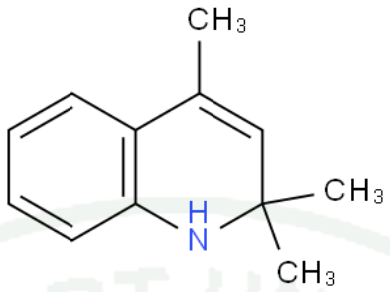

Figure 24 Structure of 2,2,4- Trimethyl-1,2-dihydroquinoline polymer (TMQ)

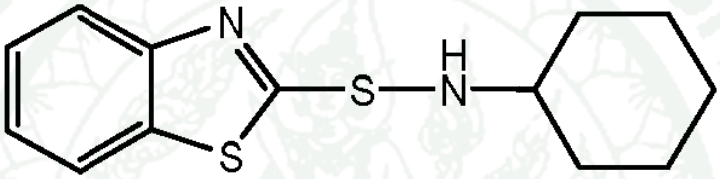

Figure 25 Structure of N- cyclohexyl-2-benzothiazole Sulphenamide (CBS)

Equipments

- Two-roll Mill
- Moving Die Rheometer (MDR), Tech PRO
- Compression molding, G30H-15-CX, Wabash, USA.
- Universal testing mechine, Testometric (M500-25AT)
- X-ray Diffraction (XRD), JEOL JDX-3530 and Bruker (D8)
- Scanning Electron Microscopy, Phillips SEM XL30 & EDX
- Vibrating Sample Magnetometer (VSM), Lake Shore 7400 Series
- Malvern:Mastersizer 2000
- Surface area analysis (BET); Model: Autosorb 1

Methods

1. Prparation of magnetic Fiilers ($BaFe_{12}O_{19}$ hexaferrite, $Ba_{1-x}La_xFe_{12}O_{19}$ hexaferrite $Ba_{1-x}La_xFe_{12-x}Zn_xO_{19}$ hexaferrite)

1.1 Preparation of $BaFe_{12}O_{19}$ hexaferrite

$BaFe_{12}O_{19}$ was prepared by the oxide one pot synthesis (OOPS) process. The mixture solution of metal ions was prepared by dissolving $Ba(NO_3)_2$, $Fe(NO_3)_3.9H_2O$ in the solution of ethylene glycol (EG) and triethanolamine (TEA) at 100 ˚C and stirring. The clear solution was heated to 120 ˚C for 2 hours with constant stirring then the precursor was formed. The precursor was washed with ethanol, filtered and then calcined at 1200 ˚C for 2 hours. The formulations of substances are shown in Table 6 and the diagram of the oxide one pot synthesis (OOPS) process is present in Figure 24.

Table 6 Formulation of $BaFe_{12}O_{19}$ preparation

Ingredient	Mole ratio
Triethanolamine (TEA)	11
$Ba(NO_3)_2$	1
$Fe(NO_3)_3.9H_2O$	10

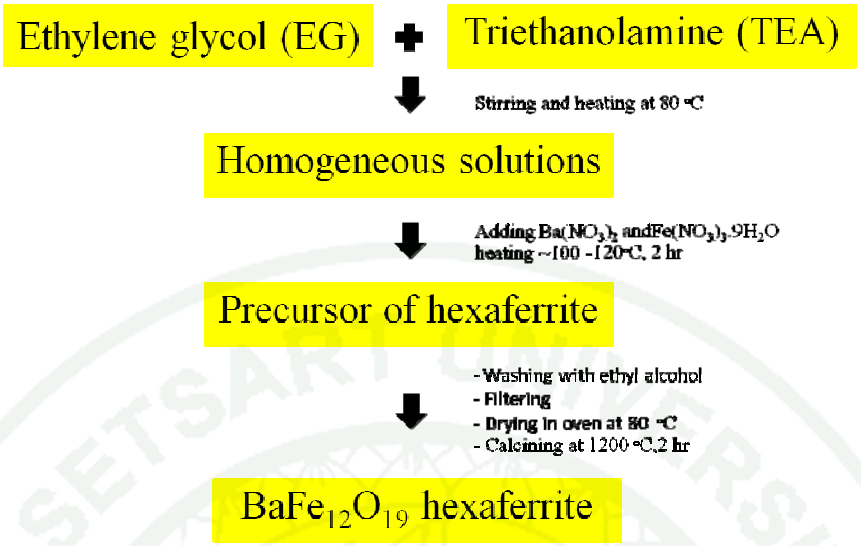

Figure 26 Diagram of the oxide one pot synthesis (OOPS) process

1.2 Preparation of $Ba_{1-x}La_xFe_{12}O_{19}$ hexaferrite

Factor 1: Study the effect of La substituted barium ferrite on magnetic properties. The formulations are shown in Table 7

The reagents of $Ba(NO_3)_2$, $Fe(NO_3)_3.9H_2O$, $La(NO_3)_3.6H_2O$ were dissolving in the solution of ethylene glycol (EG) and triethanolamine (TEA) at 100 ° C with stirring. The precursor of La doped barium hexaferrite was prepared by the oxide one pot synthesis (OOPS) process by varying the amount of $La(NO_3)_3.6H_2O$ from x = 0.00 to x = 0.20. The clear solution was heated to 120°C for 2 hours with constant stirring then the precursor was formed. The precursor was washed with ethanol, filtered and then calcined at 1200°C for 2 hours. The formulations of $Ba_{1-x}La_xFe_{12}O_{19}$ are shown in Table 7.

Table 7 The formulation of $Ba_{1-x}La_xFe_{12}O_{19}$,(x = 0.00-0.20)

Ingredient	Mole ratio				
	BaF	BaF 1	BaF 2	BaF 3	BaF 4
Triethanolamine (TEA)	11	11	11	11	11
$Ba(NO_3)_2$	1	0.95	0.90	0.85	0.80
$La(NO_3)_3.6H_2O$	0	0.05	0.10	0.15	0.20
$Fe(NO_3)_3.9H_2O$	10	10	10	10	10

1.3 Preparation of $Ba_{1-x}La_xFe_{12-x}Zn_xO_{19}$ hexaferrite

Factor 2: Study the effect of Zn substituted $Ba_{0.85}La_{0.15}Fe_{12}O_{19}$ on magnetic properties. The formulations are shown in Table 8

$Ba_{1-x}La_xFe_{12-x}Zn_xO_{19}$ (x = 0.00 -0.20) ferrite powders were prepared according to Figure 26. The mixture solution of metal ions was prepared by dissolving $Ba(NO_3)_2$, $Fe(NO_3)_3.9H_2O$, $La(NO_3)_3.6H_2O$ and $Zn(NO_3)_2.6H_2O$ in the solution of ethylene glycol (EG) and triethanolamine (TEA) at 100 °C and stirring. The amount of $Zn(NO_3)_2.6H_2O$ was varied from x = 0.05 to x = 0.20. The clear solution was heated up to 120°C for 2 hours with constant stirring then the precursor was formed. The precursor was washed with ethanol, filtered and then calcined at 1200°C for 2 hours. The ingredients of $Ba_{1-x}La_xFe_{12-x}Zn_xO_{19}$ are shown in Table 8.

Table 8 The formulations of $Ba_{1-x}La_xFe_{12-x}Zn_xO_{19}$ preparation.

Ingredient	Mole ratio				
	BaF 3	BaF 5	BaF 6	BaF 7	BaF 8
Triethanolamine (TEA)	11	11	11	11	11
$Ba(NO_3)_2$	0.85	0.85	0.85	0.85	0.85
$La(NO_3)_3.6H_2O$	0.15	0.15	0.15	0.15	0.15
$Fe(NO_3)_3.9H_2O$	1	0.95	0.90	0.85	0.80
Zn	0	0.05	0.10	0.15	0.20

2. Preparation and valcanization of rubber compounds

All ingredients were incorporated in a natural rubber matrix. The formulations of rubber ferrite composites are shown in Table 9. The mixing was done in a two-roll mill at 70 °C for 15 minutes. Finally, the curatives were added and mixed with the compounds and after homogenization they were sheeted out and kept at room temperature for 24 hours before testing.

Table 9 The ingredient of rubber ferrite composite (RFCs)

Ingredient	phr (part per hundred rubber)
Natural Rubber (STR5L)	100
Stearic acid	1
Zinc oxide	5
Accelerator (CBS)	0.6
Antioxidant (TMQ)	1
Sulfur	1.5
Barium hexaferrite	60

*CBS: N- cyclohexyl-2-benzothiazole Sulphenamide ; TMQ: 2,2,4-Trimethyl-1,2-dihydroquinoline polymer.

Prior to vulcanize the mixes, a vulcanization time was determined by means of Moving Die Rheometer (MDR). The Moving Die Rheometer measures the change in stiffness of a rubber sample, compressed between two heated platens, by an applied oscillating force. The degree of vulcanization determines the cure characteristic of the sample as it is heated and compressed. The test is known as a cure curve such as scorch time, time to percentage cure, maximum and minimum torques. The mixes were compression molded using a hydraulic hot press at 150 °C, under pressure of 15 MPa.

3. Phase morphology

3.1 X-ray diffraction (XRD) analysis

The information of structure and crystallographic orientation of barium hexaferrite was obtained from XRD measurement with CuKα (λ = 1.54 Å and 2θ = 20-70 degree).

3.2 Scanning Electron Microscope (SEM) analysis

The phase morphology of the barium hexaferrites powder and rubber ferrite composite was studied by using scanning electron microscope (model JEOL-JSM-5410LV). The dried surfaces of the samples were gold coated and then examined by SEM

3.3 Energy dispersive X ray spectroscopy

The intensity of element in sample was investigated by EDX. Qualitative analysis involves the identification of the lines in the spectrum and is fairly straightforward owing to the simplicity of X-ray spectra. Quantitative analysis (determination of the concentrations of the elements present) entails measuring line intensities for each element in the sample. All elements from atomic number 4 (Be) to 92 (U) can be detected in principle

4. Cure Characteristics

The cure characteristics of rubber compound having sulfur as curing agent were assessed by Moving Die Rheometer (MDR). Vulcanization was performed using a compression-molding machine. The various rubber compounds were compression molded at 150°C according to their respective optimum cure times. Cure time was determined from the time to reach 90% (t_{c90}).

Figure 27 The Moving Die Rheometer (MDR)

5. Mechanical Properties

5.1 Tensile strength

The vulcanized samples were cut into tensile specimens by using the punching machine. The cutting die punched the sample into dumbbell-shape. Testing was carried out on tensile testing machine in accordance with ASTM D412-92. The following tensile properties were measured: 100, 300, and 500% modulus, tensile

strength (stress of rupture of specimen) and the elongation at break according to ASTM D 412-92 using the Universal Testing Machine with the load cell of 2500 kN as shown in Figure 28.

Figure 28 The tensile testing machine

Tensile strength were calculated from the following equation

$$\sigma = F/A$$

where: σ= stress (N/mm^2)

F = force (N)

A = cross-sectional area of unstreched specimens (mm^2)

6. Magnetic testing

A vibrating sample magnetometer (VSM) operates on Faraday's Law of Induction, which tells us that a changing magnetic field will produce an electric field. This electric field can be measured and can tell us information about the changing magnetic field. Magnetic Properties of the sample were examined at room temperture using Vibration Samples Magnetometer (VSM) up to 5 kOe. The magnetic parameters

including coercivity (Hc), saturation magnetization (Ms), magnetic remanence (Mr) were obtained from these measurements.

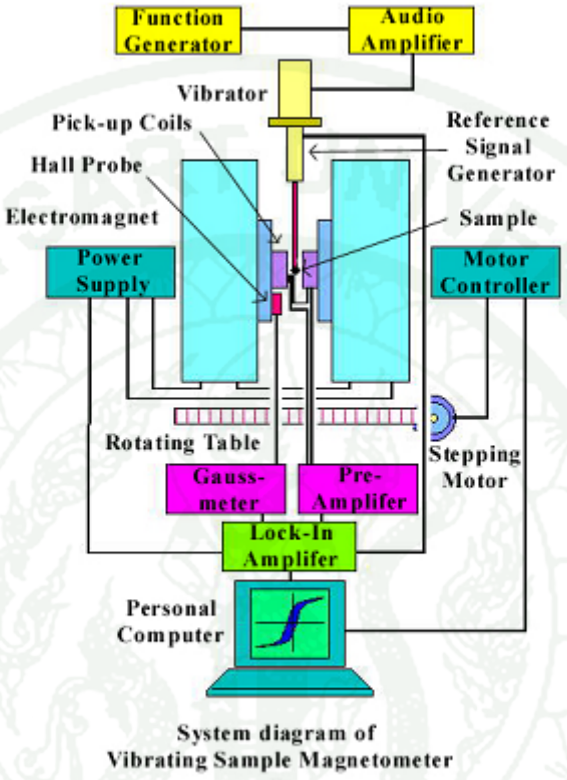

Figure 29 Vibrating Sample Magnetometer

RESULTS AND DISCUSSION

1. Filler characterization

1.1 X-ray diffraction analysis

This part emphasizes on the characterization of the structure and morphology of barium hexaferrite La-substituted barium hexaferrite and La-Zn substituted barium hexaferrite synthesized by the oxide one pot synthesis (OOPS) process. The information of structure and crystallographic orientation of substituted barium hexaferrite was obtained from XRD measurement. The determination of the crystalline phase was carried out by X-ray diffractometer (XRD) with CuKα (λ = 1.54 Å and 2θ = 20-70 degree). The XRD patterns were matched with the database of barium hexaferrite and possible intermediates are shown in Figure 30 to Figure 33.

1.1.1 $BaFe_{12}O_{19}$ hexaferrites powder

X-ray diffraction (XRD) pattern of barium hexaferrite ($BaFe_{12}O_{19}$) calcined at 1200 °C for 2 hours was matched with $BaFe_{12}O_{19}$ pattern (PDF No: 00-043-0002), $BaFe_2O_4$ pattern (PDF No: 00-025-1191) and α-$Fe_{1.76}O_3$ (Hematite) pattern (PDF No: 01-076-9683) as shown in Figure 33. It was confirmed that barium hexaferrite has some impurity as a result of the matching of XRD pattern with $BaFe_2O_4$ and α-$Fe_{1.76}O_3$ (hematite) which are considered as intermediates. Figure 33 shows that the diffraction peaks of barium hexaferrite ($BaFe_{12}O_{19}$) were dominant, while the diffraction peaks of α-$Fe_{1.76}O_3$ (hematite) and $BaFe_2O_4$ became very weak, indicating that the sample mainly consists of $BaFe_{12}O_{19}$ and a small amount of α-$Fe_{1.76}O_3$ (hematite) and $BaFe_2O_4$. The $BaFe_{12}O_{19}$ is formed by the following reaction process (Wang et al., 2010):

$$BaFe_2O_4 + 5Fe_2O_3 \rightarrow BaFe_{12}O_{19}$$

It should be noted here that there was an appearance of intermediate phase for the synthesis process of barium hexaferrite calcined at 1200 °C for 2 hours. From many researchers, it was found that barium hexaferrite (BaF) came from the reaction between $BaFe_2O_4$ and Fe_2O_3 (Wang et al., 2010). Therefore, it was interesting to further study by increasing the calcinations time to prepare more purity of barium hexaferrite.

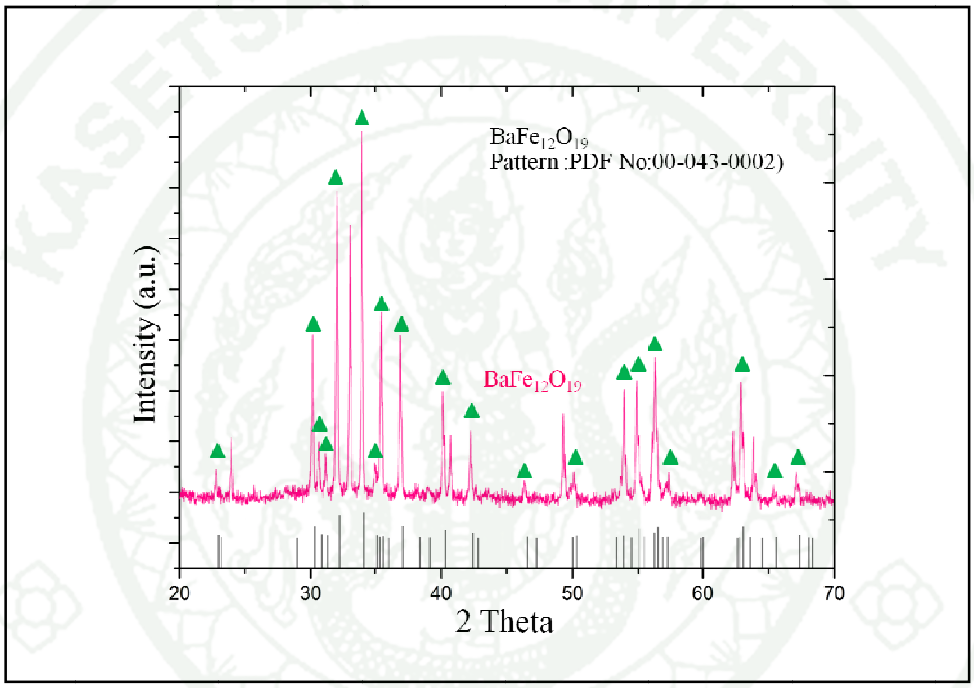

Figure 30 XRD pattern of barium hexaferrite ($BaFe_{12}O_{19}$) matched with $BaFe_{12}O_{19}$ pattern PDF No:00-043-0002

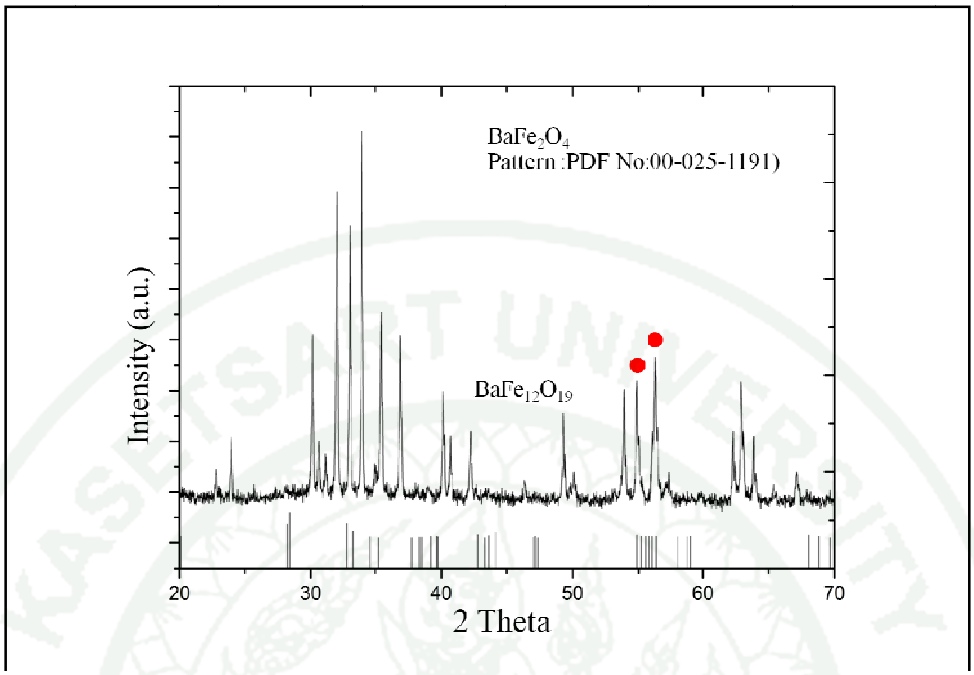

Figure 31 XRD pattern of barium hexaferrite ($BaFe_{12}O_{19}$) matched with $BaFe_2O_4$ pattern PDF No:00-025-1191

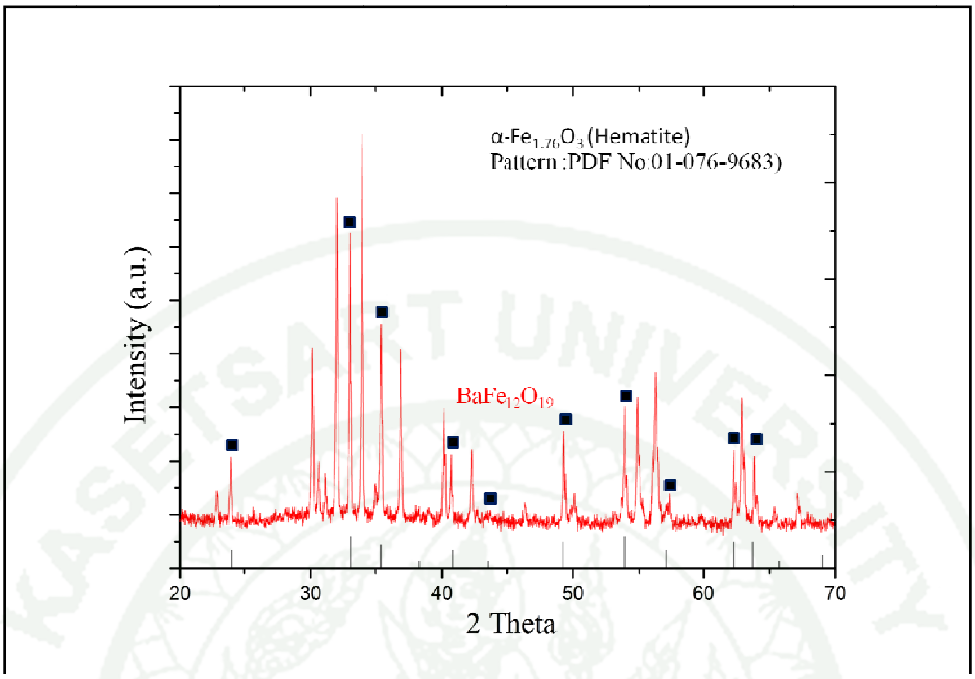

Figure 32 XRD pattern of barium hexaferrite ($BaFe_{12}O_{19}$) matched with hematite (Fe_2O_3) pattern PDF No:01-076-9683

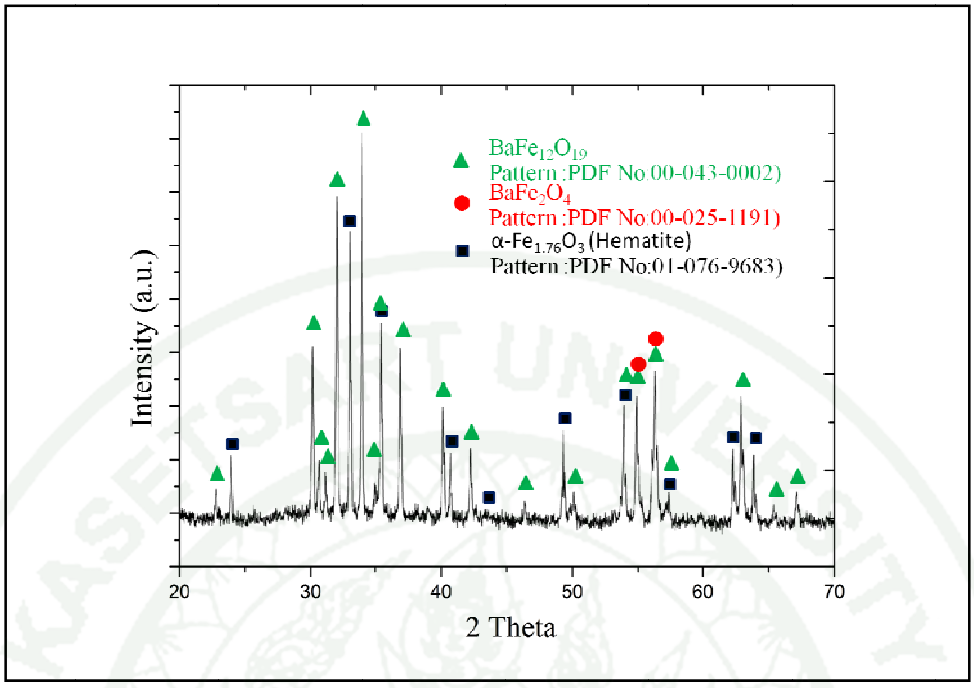

Figure 33 XRD pattern of barium hexaferrite ($BaFe_{12}O_{19}$) matched $BaFe_{12}O_{19}$ pattern PDF No:00-043-0002, $BaFe_2O_4$ pattern PDF No:00-025-1191and hematite (Fe_2O_3) pattern PDF No:01-076-9683

1.1.2 $Ba_{1-x}La_xFe_{12}O_{19}$ hexaferrites powders.

The major aim of this part was to investigate the descent of the crystalline phase of $Ba_{1-x}La_xFe_{12}O_{19}$ hexaferrites with varying the amount La substituted from x = 0.00 to x = 0.20. The barium ferrite powders after being substituted were characterized using x-ray diffractometer (XRD).

All X-ray diffraction patterns of the $Ba_{1-x}La_xFe_{12}O_{19}$ (x=0.00-0.20) samples are shown in Figure 34. The refinements of the XRD patterns were performed by using profile matching and all of the XRD peaks correspond to Bragg positions of the magnetoplumbite structure with hexagonal symmetry and space group $P6_3/mmc$ (Ounnunkad, 2006). That is mean the La can be completely substitute into the hexaferrite in the substitution range because the intermediate such as $LaFe_{12}O_{19}$,

La_2O_3 was not found in the XRD pattern. However, it should be noted here that the intermediate phase, $BaFe_2O_4$ and Fe_2O_3 were found along with the major phase, $BaFe_{12}O_{19}$. At all amount of La substituted barium hexaferrite (x = 0.00 – x = 0.20). The appearance of intermediate phase was not form the substitution of La but from the condition of synthesis process not being optimized.

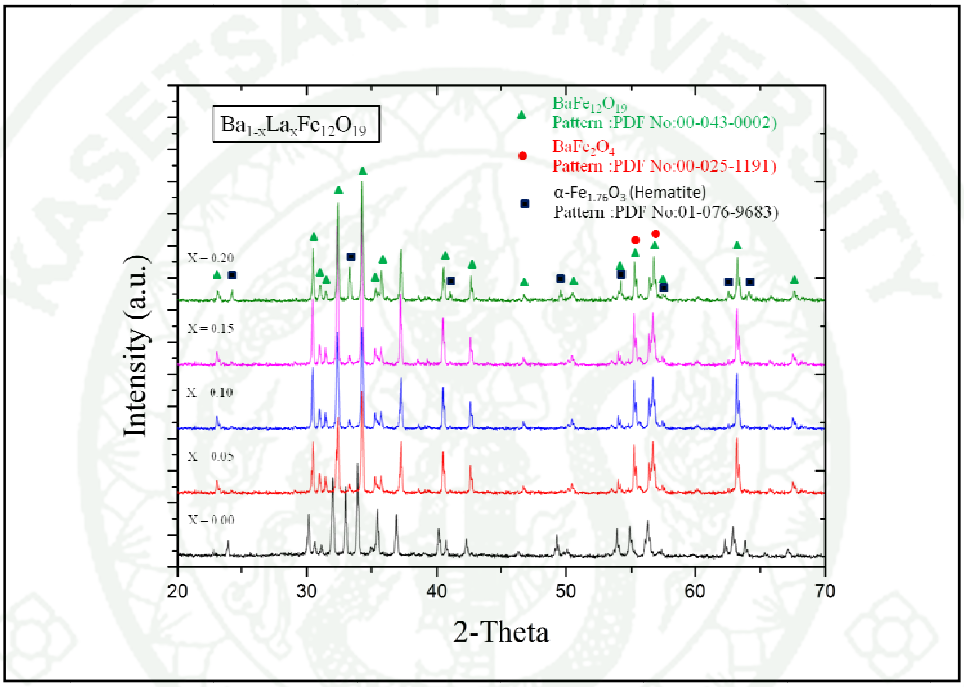

Figure 34 XRD pattern of $Ba_{1-x}La_xFe_{12}O_{19}$ (x = 0.00-0.20) $BaFe_{12}O_{19}$ pattern PDF No:00-043-0002, $BaFe_2O_4$ pattern PDF No:00-025-1191and hematite (Fe_2O_3) pattern PDF No:01-076-9683

The lattice parameters a and c were calculated from following equation:

$$d\,(h\,k\,l) = \left(\frac{4}{3}\frac{h^2 + hk + k^2}{a^2} + \frac{l^2}{c^2}\right)^{-1/2}$$

where $d_{h\ k\ l}$ corresponding to (1 0 7) and (1 1 4) peaks. Lattice parameters (a and c) of the $Ba_{1-x}La_xFe_{12}O_{19}$ (x=0.00-0.20) are listed in Table 10.It was

found that the lattice parameters of pure sample (x = 0.00) were higher than those of doped haxaferrite specimens because the radius of La^{3+} (1.22 Å) was smaller than Ba^{2+}(1.49 Å) and radius of Fe^{2+}(0.80 Å) was larger than Fe^{3+}(0.67 Å) (Hua et al., 2007). The slight changes of the lattice parameter may have been caused by the La^{3+} substitution for $Ba^{2+}$and valence change of Fe ions. Therefore, the increasing La substitution contents made the lattice parameters systematically decreased. This result shows that the crystal structures of barium hexaferrites were contracted after being doped with La ions.

Table 10 Lattice parameters of the $Ba_{1-x}La_xFe_{12}O_{19}$ hexaferrite

x (La content)	**a (Å)**	**c (Å)**
0.00	5.9205	23.4993
0.05	5.9015	23.2768
0.10	5.8882	23.1572
0.15	5.8856	23.1539
0.20	5.8853	23.1477

1.1.3 $Ba_{0.85}La_{0.15}Fe_{12-x}Zn_xO_{19}$ hexaferrite powders

From theoretically the doping by non-magnetic Zn^{2+} ion, which occupies the $4f_1$ sites, will increase the value of specific saturated magnetization M_s. This is because the zinc ions greatly prefer tetrahedral positions, and in M ferrites the tetrahedral sites oppose the spin of most of the octahedral sites, which produce the net moment. Therefore, substitution with Zn^{2+} reduces this negative contribution, increasing the net magnetic moment (Pullar, 2012).

In this section, the influence of Zn ion on the crystalline phase of barium hexaferrite was investigated. The observation of crystal structure was received by X-ray diffractometer (XRD). The XRD patterns of $Ba_{0.85}La_{0.15}Fe_{12-x}Zn_xO_{19}$ hexaferrites with x = 0.00 to x= 0.20 was matched with reference of barium

hexaferrite and intermediate as shown in Figure 35 to figure 39. The results were discussed and reported.

Figures 35-39 show that XRD patterns of $Ba_{0.85}La_{0.15}Fe_{12-x}Zn_xO_{19}$ (x = 0.05) hexaferrites with various Zn content (x= 0.00 – x = 0.20) matched with references, in which Figure 35 matched with the reference pattern of $BaFe_{12}O_{19}$ (PDF No:00-007-0276), Figure 36 matched with $BaFe_2O_4$ pattern (PDF No:00-025-119), Figure 37 matched with $ZnFe_2O_4$ pattern (PDF No:00-001-1108) and Figure 38 matched with α-$Fe_{1.76}O_3$ (hematite) pattern (PDF No:01-076-9683). Moreover, it should be noted here that, the intermediates phase appeared in all Zn^{2+} substituted barium hexaferrite. It was also observed that, the concentration of the hematite phase decreased with increasing Zn contents but the formation of $ZnFe_2O_4$ increased.

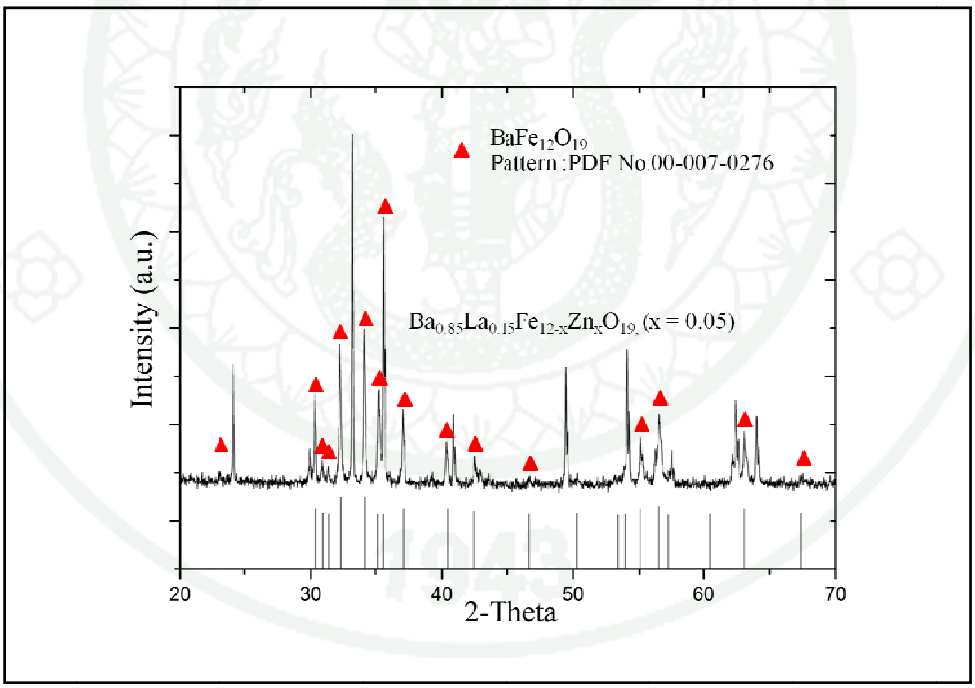

Figure 35 XRD pattern of $Ba_{0.85}La_{0.15}Fe_{12-x}Zn_xO_{19}$ (x = 0.05) matched with $BaFe_{12}O_{19}$ PDF No: 00-007-00276

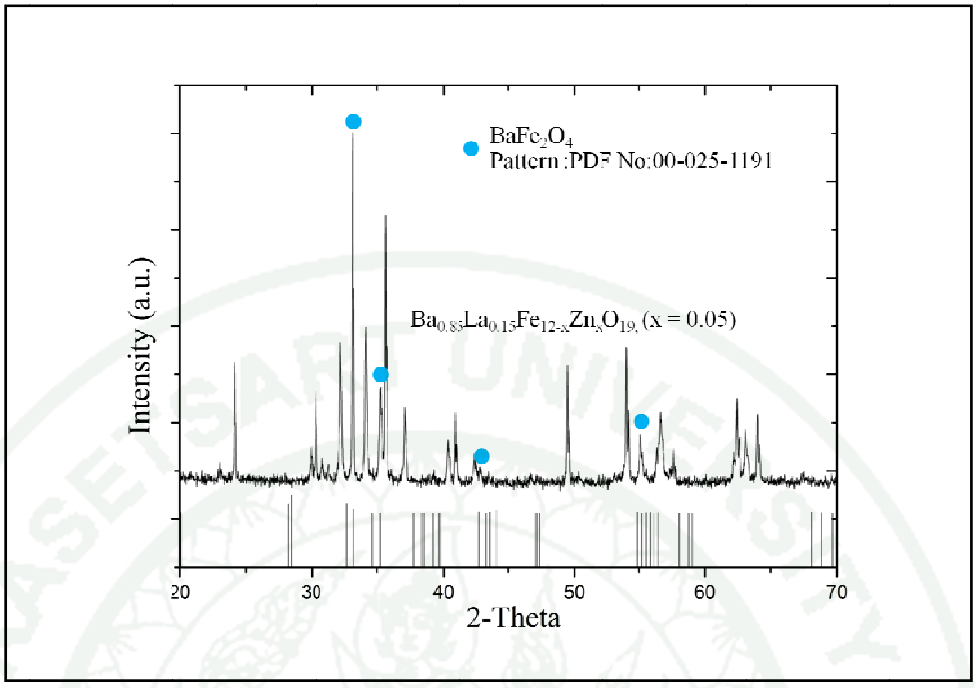

Figure 36 XRD pattern of $Ba_{0.85}La_{0.15}Fe_{12-x}Zn_xO_{19}$ (x = 0.05) matched with $BaFe_2O_4$ PDF No: 00-025-1191

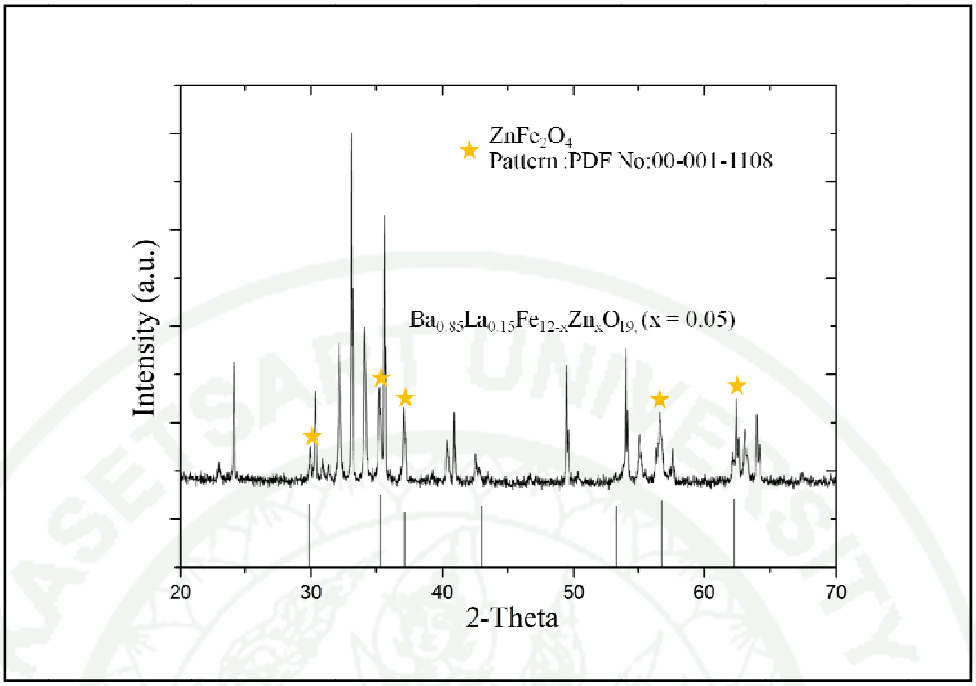

Figure 37 XRD pattern of $Ba_{0.85}La_{0.15}Fe_{12-x}Zn_xO_{19}$ (x = 0.05) matched with $ZnFe_2O_4$ PDF No: 00-001-1108

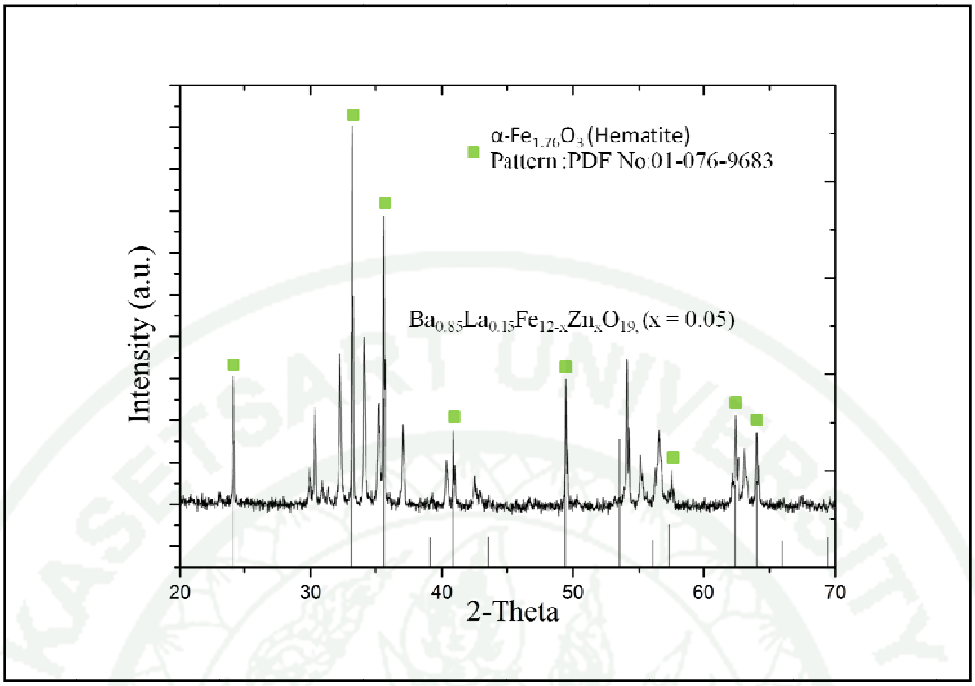

Figure 38 XRD pattern of $Ba_{0.85}La_{0.15}Fe_{12-x}Zn_xO_{19}$ (x = 0.05) matched with Fe_2O_3 PDF No: 00-076-9683

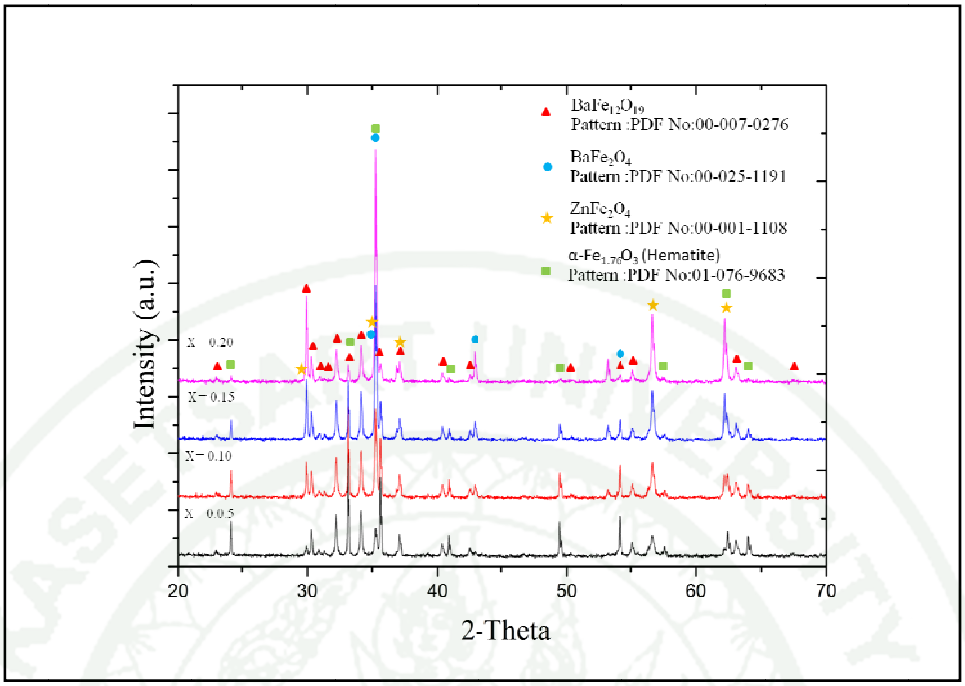

Figure 39 XRD pattern of $Ba_{0.85}La_{0.15}Fe_{12-x}Zn_xO_{19}$ (x = 0.05- 0.20) matched with $BaFe_{12}O_{19}$ PDF No: 00-007-00276, $BaFe_2O_4$ PDF No: 00-025-1191, $ZnFe_2O_4$ PDF No: 00-001-1108, Fe_2O_3 PDF No: 00-076-9683.

Lui et al., proposed the mechanism of the formation of barium hexaferrite as following (Liu et al., 2010)

$$BaCO_3+Fe_2O_3 = BaFe_2O_4 + CO_2 \quad (1)$$

$$BaCO_3+6Fe_2O_3 = BaFe_{12}O_{19} + CO_2 \quad (2)$$

$$BaFe_2O_4+5Fe_2O_3 = BaFe_{12}O_{19} \quad (3)$$

Crystalline $BaFe_2O_4$ was reported as an essential intermediate phase for formation of BaM. $BaFe_2O_4$ is a compound similar to Fe_3O_4 in which Ba^{2+} is replaced by Fe^{2+}(Liu et al., 2010). (Seifert et al., 2009) found Fe_3O_4 in their preparation for La-substituted M-type SrM, where the trivalent La^{3+} ion may force Fe^{3+} ions to be reduced to Fe^{2+} when it is substituted for the divalent Sr^{2+}ion. So when the Fe_3O_4 formed, the Fe^{2+} ions in their stucture may be replacing by Ba^{2+} and Zn^{2+} in the Fe^{2+} site of Fe_3O_4 structure to form $BaFe_2O_4$ as an intermediate and $ZnFe_2O_4$.

$ZnFe_2O_4$ is a stable phase which is detected in XRD pattern after being doped. The concentraton of $ZnFe_2O_4$ increased with increasing Zn contents. Zn ion is easier to replace into Fe_2O_3 than Ba because Zn radii is nearly with Fe ion as shown in Figure 39.

However, it was found from XRD pattern that there were peaks of $BaFe_2O_4$, Fe_2O_3 and $ZnFe_2O_4$ formed in this synthesis condition but the formation of $BaFe_{12}O_{19}$ can convert from reaction between $BaFe_2O_4$ and Fe_2O_3. So, the longer calcination time or higher calcintion temparature are needed to convert intermadaite to form BaM.

1.2. SEM analysis

1.2.1 $Ba_{1-x}La_xFe_{12}O_{19}$ hexaferrites powders.

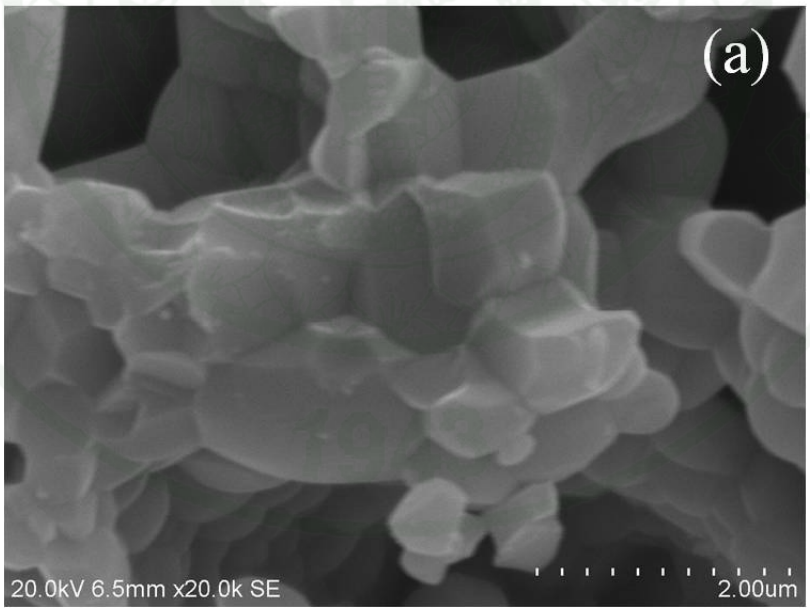

Figure 40 SEM imagines for $Ba_{1-x}La_xFe_{12}O_{19}$ samples of different substituted amount.(a) x = 0.00; (b) x = 0.05; (c) x = 0.10;(d) x = 0.15; (d) x = 0.20.

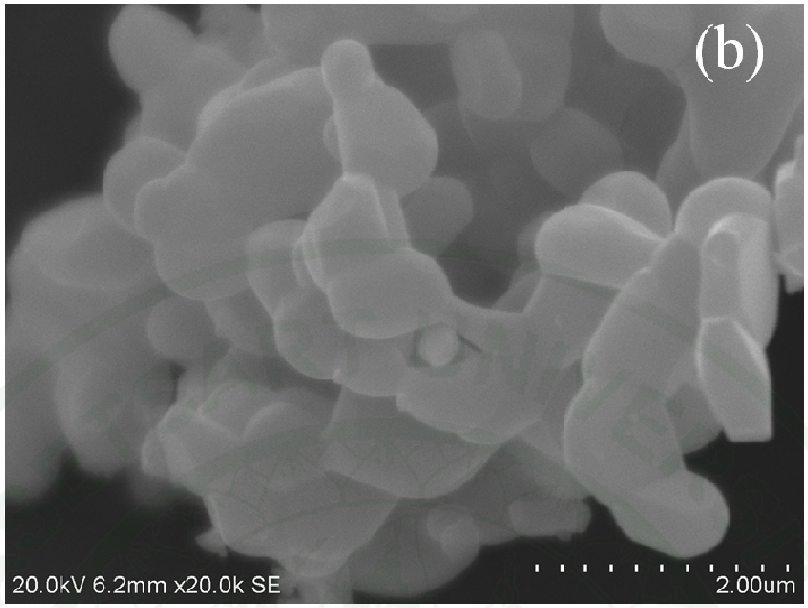

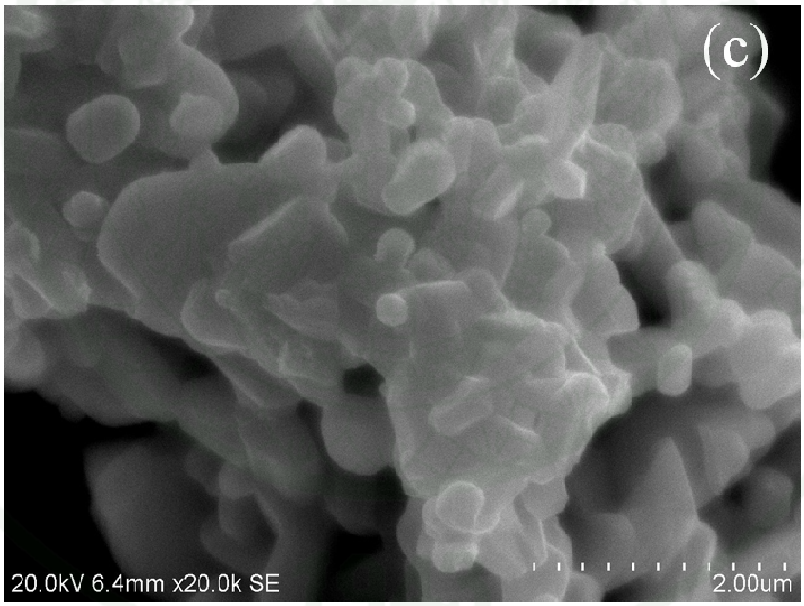

Figure 40 (Continued)

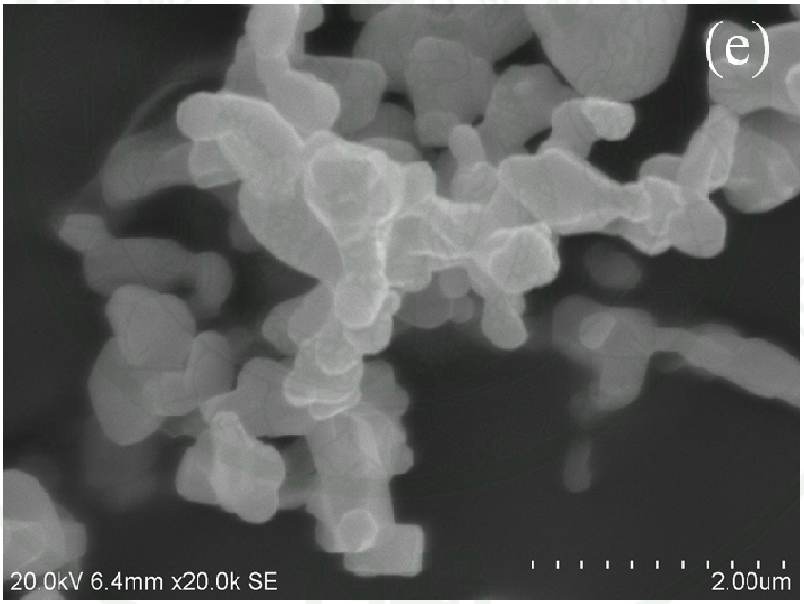

Figure 40 (Continued)

The scanning electron microscopic (SEM) pictures of barium ferrite powders are shown in Figure 40. It was found that crystal structures of barium ferrite substituted with La at lower content (x=0.00-0.20) showed hexagonal shape. However, the particle size of barium hexaferrites decreased with increasing La content. It was confirmed by the decrease in lattice parameters as seen in Table 10 discussed earlier.

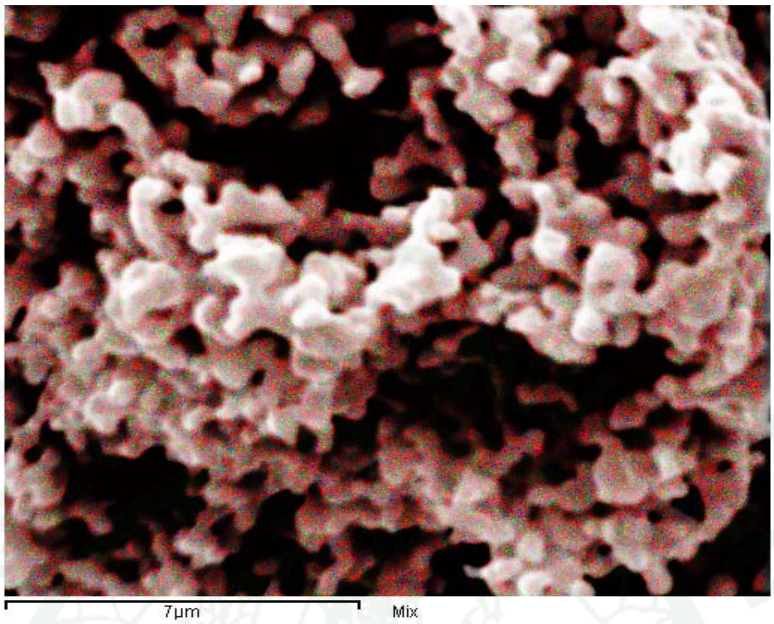

(a) SEM-mapping of $Ba_{1-x}La_xFe_{12}O_{19}$ (x = 0.15), Ba^{2+}: green, La^{3+}: blue

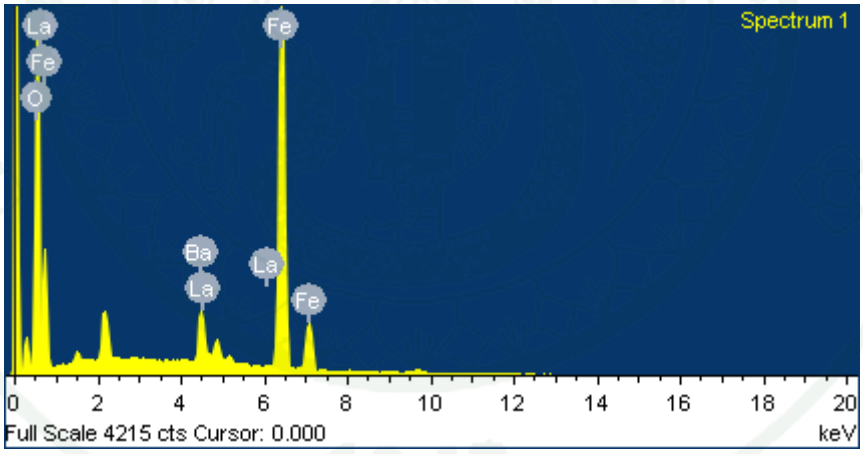

(b) Energy dispersive X-ray (EDX) of $Ba_{1-x}La_xFe_{12}O_{19}$

Figure 41 (a) SEM mapping of $Ba_{1-x}La_xFe_{12}O_{19}$ (x = 0.15), (b) energy dispersive X-ray (EDX)

The chemical composition of $Ba_{1-x}La_xFe_{12}O_{19}$ hexaferrite as seen in Figure 41was carried out using SEM mapping and SEM-EDX. The SEM mapping can be used to observe the distribution of ion in the sample while the SEM-EDX was used to confirm that the substitution of La into barium hexaferrite was successful. It was confirmed from the results that La can be completely substitution in barium hexaferrite structure.

1.2.2 $Ba_{0.85}La_{0.15}Fe_{12-x}Zn_xO_{19}$ hexaferrite powders.

The SEM pictures of $Ba_{0.85}La_{0.15}Fe_{12-x}Zn_xO_{19}$ hexaferrite powders with different Zn content were observed at 30000 magnification. It was shown that the crystal structures have irregular shape. This may be caused by the fact that there were intermedaite phase along with barium hexaferrite in which intermediate has cubic shape such as $ZnFe_2O_4$ and $BaFe_2O_4$. The results from SEM were consistent with that from XRD discussion.

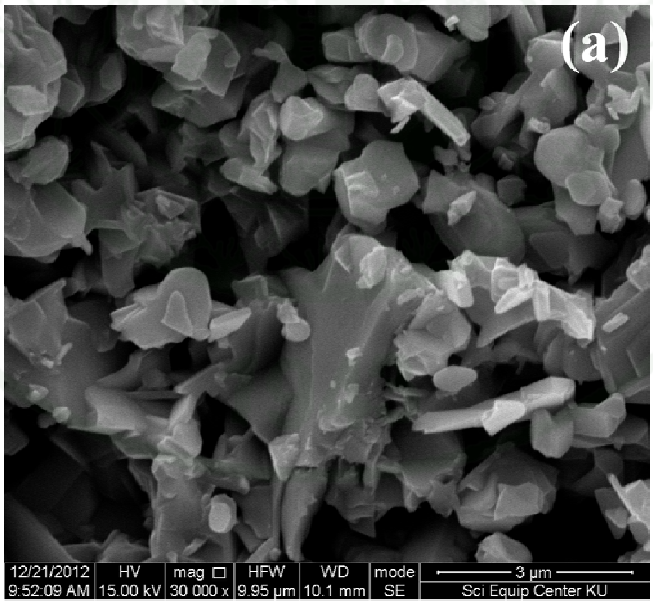

Figure 42 Scanning microscope picture of $Ba_{0.85}La_{0.15}Fe_{12-x}Zn_xO_{19}$ (a) x = 0.05, (b) x = 0.10, (c) x = 0.15 and (d) x = 0.20

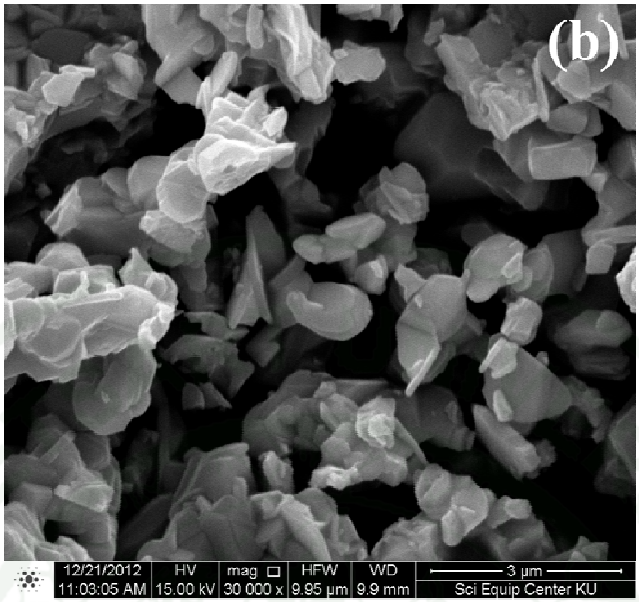

Figure 42 (Continued)

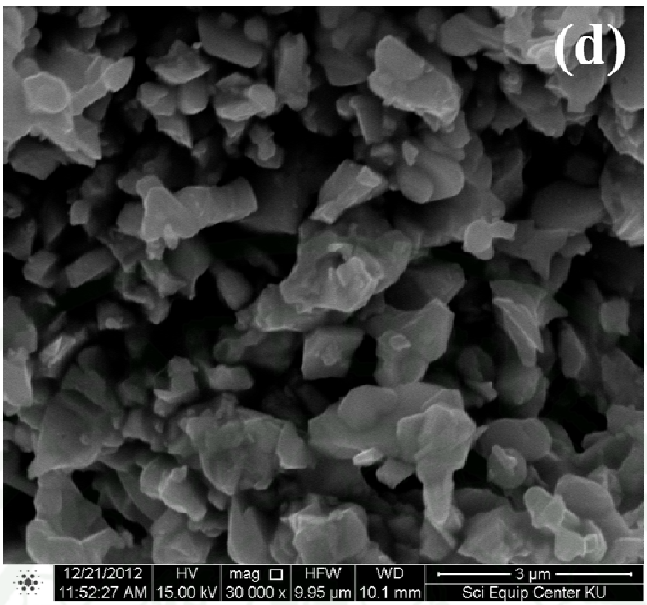

Figure 42 (Continued)

2. Magnetic properties of fillers

The magnetic properties of barium hexaferrite series were obtained by using vibrating sample magnetometer (VSM) with magnetic field up to 8 kOe. The VSM can give information about the magnetic behaviors of the sample including the saturation magnetization (Ms) and coercivity (Hc). The magnetic field applied both of positive and negative field. After applying the magnetic field into the sample, the loops of the magnetic behavior called hysteresis loops were obtained.

2.1 $Ba_{1-x}La_xFe_{12}O_{19}$ hexaferrite (x=0.00-0.20)

The hysteresis loops of the $Ba_{1-x}La_xFe_{12}O_{19}$ hexaferrite with x=0.00-0.20 are reported in Figure 43. It was found that the samples showed behavior of hard magnets as a result of increasing of coercive field (H_c) with an increase in La content. From XRD pattern, it was found that the impurity of sample is effect on the magnetic properties. When increased the La content, the intermediates was decreased which

related with the hysteresis in Figure 43. The hysteresis loops of barium hexaferrite substituted with La at 15% and 20% showed the smooth of hysteresis loops because the lower intermediate after being doped with La. The variations of Ms and Hc values were listed in Table 11.

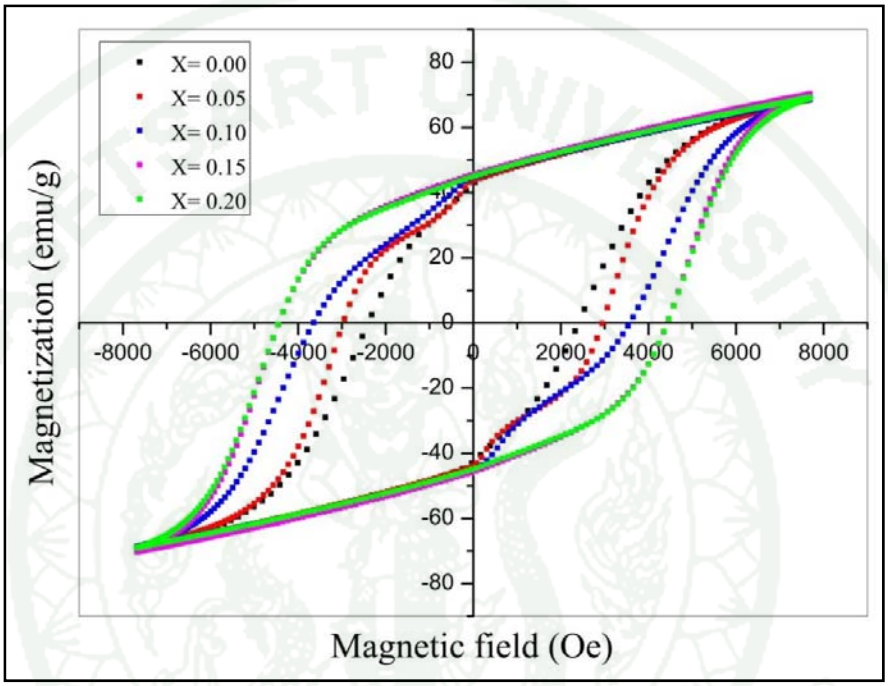

Figure 43 The hysteresis loops of $Ba_{1-x}La_xFe_{12}O_{19}$ with x = 0.00-0.20

Table 11 The lists of magnetic properties of $Ba_{1-x}La_xFe_{12}O_{19}$ with x = 0.00-0.20

La Content (x)	Saturation magnetization (M_s)	Coercivity (H_c)
0.00	68.50	2320.47
0.05	68.53	2941.55
0.10	68.55	3645.40
0.15	70.14	4453.2
0.20	69.24	4460.5

Saturation magnetizations (M_s) of $Ba_{1-x}La_xFe_{12}O_{19}$ with x = 0.00-0.20 are reported in Figure 44 (a). It was found that M_s increased with increasing La substituted up to x = 0.15 and then decreased due to the enhancement of hyperfine field at 12*k* and 2*b* sublattice sites or the increasing in Fe^{3+}-O-Fe^{3+} superexchange interaction and spin canting (Ounnunkad, 2006). This deviated from the collinear to a non-collinear arrangement. In addition, the decrease in the M_S of $Ba_{1-x}La_xFe_{12}O_{19}$ with x = 0.20 was due to a Fe^{3+}($3d^5$ high spin) ion forming into Fe^{2+} state ($3d^6$ =low spin) per substitution of one La^{3+}ion, giving a weaken Fe^{3+}-O-Fe^{3+} super exchange interaction and dilution of internal magnetic field strength (Ounnunkad et al., 2006; Pullar, 2012). Furthermore, the coercive force (H_c) remarkably increased with increasing La content, as illustrated in Figure 44 (b) The enhancement of coercivity was probably due to an increase in the magnetocrystalline anisotropy constant and reduction of grain size. In the barium hexaferrite, the Fe^{3+} ions are distributed over five different sites: three octahedral sites (12*k*,4f_2, and 2*a*), one tetrahedral site (4f1), and one bipyramidal site (2b) (Anterpreet Singha, 2010; Ounnunkad, 2006). In the La-substituted samples for making LaM, La^{3+}ions are expected to enter the Ba^{2+}sites because of their compatibility in radius. It leads to a valence change of $Fe^{3+}$to Fe^{2+}at 2*a* or 4f_2 site to conserve the charge neutrality that the Fe^{2+} has larger orbital moment and therefore larger spin orbit coupling than Fe^{3+} . Because of this, the anisotropy constant for lanthanum ferrite (LaM) is greater than BaM (Pullar, 2012).

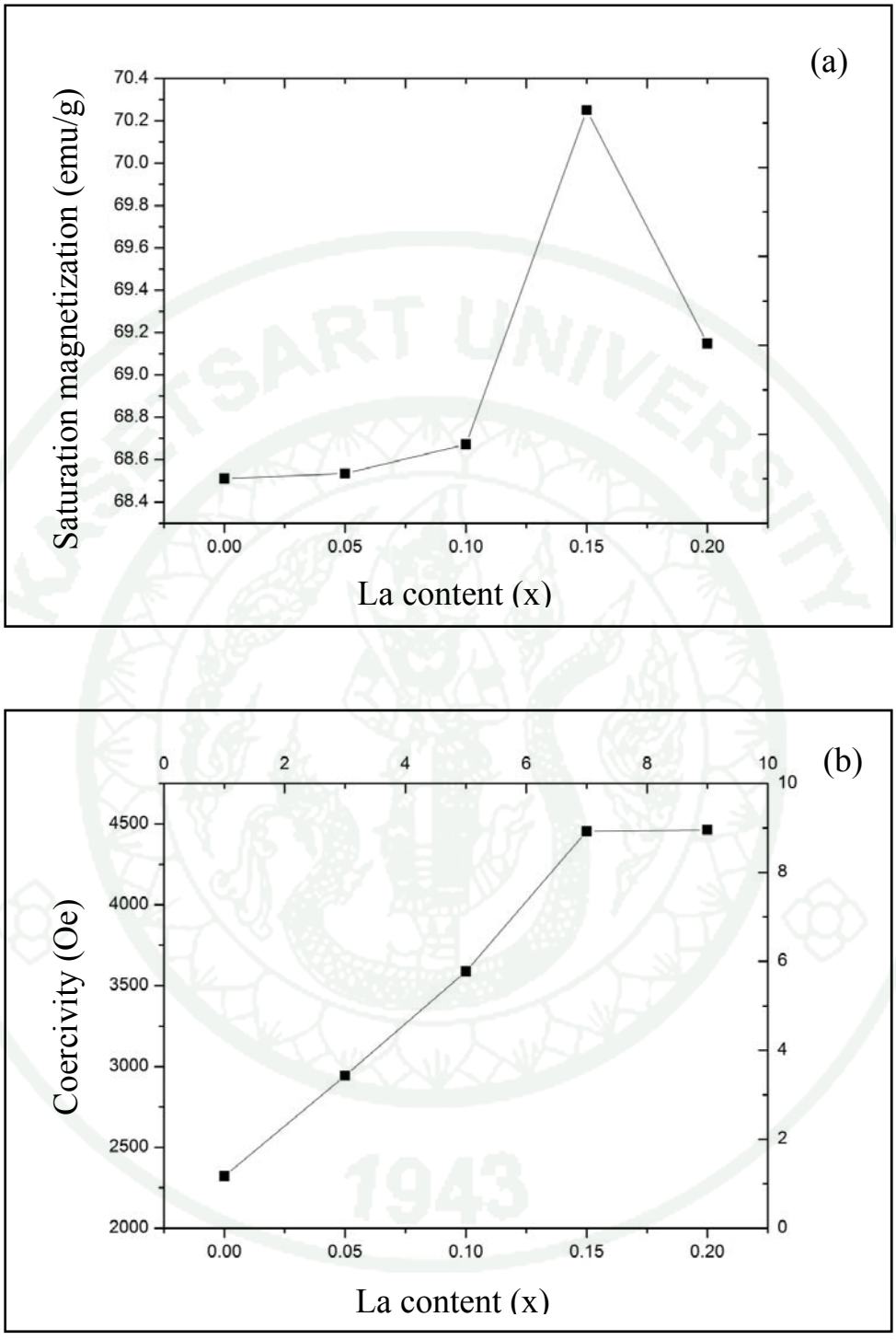

Figure 44 (a)The saturation magnetization (*Ms*) and (b) Coercivity (*Hc*) behaviors of La substituted barium hexaferrite with different La content

2.2 $Ba_{0.85}La_{0.15}Fe_{12-x}Zn_xO_{19}$ (x = 0.00- 0.20) hexaferrite powders.

Magnetic behaviors of $Ba_{0.85}La_{0.15}Fe_{12-x}Zn_xO_{19}$ (x = 0.00- 0.20) were investigated using vibrating sample magnetometer at 8kOe as shown in Figure 45.

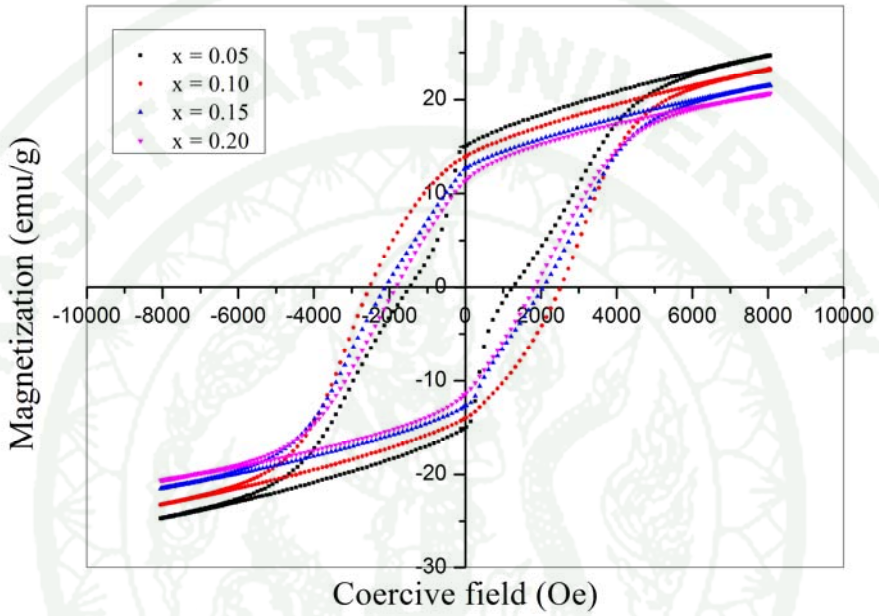

Figure 45 The hysteresis loops of $Ba_{0.85}La_{0.15}Fe_{12-x}Zn_xO_{19}$ (x = 0.00- 0.20)

Table 12 The lists of magnetic properties of $Ba_{0.85}La_{0.15}Fe_{12-x}Zn_xO_{19}$ (x = 0.00- 0.20)

Zn Content (x)	Saturation magnetization (M_s)	Coercivity (H_c)
0.05	24.7322	1555.97
0.10	23.1505	2490.86
0.15	21.4361	2140.79
0.20	20.632	1908.84

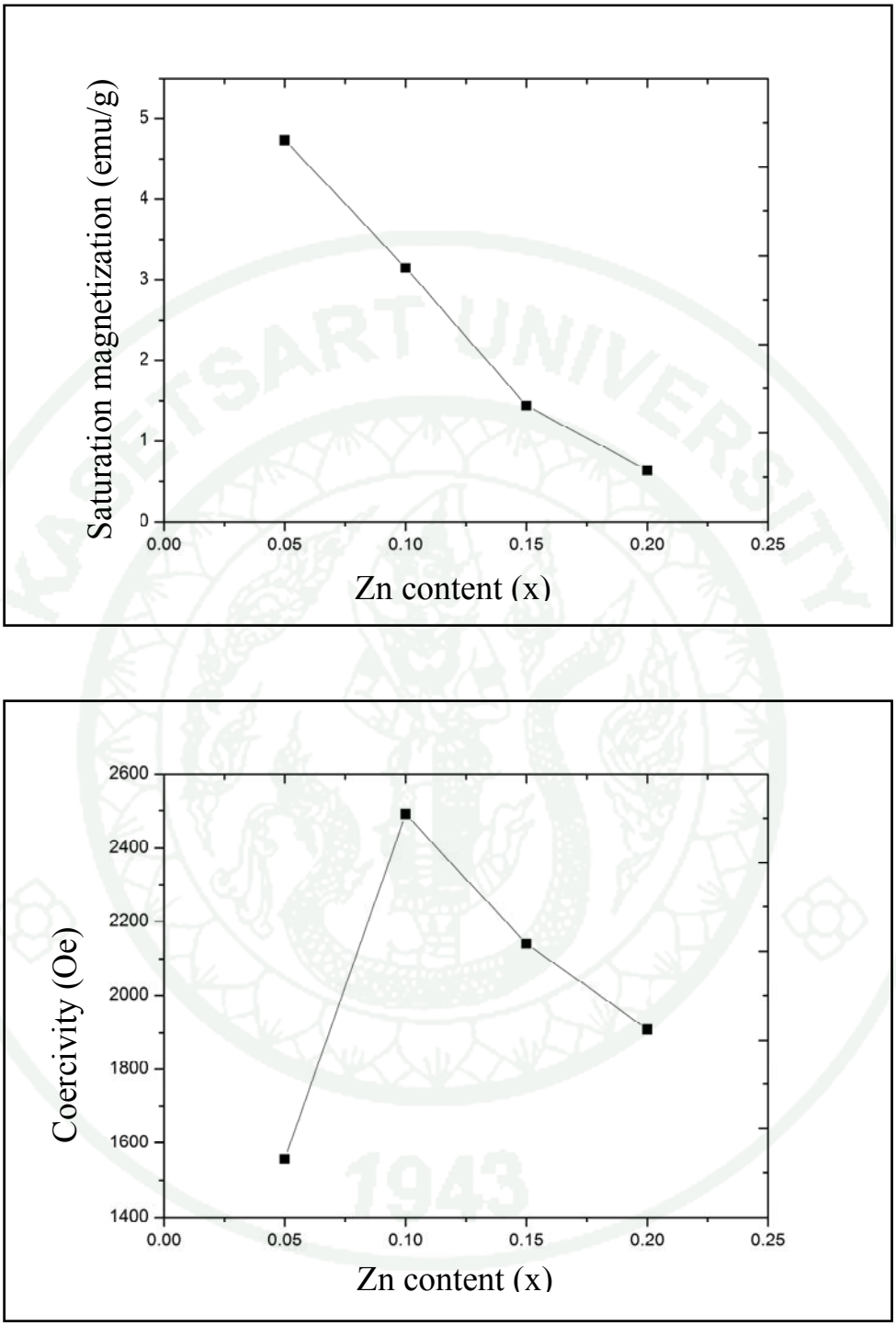

Figure 46 The magnetic properties of $Ba_{0.85}La_{0.15}Fe_{12-x}Zn_xO_{19}$ (x = 0.00- 0.20) (a) saturation magnetization (*Ms*) (b) Coercivity (*Hc*)

From theoretically the doping by non-magnetic Zn^{2+} ion, which occupies the $4f_1$ sites, will increase the value of specific saturated magnetization M_s but the experimental results has usually been found the opposite trend, where in Zn^{2+} doping reduced Ms, especially with larger amounts of dopant (Pullar, 2012).

In this study the problems of incomplete conversion of intermediate to form barium hexaferrite and the formation of zinc ferrite were obtained, resulting in lower magnetic properties. Therefore, the longer reaction time and higher calcination temperature may be needed to further study.

From the above results, La substituted barium hexaferrite at x = 0.15 was the optimized condition, leading to the highest saturation magnetization and coercivity. Therefore, in the next section $Ba_{0.85}La_{0.15}Fe_{12}O_{19}$ was chosen as fillers for making rubber ferrite composites. The comparisons of three types of composites which are filled with different type of magnetic fillers, RFC 1 (commercials grade $BaFe_{12}O_{19}$), RFC 2 ($BaFe_{12}O_{19}$) and RFC 3 ($Ba_{0.85}La_{0.15}Fe_{12}O_{19}$) on cure characteristic, magnetic properties and mechanical properties were discussed and reported.

3. Rubber ferrite composites (RFCs)

3.1 SEM analysis of rubber ferrite composites (RFCs)

The dispersion of fillers in matrix was investigated using the scanning electron microscope pictures as seen in Figure 47 and Figure 48 in which Figure 47 shows the SEM images of RFCs at low (200) magnification while Figure 48 shows the SEM images of RFCs at high (30000) magnification. It was observed that the dispersion of magnetic filler, barium hexaferrite, was quite good but some of the magnetic fillers was agglomerated due to the nature of magnetic fillers which made the interaction between filler-filler interactions are more effect than filler-matrix interaction. Moreover, it should be pointed out here that the particle size distribution

of barium hexaferrites was quite board which influence the mechanical properties of rubber ferrite composites discussed in the next section.

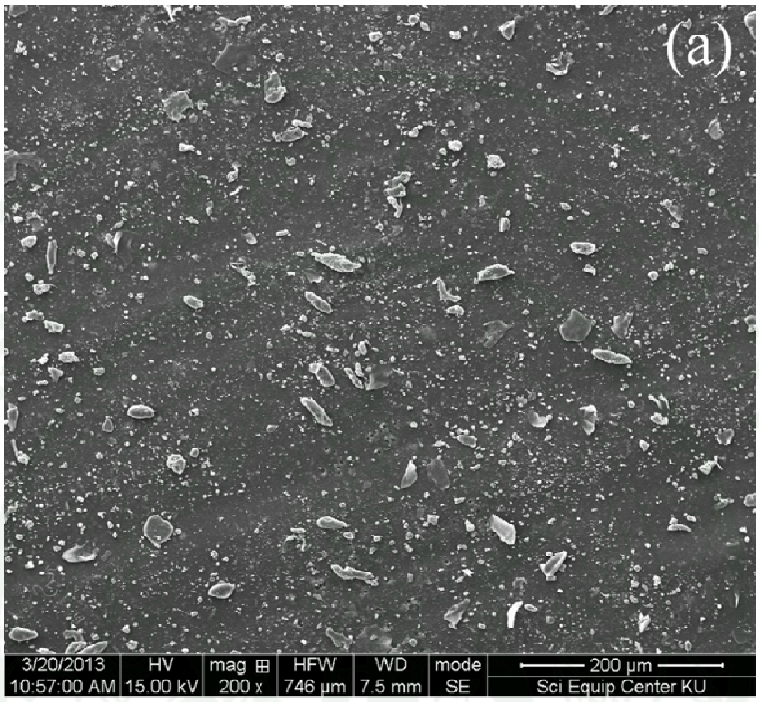

Figure 47 SEM images of RFCs filled $BaFe_{12}O_{19}$ (a) commercial grade $BaFe_{12}O_{19}$ (RFC 1), (b) $BaFe_{12}O_{19}$ synthesized by OOPS process (RFC 2), (c) $Ba_{0.85}La_{0.15}Fe_{12}O_{19}$ (RFC 3) with 200 magnification

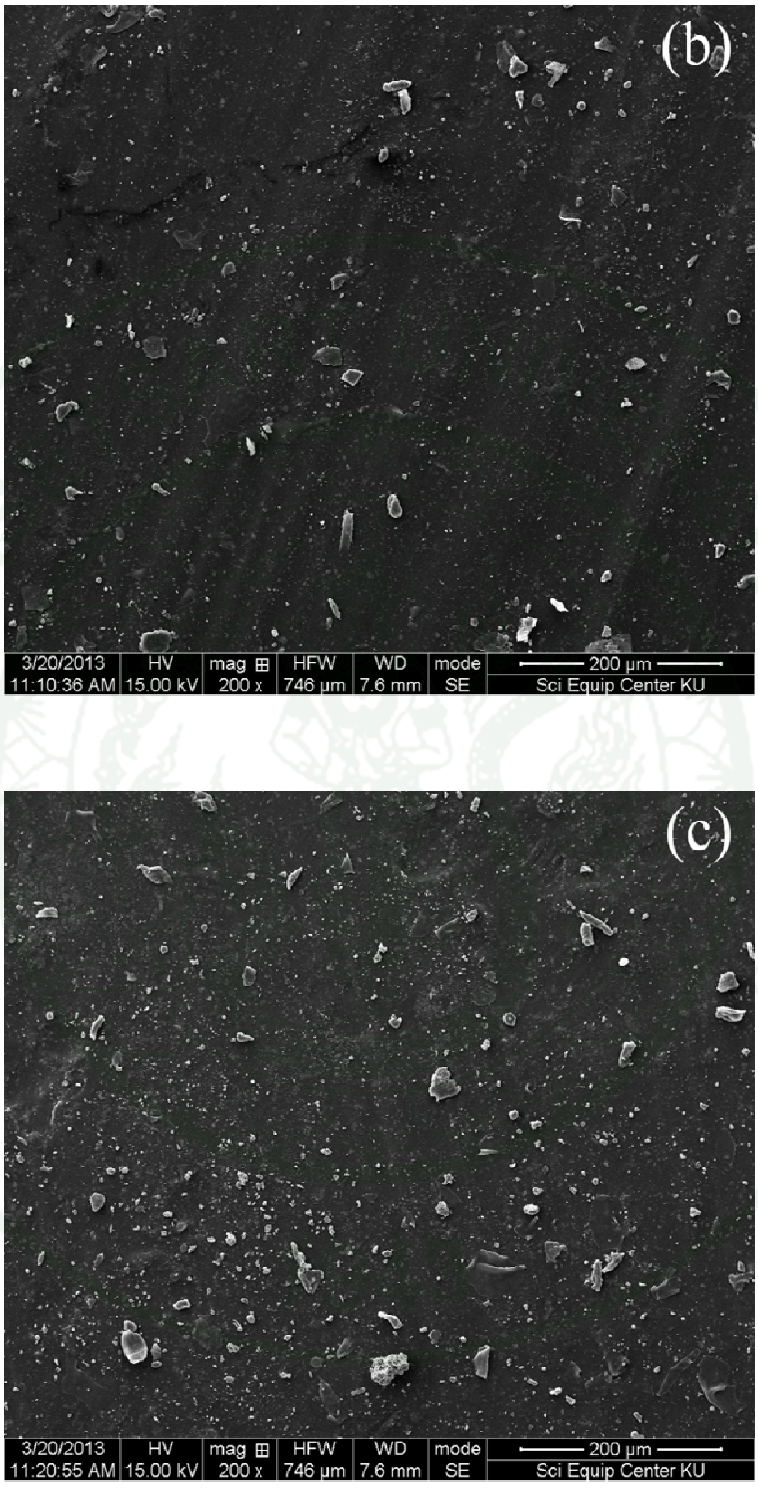

Figure 47 (Continued)

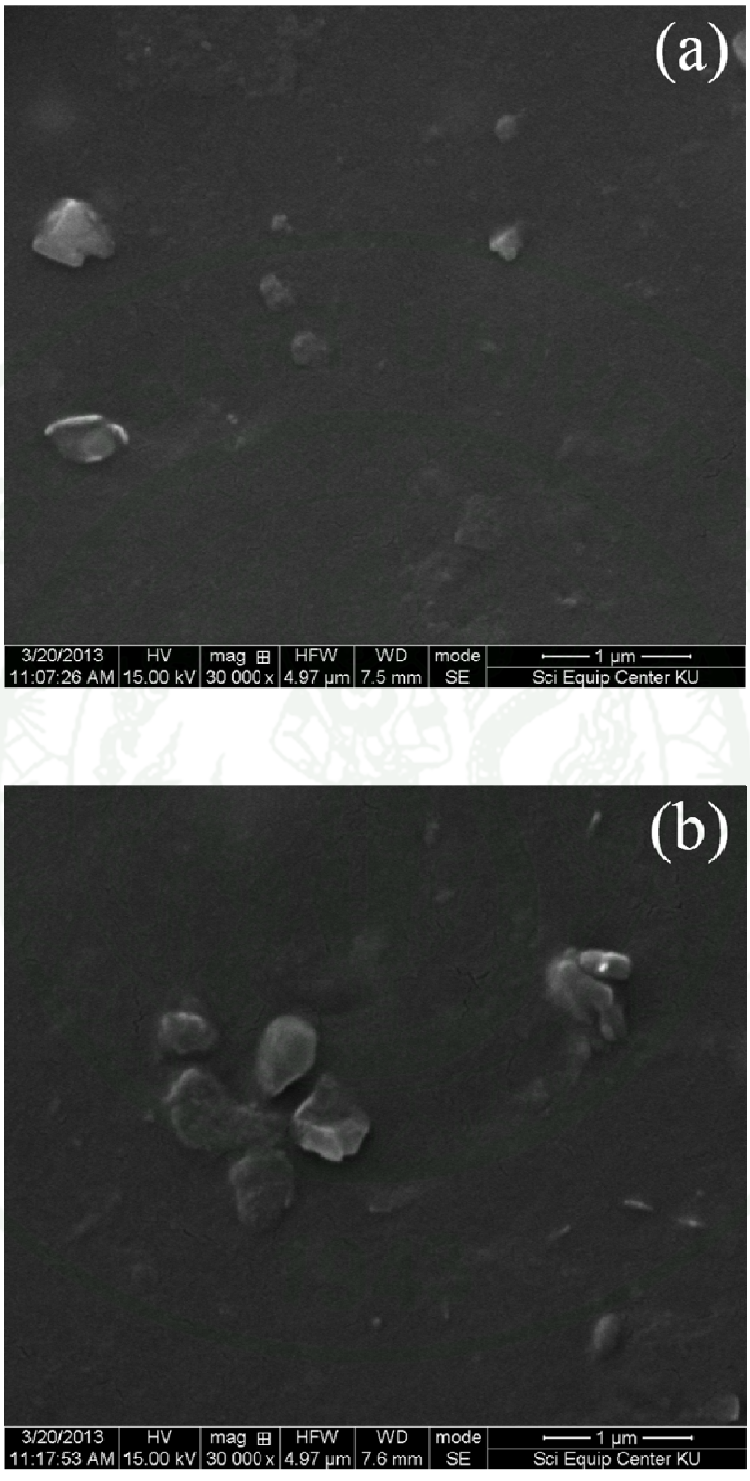

Figure 48 SEM images RFCs filled $BaFe_{12}O_{19}$ (a) commercial grade $BaFe_{12}O_{19}$ (RFC 1), (b) $BaFe_{12}O_{19}$ synthesized by OOPS process (RFC 2), (c) $Ba_{0.85}La_{0.15}Fe_{12}O_{19}$ (RFC 3) with 30000 magnification

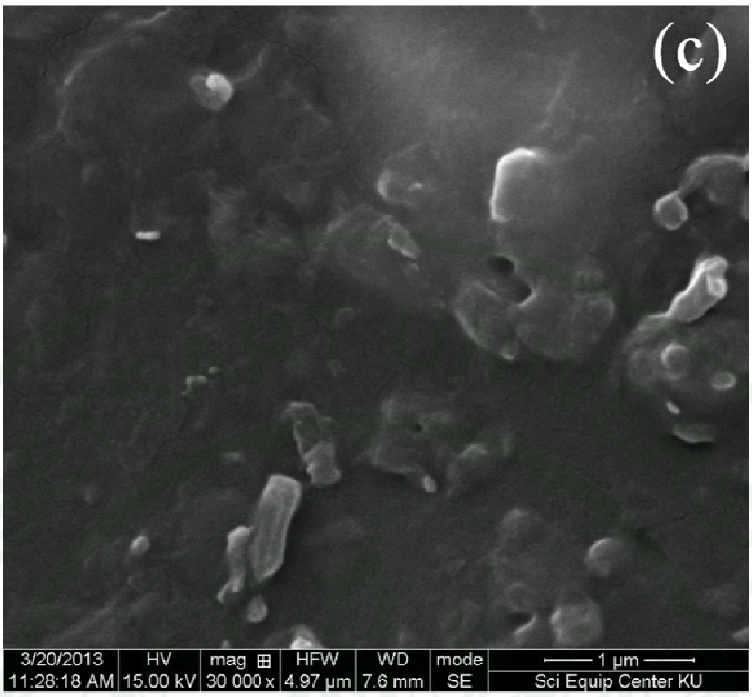

Figure 48 (Continued)

Figure 47, The SEM images of RFCs at 200 magnification and Figure 48, the SEM images of RFCs at 30000 magnification are shown the microstructures of the RFC 1, RFC 2, and RFC 3 at low and high magnification respectively. It was observed that all types of ferrite particles dispersed in the matrix and the surface of rubber ferrite composites

3.2 Cure characteristic of rubber ferrite composites.

Cure characteristics of rubber ferrite composites were determined by using Monsato MDR at 150 ◦C. Table 13 shows the results of scorch time, t_{s2} and cure time, t_{c90} of ferrite filled rubber composites. This section was aimed to compare the cure characteristic of RFCs filled with commercial grade barium hexaferrite , synthesized barium hexaferrite calcined at 1200 ◦C and La substituted barium hexaferrite at the same amount of loading (60 phr).

Table 13 The results of scorch time, t_{s2} and cure time, t_{90}

Cure characteristic	RFC 1	RFC 2	RFC 3
Maximum torque, M_H (lb.in)	2.71±0.02	3.11±0.02	3.22±0.12
Minimum torque, M_L (lb.in)	0.15±0.01	0.20±0.06	0.18±0.02
Scorch time, t_{s2} (min)	5.90±0.08	6.20±0.06	6.29±0.06
Optimum cure time, t_{c90} (min)	6.82±0.01	7.79±0.04	7.99±0.02

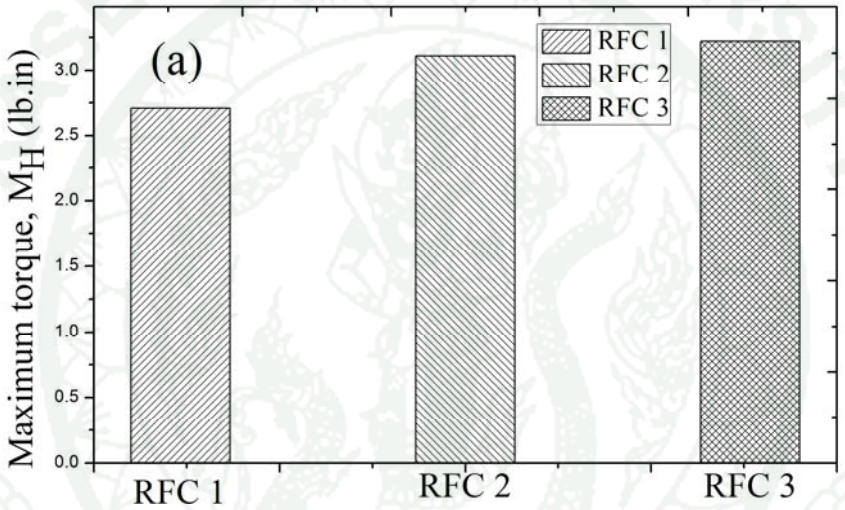

Figure 49 The variation of cure characteristic of RFCs with different BaF type (a) maximum torque, M_H and (b) minimum torque, M_L.

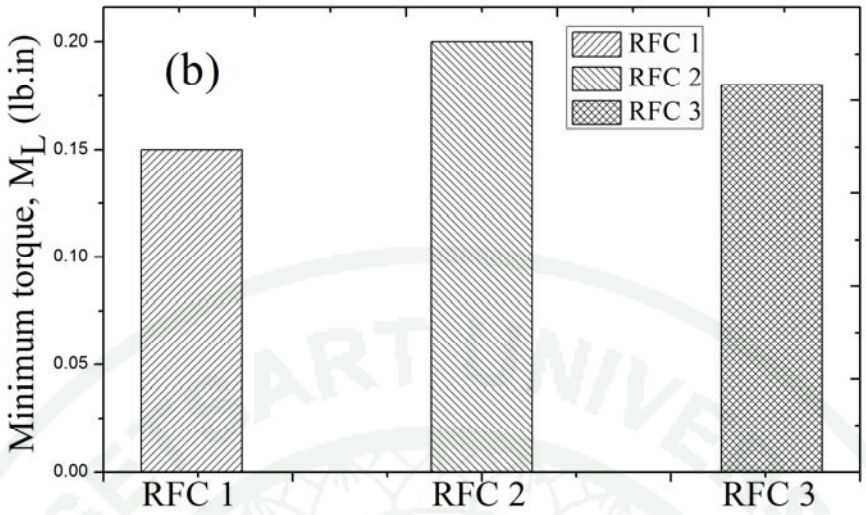

Figure 49 (Continued)

Table 14 Physical properties of barium ferrite powders

Barium hexaferrite	Particle size (μm)	Surface area (m^2/g)
Commercial	13.877	6.060
$BaFe_{12}O_{19}$	22.743	0.091
$Ba_{0.85}La_{0.15}Fe_{12}O_{19}$	16.720	1.430

Figure 49 shows the results of (a) maximum torque, M_H and (b) minimum torque, M_L. The M_L is measure of the viscosity of the uncured compound. It was found that M_L of RFC 1 is lower than both of RFC 2 and RFC 3. This may be caused by the fact that the fillers size of commercial grade barium hexaferrite is smaller than barium hexaferrite synthesized by the OOPS process as seen in Table 14. The bigger particle size interrupts the flow of the matrix more than smaller size. In case of RFC 2 and RFC 3, M_L of both RFC 2 and RFC 3 were not significant different due to size of particle depends on the calcination temperature (Lalita *et al*., 2009) , in which RFC 2 and RFC 3 calcined at the same temperature leading to the same size. Moreover, M_H is a measure of cure state during the specific period of time where no returning of cure, maximum torque can be related to vulcanizate modulus and hardness. It was

observed that M_H value of the RFCs with different types of BaF showed the similar trend as M_L.

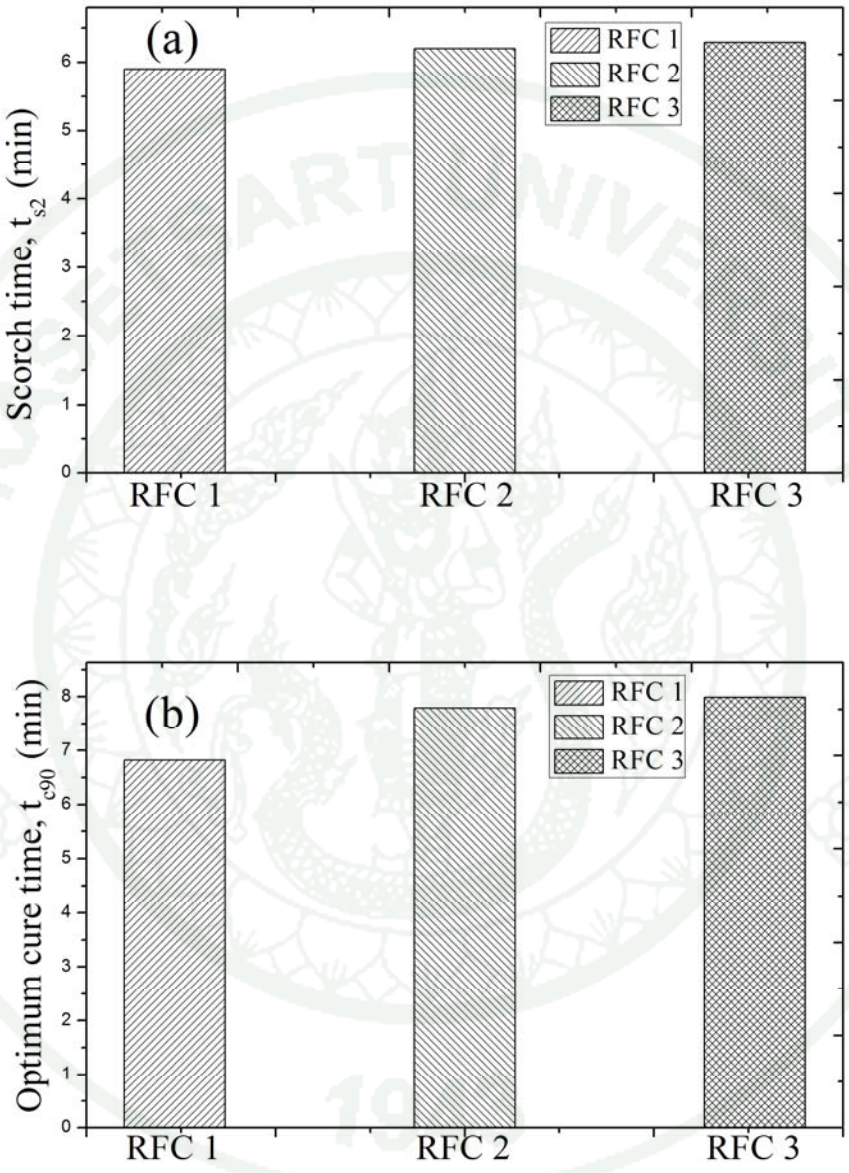

Figure 50 The cure characteristic of RFCs (a) scorch time t_{s2} (min) and (b) optimum cure time t_{c90} (min)

It was observed from Figure 50(a) that the scorch time (ts_2) or processing safety, a time before curing occurred, of rubber ferrite composite filled with commercial grade barium hexaferrite is lower than those of BaF synthesized from

OOPS process. This may be caused by the fact that the particle size of commercial grade barium ferrite was smaller than those of barium hexaferrite synthesized by the OOPS process as discussed earlier in Table 13. The smaller size gave higher surface area, thus, when the particle received heat, the accumulation was occurred in the particle which is transfered to matrix as well. The fact that commercial grade BaF has smaller particle size than synthesized BaF leading to lower ts_2 in rubber compound filled with commercial grade BaF (RFC 1) than that of BaF synthesized from OOPs process (RFC 2) and La substituted barium ferrite synthesixed by OOPs process (RFC 3). Furthermore, cure time is time needed for rubber compounds to reach maximum viscosity or elastic modulus at a given temperature. From Figure 50(b), it shows that the cure time of RFC 1 is lowest compared with that of RFC 2 and RFC 3 because the surface area of the commercial grade barium hexaferrite are higher, resulting in greater rate of heat transfer to matrix leading to the lower cure time.

3.3 Magnetic properties of rubber ferrite composites

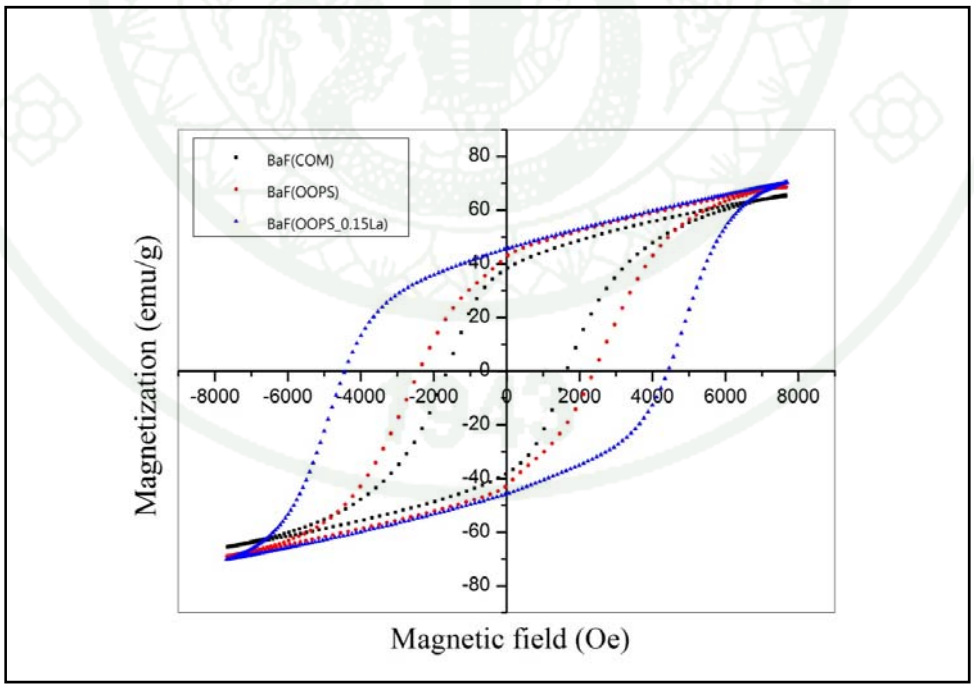

Figure 51 The hysteresis loops of different type of BaF

Figure 51 shows hysteresis loops of barium ferrite (commercial grade), barium ferrite synthesized by OOPS process and La substituted barium ferrite synthesized by OOPS process. It was found that La substituted barium ferrite synthesized by OOPS process gave the highest in saturation magnetization and coercive field. The value of saturation magnetization and coercive field are listed in Table 15.

Table 15 The lists of magnetic properties of different type of barium hexaferrite.

Barium ferrite	Saturation magnetization(M_s) emu/g)	Coercive field (H_c) (Oe)
BaF(COM)	65.1939	1676.25
BaF	68.5024	2320.47
BaF 3	70.1416	4453.20

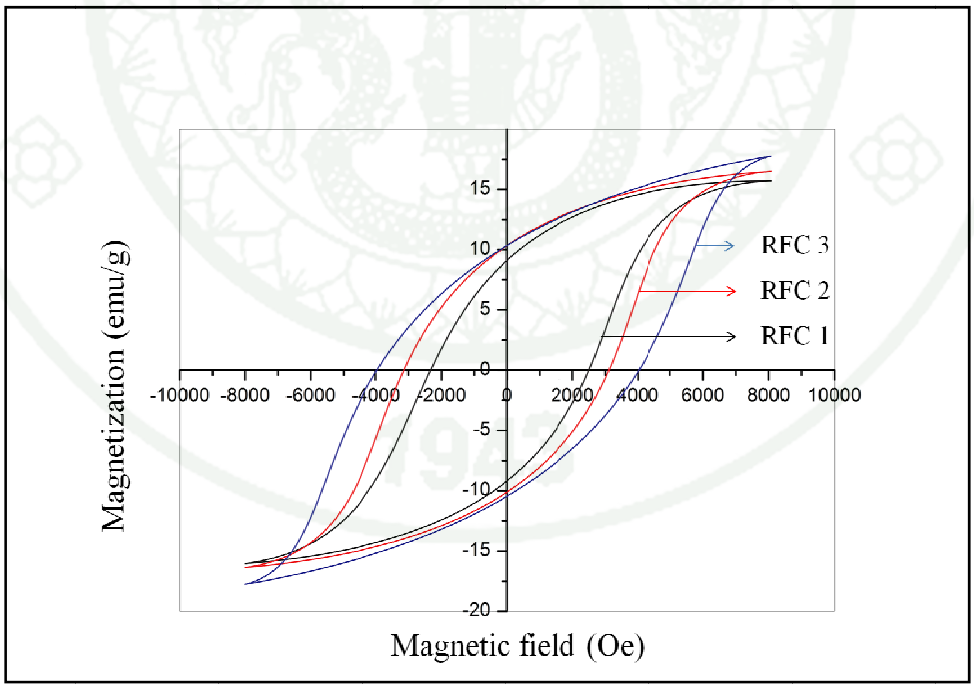

Figure 52 The variation of hysteresis loops of RFCs with different BaF types.

Table 16 The magnetic properties of RFCs with different BaF types.

Rubber Compound	Saturation magnetization (M_s) (emu/g)	Coercive field (H_c) (Oe)
RFC 1	15.2895	2395.65
RFC 2	16.8225	3158.80
RFC 3	18.1045	4027.24

*RFC 1(commercial grade $BaFe_{12}O_{19}$), RFC 2 ($BaFe_{12}O_{19}$_OOPS), RFC 3 ($Ba_{0.85}La_{0.15}Fe_{12}O_{19}$)

The averages of saturation magnetization and coercivity of rubber ferrite composites filled with different barium ferrite types are reported in Table 16. It was found that RFC 1 has the lowest magnetic properties and RFC 3 shows the highest magnetic properties because the $Ba_{0.85}La_{0.15}Fe_{12}O_{19}$ hexaferrite gave higher in saturation magnetization and coercivity when compared with commercial grade BaF and synthesized BaF as shown in Table 15. Furthermore, it was found the drop of saturation magnetization of barium hexaferrite in all of composites compared with barium hexaferrite powders since the saturation magnetization was calculated based on weight. After the magnetic fillers were incorporated into natural rubber matrix, the weights of the composites were lower than the pure magnetic fillers, resulting in lower saturation magnetization. However, it was discovered that the coercivity of composites is rather similar to magnetic fillers. That is to say the saturation magnetization is dependent on the amount of magnetic fillers in rubber matrix, whereas the coercivity is dependent on the magnetic properties of magnetic fillers. The results were in agreement with Lalita et al., (2009) which studied the magnetic and mechanical properties of RFCs with different ferrite loading. They found that the higher loading gave the higher magnetic properties.

3.3 Mechanical properties

The mechanical properties, including tensile strength and elongation at break, of RFCs were obtained by means of material testing machine followed

standard ASTM D412 with 2500 kg loading cell at 500 mm/min. The sample was in dumbbell type with 115 mm of sample length 3.8 mm of thickness and 6 mm of width. The results were reported in Table 17. Usually, The mechanical properties depend on size, shape, loading and dispersion of the magnetic fillers, as well as the matrix properties and the interfacial adhesion between the filler and the polymer matrix (Makled et al., 2005).

Table 17 Mechanical properties of RFC with different BaF type.

Compound	Tensile strength (N)	Elongation at break (mm)
RFC 1	100.2±1.05	513.2±40.11
RFC 2	89.9±1.23	473.4±32.45
RFC 3	89.2±0.84	457.5±26.76

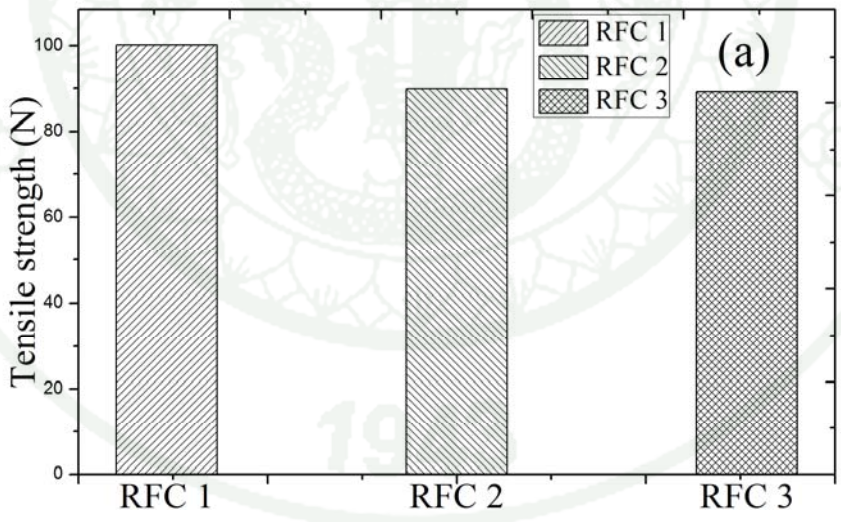

Figure 53 Mechanical properties of RFCs with different BaF type, (a) tensile strength and (b) elongation at break.

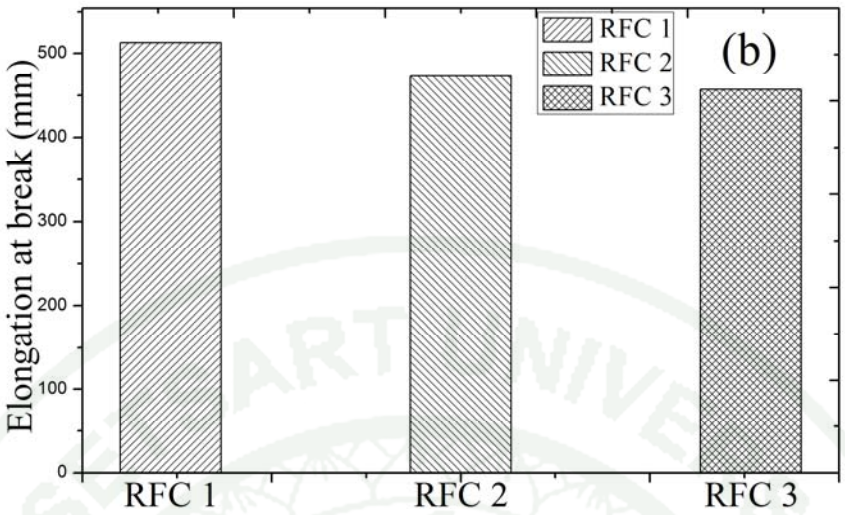

Figure 53 (Continued)

Figure 53(a) shows that the tensile strength of RFC 1 is greater than that of RFC 2 and RFC 3. This is because the smaller particle size of commercial grade BaF means the higher in surface areas which make interaction between fillers and matrix better than the bigger particle size. Moreover, it seems reasonable then that this stress transfer will be better if the filler particles were smaller, because greater surface was thereby exposed for a given filler concentration. A compound's physical/mechanical properties can be strongly influenced by the surface activity of the filler, which is the ability of the filler's surface to bond with the matrix, for instance, an air gap between a filler particle and the matrix. The filler must make intimate contact with the elastomer chains if it is going to contribute to reinforcement of the rubber-filler composite. Fillers that have a high surface area have more contact area available, and therefore have a higher potential to reinforce the rubber chains (Lalita *at al.,* 2009).

The elongation at break of RFCs with different BaF types at the same BaF loading was found to be a similar trend as the tensile strength as seen in Figure 53(b). The rigid fillers behave like a reinforcement. The interaction between rubber

and filler of BaF (com) is stronger than those of RFC 2 and RFC 3, leading to the greater elongation at break because the size effect of filler.

CONCLUSION

The purpose of this study was to improve the magnetic properties of rubber ferrite composites (RFCs) by La substituted and La-Zn substituted barium hexaferrite ($BaFe_{12}O_{19}$, BaF) synthesized by the oxide one pot synthesis (OOPS) process. The synthesized barium hexaferrite with the best magnetic properties was incorporated into natural rubber for making a composites. The comparison of RFCs with different BaF type was investigated. From the experimental results and discussion of this study, the conclusion can be drawn as follow :

1. The preparation of BaF was successful. The precursor was calcined at 1200 °C for 2 hours. It was found that the intermediates, Fe_2O_3 and $BaFe_2O_4$ appeared along with the $BaFe_{12}O_{19}$ because of the reaction between Fe_2O_3 and $BaFe_2O_4$ to convert to $BaFe_{12}O_{19}$ was incomplete. The saturation magnetization and coercivity were 68.5024 emu/g and 2320.47 Oe respectively.

2. The lattice parameters of the La substituted barium hexaferrite decreased with increasing La content corresponding with the SEM pictures. The magnetic properties of La substituted barium hexaferrite increased up to x = 0.15 and then decreased. Moreover, the co-substituted of La-Zn was not complete because the formation of $ZnFe_2O_4$ and incomplete reaction of intermediates phase, leading to the decreased in magnetic properties after being doped with La-Zn. The optimization of La substituted was at x = 0.15. The saturation magnetization was equal to 70.1416 emu/g and coercivity was equal to 4453.20.

3. (i) The cure characteristics, including the maximum torque (M_H),minimum torque (ML), scorch time (t_{s2}) and cure time (t_{c90}) of rubber compounds filled with all BaF types were investigated. It was found to be similar trend because the effect of the particle size. The particle size of commercial grade barium ferrite was smaller than both of synthesized barium ferrite, leading to higher surface areas and greater interaction between filler and rubber matrix making higher heat transfer rate.

(ii) The tensile strength and elongation at break of RFCs with all BaF types shared similar trend. This is because the magnetic filler act like reinforcement filler. Synthesized barium hexaferrite had a bigger size than commercial grade barium hexaferrite, resulting in lower rubber filler interaction and lower mechanical properties.

(iii) The magnetic properties of rubber ferrite composites, including the saturation magnetization (M_s) and coercivity (*Hc*) were also investigated. It was found that the *Ms* and *Hc* of RFC 3 gave the highest saturation magnetization because the *Ms* is dependent on the magnetic properties.

LITERATURE CITED

Singha, A., B. Narangb, O.P. Pandeyd and R.K. Kotnalae. 2010. Electrical and magnetic properties of rare earth substituted strontium hexaferrites. **Journal of Ceramic Processing Research**. 11:241-249.

Jianmin, B., L. Xiaoxi, X. Tian, W. Fulin, and Y. Zheng. 2000. The effects of La–Zn substitution on the magnetic properties of Sr-magnetoplumbite ferrite nano-particles. **Materials Science and Engineering: B** 68:182-185.

Sun, C., K. Sun and P. Chui. 2012. Microwave absorption properties of Ce-substituted M-type barium ferrite. **Journal of Magnetism and Magnetic Materials** 324:802-805.

Corral-Huacuz J.C. and G. Mendoza-Suárez 2002. Preparation and magnetic properties of Ir–Co and La–Zn substituted barium ferrite powders obtained by sol–gel. **Journal of Magnetism and Magnetic Materials** 242–245, Part 1:430-433.

Grusková A., M. Papánová, D. Kevická, J. Sláma, V. Jančárik, J. Lipka, A. González-Angeles and J. Šubrt. 2004. Influence of Zn-Zr Ions on Microstructural and Magnetic Properties of Ba Hexaferrites. Czechoslovak **Journal of Physics** 54:671-674.

_____, J. Lipka, M. Papánová, J. Sláma, I.Tóth, D. Kevická, G. Mendoza, J. C. Corral and J. Šubrt. 2005. La–Zn Substituted Hexaferrites Prepared by Chemical Method. **Hyperfine Interactions** 164:27-33.

Hua, Z.H., S.Z. Li, Z.D. Han, D.H. Wang, M. Lu, W. Zhong, B.X. Gu and Y.W. Du. 2007. The effect of La–Zn substitution on the microstructure and magnetic properties of barium ferrites. **Materials Science and Engineering: A** 448:326-329.

Kanagesan, S., S. Jesurani, R. Velmurugan, M. Sivakumar, C. Thirupathi and T. Kalaivani. 2012. Synthesis and magnetic properties of conventional and microwave calcined barium hexaferrite powder. **Journal of Materials Science: Materials in Electronics** 23:635-639.

Kantiyong, L., W. Keawwattana, N. koonsaeng, P. Jantaratana. 2009. **Magnetic and Mechanical Properties of Barium Ferrite-Natural Rubber Composites**., M.S. Thesis, Kasetsart University.

Laobuthee, A., S. Wongkasemjit, E. Traversa and R.M. Laine 2000. MgAl2O4 spinel powders from oxide one pot synthesis (OOPS) process for ceramic humidity sensors. **Journal of the European Ceramic Society** 20:91-97.

Lee, S.W., S.Y. An, I.B. Shim and C.S. Kim. 2005. Mössbauer studies of La–Zn substitution effect in strontium ferrite nanoparticles. **Journal of Magnetism and Magnetic Materials** 290–291, Part 1:231-233.

Li, J., H.W. Zhang, Y.X. Li, Q. Li and J.F. Qin. 2012. Study on the structural and magnetic properties of La-doped barium ferrites. Wuli Xuebao/**Acta Physica Sinica** 61.

Lisjak, D. and M. Drofenik. 2004. Synthesis and characterization of A–Sn-substituted (A=Zn, Ni, Co) BaM–hexaferrite powders and ceramics. **Journal of the European Ceramic** Society 24:1841-1845.

Litsardakis, G., I. Manolakis and K. Efthimiadis. 2007. Structural and magnetic properties of barium hexaferrites with Gd–Co substitution. **Journal of Alloys and Compounds** 427:194-198.

Liu, Y., M.G.B. Drew and Y. Liu. 2012. Optimizing the methods of synthesis for barium hexagonal ferrite—An experimental and theoretical study. **Materials Chemistry and Physics** 134:266-272.

_____, _____, J.Wang and M. Zhang. 2010. Efficiency and purity control in the preparation of pure and/or aluminum-doped barium ferrites by hydrothermal methods using ferrous ions as reactants. **Journal of Magnetism and Magnetic Materials** 322:366-374.

Lixi, W., H. Qiang, M. Lei and Z. Qitu. 2007. Influence of Sm3+ Substitution on Microwave Magnetic Performance of Barium Hexaferrites. **Journal of Rare Earths** 25, Supplement 2:216-219.

Makled, M.H.and T. Matsui. 2009. Magnetic and mechanical characterisation of natural rubber coprecipitated barium ferrite composites at high loading. **Plastics, Rubber and Composites** 38:297-301.

_____, _____, H. Tsuda, H. Mabuchi, M.K. El-Mansy and K. Morii. 2005. Magnetic and dynamic mechanical properties of barium ferrite–natural rubber composites. **Journal of Materials Processing Technology** 160:229-233.

Mohsen, Q. 2010. Barium hexaferrite synthesis by oxalate precursor route. **Journal of Alloys and Compounds** 500:125-128.

Naiden, E.P., V.Y. Kreslin, M.V. Politov and A.G. Chesnokov. 2000. The Effect of Cation Substitution on Magnetic Anisotropy of M-Type Hexagonal Ferrites. **Russian Physics Journal** 43:790-796.

Ogasawara, T. and M.A.S. Oliveira. 2000. Microstructure and hysteresis curves of the barium hexaferrite from co-precipitation by organic agent. **Journal of Magnetism and Magnetic Materials** 217:147-154.

Otaigbe, J.U., H.S. Kim and J. Xiao. 1999. Effect of coupling agent and filler particle size on melt rheology of polymer-bonded Nd-Fe-B magnets. **Polymer Composites** 20:697-704.

Ounnunkad, S. 2006. Improving magnetic properties of barium hexaferrites by La or Pr substitution. **Solid State Communications** 138:472-475.

_____ and P. Winotai. 2006. Properties of Cr-substituted M-type barium ferrites prepared by nitrate–citrate gel-autocombustion process. **Journal of Magnetism and Magnetic Materials** 301:292-300.

_____, _____ and S. Phanichphant. 2006. Effect of La doping on structural, magnetic and microstructural properties of Ba1 − x La x Fe12O19 ceramics prepared by citrate combustion process. **Journal of Electroceramics** 16:357-361.

Pullar, R.C. 2012. Hexagonal ferrites: A review of the synthesis, properties and applications of hexaferrite ceramics. **Progress in Materials Science** 57:1191-1334.

Qiu, J., and M. Gu. 2006. Crystal structure and magnetic properties of barium ferrite synthesized using GSPC and HEBM. **Journal of Alloys and Compounds** 415:209-212.

Seifert, D., J. Töpfer, F. Langenhorst, J.M Le Breton, H. Chiron and L. Lechevallier. 2009. Synthesis and magnetic properties of La-substituted M-type Sr hexaferrites. **Journal of Magnetism and Magnetic Materials** 321:4045-4051.

Sindhu, S., M.R. Anantharaman, B. Thampi, K.A. Malini and P. Kurian. 2002. Evaluation of a.c. conductivity of rubber ferrite composites from dielectric measurements**. Bulletin of Materials Science** 25:599-607.

Sözeri, H., I. Küçük and H.Özkan. 2011. Improvement in magnetic properties of la substituted BaFe 12O 19 particles prepared with an unusually low Fe/Ba molar ratio. Journal of **Magnetism and Magnetic Materials** 323:1799-1804.

Tsutaoka, T. and N.Koga. 2013. Magnetic phase transitions in substituted barium ferrites BaFe12−x(Ti0.5Co0.5)xO19 (x=0–5). **Journal of Magnetism and Magnetic Materials** 325:36-41.

Wang, H.Z., Q. He, G.H. Wen, F. Wang, Z.H. Ding and B. Yao. 2010. Study of formation mechanism of barium hexaferrite by sintering curve. **Journal of Alloys and Compounds** 504:70-75.

Winotai, P., S. Thongmee and M. Tangab. 2000. Cation distribution in bismuth-doped M-type barium hexaferrite. **Materials Research Bulletin** 35:1747-1753.

Yanbing, H., J. Sha, S. Lina, T. Quan, L.Qin, J. Hongxiao, J. Dingfeng, B. hong, G. Hongliang and X.Wang. 2009. Tailored magnetic properties of Sm(Zn) substituted nanocrystalline barium hexaferrites. **Journal of Alloys and Compounds** 486:348-351.

Yang, J.M. and F.S. Yen. 2008. Evolution of intermediate phases in the synthesis of zinc ferrite nanopowders prepared by the tartrate precursor method. **Journal of Alloys and Compounds** 450:387-394.

You, L., L. Qiao, J. Zheng, M. Jiang, L. Jiang and J. Sheng. 2008. Magnetic properties of La-Zn substituted Sr-hexaferrites by self-propagation high-temperature synthesis. **Journal of Rare Earths** 26:81-84.

APPENDIX

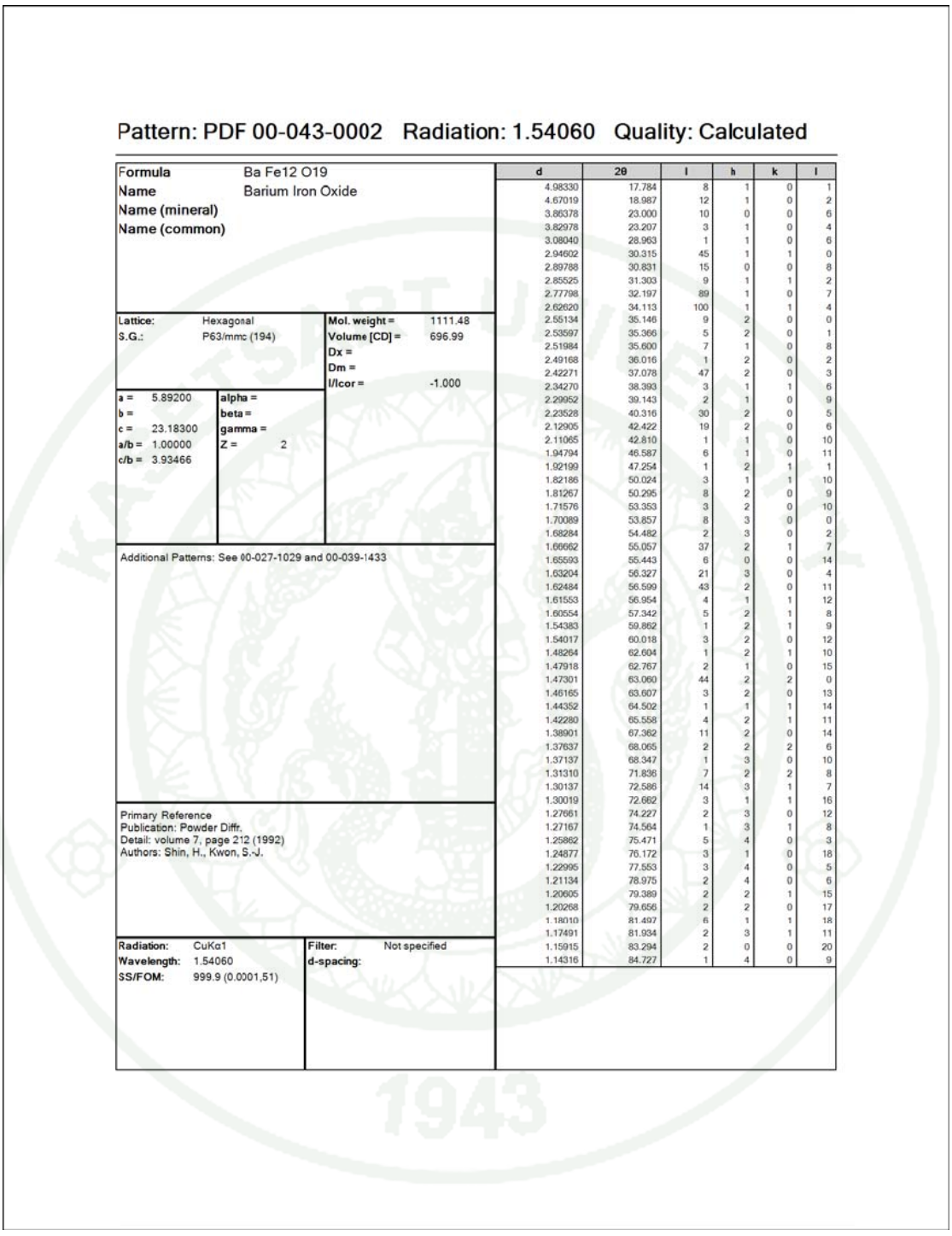

Pattern: PDF 00-043-0002 Radiation: 1.54060 Quality: Calculated

Formula	Ba Fe12 O19
Name	Barium Iron Oxide
Name (mineral)	
Name (common)	

Lattice:	Hexagonal	Mol. weight =	1111.48
S.G.:	P63/mmc (194)	Volume [CD] =	696.99
		Dx =	
		Dm =	
		I/Icor =	-1.000

a =	5.89200	alpha =	
b =		beta =	
c =	23.18300	gamma =	
a/b =	1.00000	Z =	2
c/b =	3.93466		

Additional Patterns: See 00-027-1029 and 00-039-1433

Primary Reference
Publication: Powder Diffr.
Detail: volume 7, page 212 (1992)
Authors: Shin, H., Kwon, S.-J.

Radiation:	CuKα1	Filter:	Not specified
Wavelength:	1.54060	d-spacing:	
SS/FOM:	999.9 (0.0001,51)		

d	2θ	I	h	k	l
4.98330	17.784	8	1	0	1
4.67019	18.987	12	1	0	2
3.86378	23.000	10	0	0	6
3.82978	23.207	3	1	0	4
3.08040	28.963	1	1	0	6
2.94602	30.315	45	1	1	0
2.89788	30.831	15	0	0	8
2.85525	31.303	9	1	1	2
2.77798	32.197	89	1	0	7
2.62620	34.113	100	1	1	4
2.55134	35.146	9	2	0	0
2.53597	35.366	5	2	0	1
2.51984	35.600	7	1	0	8
2.49168	36.016	1	2	0	2
2.42271	37.078	47	2	0	3
2.34270	38.393	3	1	1	6
2.29952	39.143	2	1	0	9
2.23528	40.316	30	2	0	5
2.12905	42.422	19	2	0	6
2.11065	42.810	1	1	0	10
1.94794	46.587	6	1	0	11
1.92199	47.254	1	2	1	1
1.82186	50.024	3	1	1	10
1.81267	50.295	8	2	0	9
1.71576	53.353	3	2	0	10
1.70089	53.857	8	3	0	0
1.68284	54.482	2	3	0	2
1.66662	55.057	37	2	1	7
1.65593	55.443	6	0	0	14
1.63204	56.327	21	3	0	4
1.62484	56.599	43	2	0	11
1.61553	56.954	4	1	1	12
1.60554	57.342	5	2	1	8
1.54383	59.862	1	2	1	9
1.54017	60.018	3	2	0	12
1.48264	62.604	1	2	1	10
1.47918	62.767	2	1	0	15
1.47301	63.060	44	2	2	0
1.46165	63.607	3	2	0	13
1.44352	64.502	1	1	1	14
1.42280	65.558	4	2	1	11
1.38901	67.362	11	2	0	14
1.37637	68.065	2	2	2	6
1.37137	68.347	1	3	0	10
1.31310	71.836	7	2	2	8
1.30137	72.586	14	3	1	7
1.30019	72.662	3	1	1	16
1.27661	74.227	2	3	0	12
1.27167	74.564	1	3	1	8
1.25862	75.471	5	4	0	3
1.24877	76.172	3	1	0	18
1.22995	77.553	3	4	0	5
1.21134	78.975	2	4	0	6
1.20605	79.389	2	2	1	15
1.20268	79.656	2	2	0	17
1.18010	81.497	6	1	1	18
1.17491	81.934	2	3	1	11
1.15915	83.294	2	0	0	20
1.14316	84.727	1	4	0	9

Appendix Figure 1 Data base of $BaFe_{12}O_{19}$

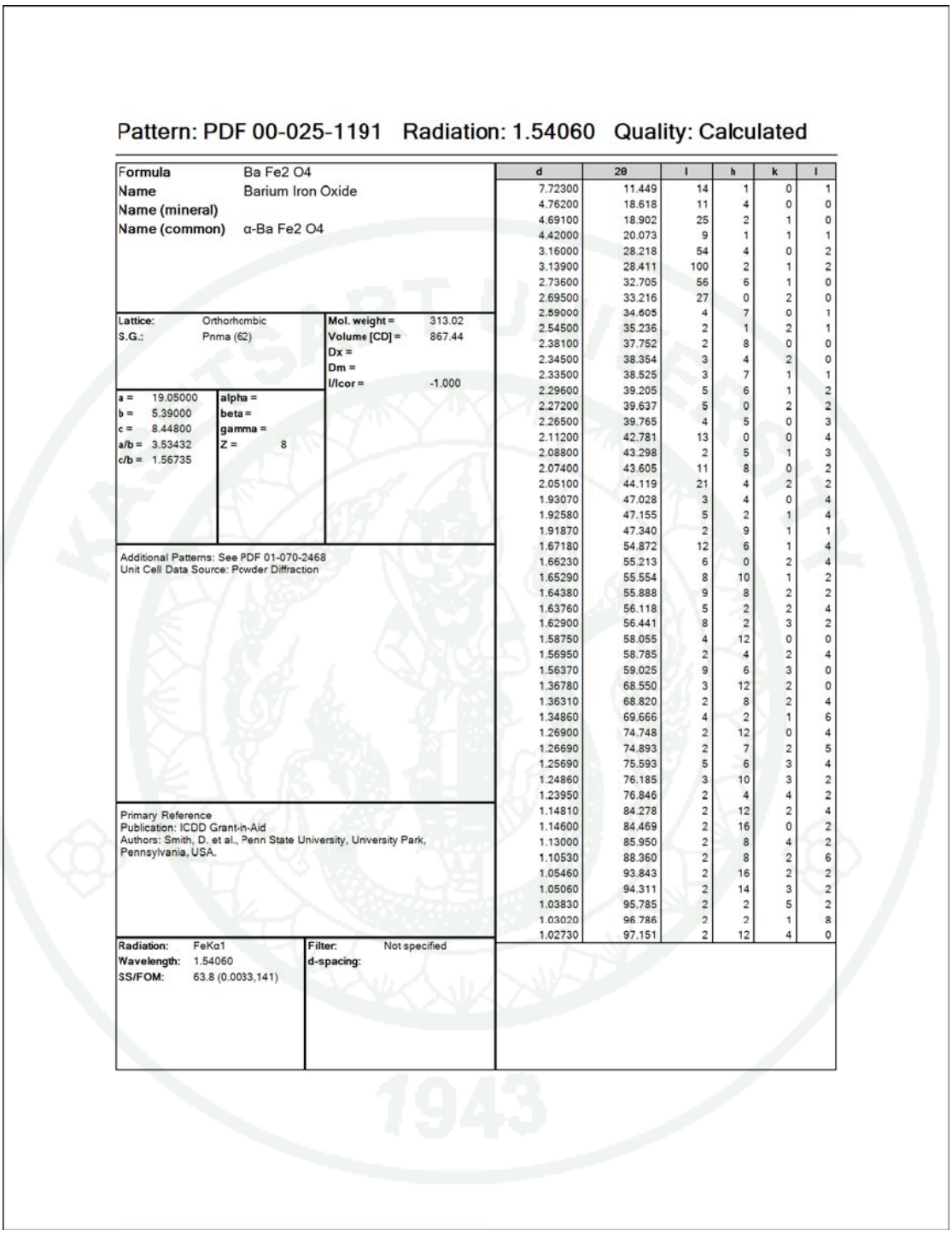

Pattern: PDF 00-025-1191 Radiation: 1.54060 Quality: Calculated

Formula	Ba Fe2 O4
Name	Barium Iron Oxide
Name (mineral)	
Name (common)	α-Ba Fe2 O4

Lattice:	Orthorhombic	Mol. weight =	313.02
S.G.:	Pnma (62)	Volume [CD] =	867.44
		Dx =	
		Dm =	
		I/Icor =	-1.000

a =	19.05000	alpha =	
b =	5.39000	beta =	
c =	8.44800	gamma =	
a/b =	3.53432	Z =	8
c/b =	1.56735		

Additional Patterns: See PDF 01-070-2468
Unit Cell Data Source: Powder Diffraction

Primary Reference
Publication: ICDD Grant-in-Aid
Authors: Smith, D. et al., Penn State University, University Park, Pennsylvania, USA.

Radiation:	FeKα1	Filter:	Not specified
Wavelength:	1.54060	d-spacing:	
SS/FOM:	63.8 (0.0033,141)		

d	2θ	I	h	k	l
7.72300	11.449	14	1	0	1
4.76200	18.618	11	4	0	0
4.69100	18.902	25	2	1	0
4.42000	20.073	9	1	1	1
3.16000	28.218	54	4	0	2
3.13900	28.411	100	2	1	2
2.73600	32.705	56	6	1	0
2.69500	33.216	27	0	2	0
2.59000	34.605	4	7	0	1
2.54500	35.236	2	1	2	1
2.38100	37.752	2	8	0	0
2.34500	38.354	3	4	2	0
2.33500	38.525	3	7	1	1
2.29600	39.205	5	6	1	2
2.27200	39.637	5	0	2	2
2.26500	39.765	4	5	0	3
2.11200	42.781	13	0	0	4
2.08800	43.298	2	5	1	3
2.07400	43.605	11	8	0	2
2.05100	44.119	21	4	2	2
1.93070	47.028	3	4	0	4
1.92580	47.155	5	2	1	4
1.91870	47.340	2	9	1	1
1.67180	54.872	12	6	1	4
1.66230	55.213	6	0	2	4
1.65290	55.554	8	10	1	2
1.64380	55.888	9	8	2	2
1.63760	56.118	5	2	2	4
1.62900	56.441	8	2	3	2
1.58750	58.055	4	12	0	0
1.56950	58.785	2	4	2	4
1.56370	59.025	9	6	3	0
1.36780	68.550	3	12	2	0
1.36310	68.820	2	8	2	4
1.34860	69.666	4	2	1	6
1.26900	74.748	2	12	0	4
1.26690	74.893	2	7	2	5
1.25690	75.593	5	6	3	4
1.24860	76.185	3	10	3	2
1.23950	76.846	2	4	4	2
1.14810	84.278	2	12	2	4
1.14600	84.469	2	16	0	2
1.13000	85.950	2	8	4	2
1.10530	88.360	2	8	2	6
1.05460	93.843	2	16	2	2
1.05060	94.311	2	14	3	2
1.03830	95.785	2	2	5	2
1.03020	96.786	2	2	1	8
1.02730	97.151	2	12	4	0

Appendix Figure 2 Data base of Barium iron oxide

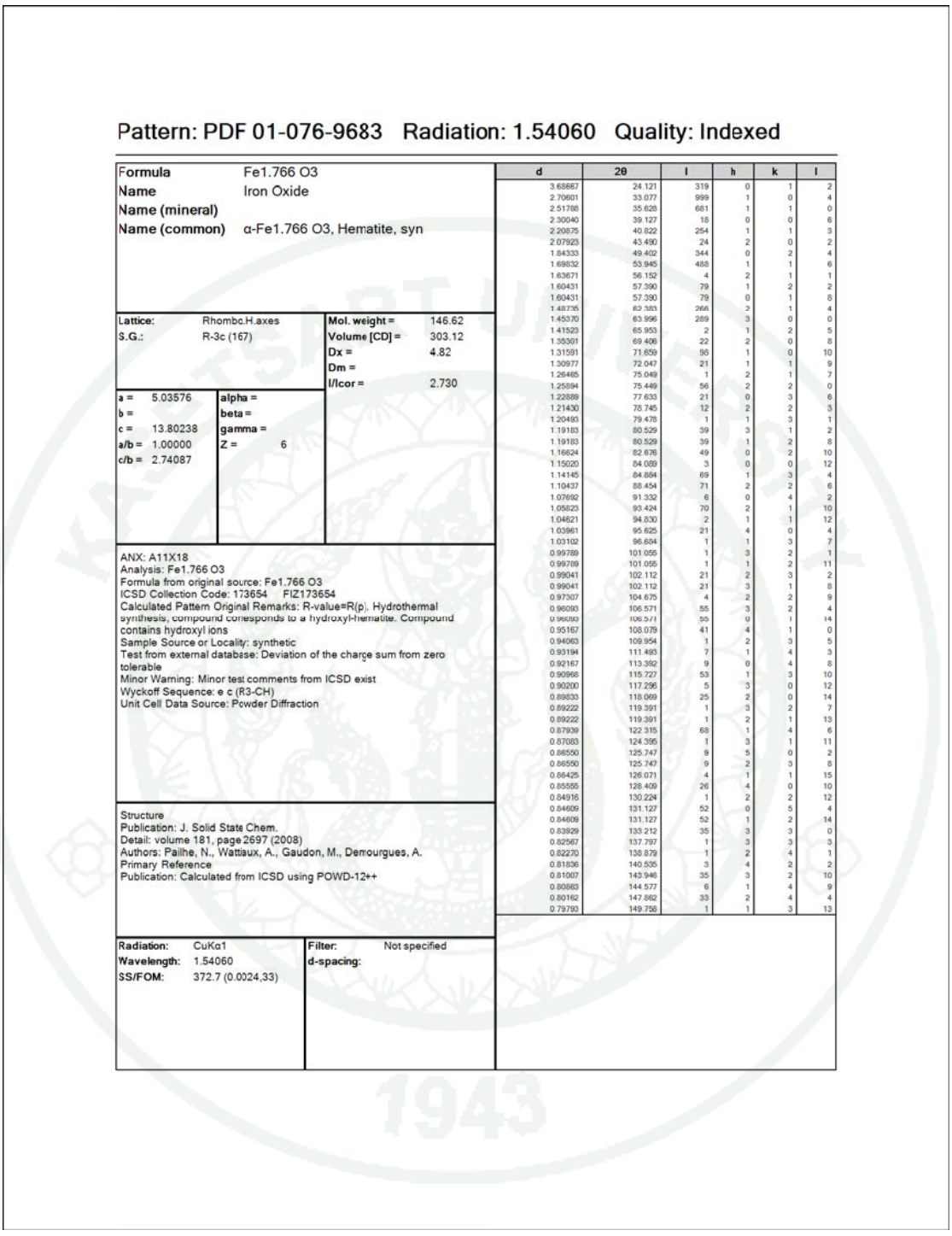

Pattern: PDF 01-076-9683 Radiation: 1.54060 Quality: Indexed

Formula	Fe1.766 O3
Name	Iron Oxide
Name (mineral)	
Name (common)	α-Fe1.766 O3, Hematite, syn

Lattice:	Rhombo.H.axes
S.G.:	R-3c (167)

Mol. weight =	146.62
Volume [CD] =	303.12
Dx =	4.82
Dm =	
I/Icor =	2.730

a = 5.03576	alpha =
b =	beta =
c = 13.80238	gamma =
a/b = 1.00000	Z = 6
c/b = 2.74087	

ANX: A11X18
Analysis: Fe1.766 O3
Formula from original source: Fe1.766 O3
ICSD Collection Code: 173654 FIZ173654
Calculated Pattern Original Remarks: R-value=R(p). Hydrothermal synthesis, compound corresponds to a hydroxyl-hematite. Compound contains hydroxyl ions
Sample Source or Locality: synthetic
Test from external database: Deviation of the charge sum from zero tolerable
Minor Warning: Minor test comments from ICSD exist
Wyckoff Sequence: e c (R3-CH)
Unit Cell Data Source: Powder Diffraction

Structure
Publication: J. Solid State Chem.
Detail: volume 181, page 2697 (2008)
Authors: Pailhe, N., Wattiaux, A., Gaudon, M., Demourgues, A.
Primary Reference
Publication: Calculated from ICSD using POWD-12++

Radiation:	CuKα1
Wavelength:	1.54060
SS/FOM:	372.7 (0.0024,33)

Filter:	Not specified
d-spacing:	

d	2θ	I	h	k	l
3.68867	24.121	319	0	1	2
2.70601	33.077	999	1	0	4
2.51788	35.628	681	1	1	0
2.30040	39.127	18	0	0	6
2.20875	40.822	254	1	1	3
2.07923	43.490	24	2	0	2
1.84333	49.402	344	0	2	4
1.69832	53.945	488	1	1	6
1.63671	56.152	4	2	1	1
1.60431	57.390	79	1	2	2
1.60431	57.390	79	0	1	8
1.48735	62.383	266	2	1	4
1.45370	63.996	289	3	0	0
1.41523	65.953	2	1	2	5
1.35301	69.406	22	2	0	8
1.31591	71.659	98	1	0	10
1.30977	72.047	21	1	1	9
1.26465	75.049	1	2	1	7
1.25894	75.449	56	2	2	0
1.22889	77.633	21	0	3	6
1.21430	78.745	12	2	2	3
1.20493	79.478	1	1	3	1
1.19183	80.529	39	3	1	2
1.19183	80.529	39	1	2	8
1.16624	82.676	49	0	2	10
1.15020	84.089	3	0	0	12
1.14145	84.894	69	1	3	4
1.10437	88.454	71	2	2	6
1.07692	91.332	6	0	4	2
1.05823	93.424	70	2	1	10
1.04621	94.830	2	1	1	12
1.03961	95.625	21	4	0	4
1.03102	96.684	1	1	3	7
0.99789	101.055	1	3	2	1
0.99789	101.055	1	1	2	11
0.99041	102.112	21	2	3	2
0.99041	102.112	21	3	1	8
0.97307	104.675	4	2	2	9
0.96093	106.571	55	3	2	4
0.96093	106.571	55	0	1	14
0.95167	108.079	41	4	1	0
0.94063	109.954	1	2	3	5
0.93194	111.493	7	1	4	3
0.92167	113.392	9	0	4	8
0.90968	115.727	53	1	3	10
0.90200	117.296	5	3	0	12
0.89833	118.069	25	2	0	14
0.89222	119.391	1	3	2	7
0.89222	119.391	1	2	1	13
0.87939	122.315	68	1	4	6
0.87083	124.395	1	3	1	11
0.86550	125.747	9	5	0	2
0.86550	125.747	9	2	3	8
0.86425	126.071	4	1	1	15
0.85555	128.409	26	4	0	10
0.84916	130.224	1	2	2	12
0.84609	131.127	52	0	5	4
0.84609	131.127	52	1	2	14
0.83929	133.212	35	3	3	0
0.82567	137.797	1	3	3	3
0.82270	138.879	1	2	4	1
0.81836	140.535	3	4	2	2
0.81007	143.946	35	3	2	10
0.80863	144.577	6	1	4	9
0.80162	147.862	33	2	4	4
0.79793	149.758	1	1	3	13

Appendix Figure 3 Data base of iron oxide

Pattern: PDF 00-001-1108 Radiation: 1.54060 Quality: Blank

Formula	Zn Fe2 O4
Name	Zinc Iron Oxide
Name (mineral)	
Name (common)	

Lattice:	Cubic
S.G.:	Fd-3m (227)

Mol. weight =	241.07
Volume [CD] =	599.08
Dx =	
Dm =	5.249
I/Icor =	-1.000

a =	8.43000	alpha =	
b =		beta =	
c =		gamma =	
a/b =	1.00000	Z =	8
c/b =	1.00000		

Color: Brownish black to black
Deleted Or Rejected By: Deleted by 00-022-1012
Melting Point: 1863 K

Primary Reference
Publication: Amer. J. Sci.
Detail: volume 19, page 67 (1930)
Authors: Poshjak.

Radiation:	MoKα1	Filter:	Not specified
Wavelength:	1.54060	d-spacing:	
SS/FOM:	5.7 (0.097,34)		

d	2θ	I	h	k	l
4.85000	18.277	20	1	1	1
2.99000	29.858	50	2	2	0
2.54000	35.308	100	3	1	1
2.42000	37.121	10	2	2	2
2.10000	43.038	40	4	0	0
1.72000	53.211	40	4	2	2
1.62000	56.783	70	5	1	1
1.49000	62.260	80	4	4	0
1.33000	70.785	20	6	2	0
1.28000	73.997	40	5	3	3
1.27000	74.679	10	6	2	2
1.12000	86.907	30	6	4	2
1.09000	89.934	50	7	3	1
1.05000	94.381	30	8	0	0
0.97000	105.145	40	6	6	2
0.88000	122.171	20	9	3	1
0.86000	127.196	30	8	4	4
0.83000	136.273	10	10	2	0
0.81000	143.974	20	10	2	2

Appendix Figure 4 Data base of Zinc iron oxide

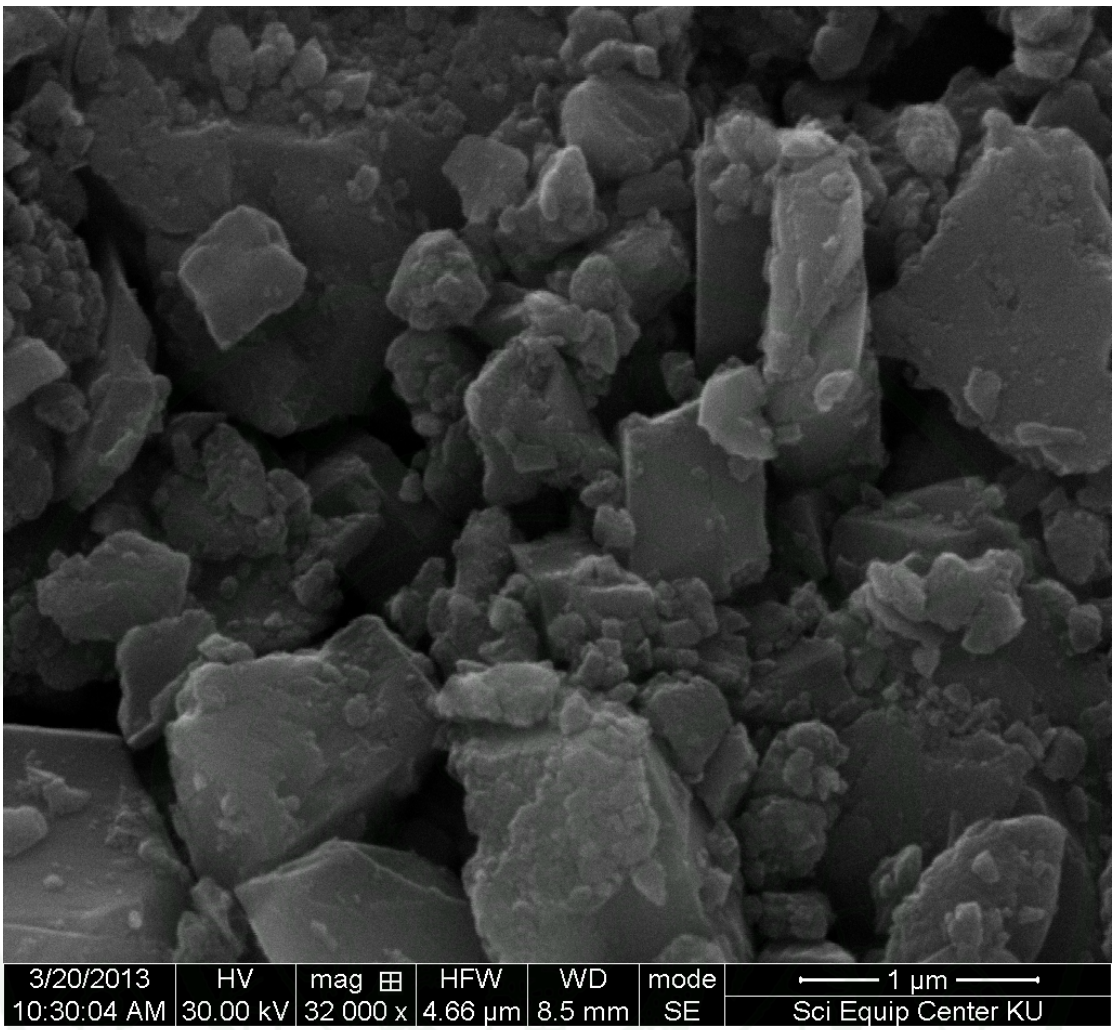

Appendix Figure 5 SEM image of commercial grade barium hexaferrite

CURRICULUM VITAE

NAME : Mr. Sitthisak Sorlateap

BIRTH DATE : Jan 1, 1988

BIRTH PLACE : Chonburi, Thailand

EDUCATION	**YEAR**	**INSTITUTE**	**DEGREE/DIPLOMA**
	2009	Kasetsart Univ.	B.Sc.(Chemistry)

POSITION/TITLE : Student

WORK PLACE : Faculty of Science, Kasetsart University

SCHOLARSHIP/AWARDS : Graduate school for publication in international journal 2010-2011
Postgraduate Education and Research Program in Physical Chemistry (ADB KU-Chem) 2010-2011

PUBLICATION : Sorlateap S., Keawwattana W. (2013) Preparation and magnetic properties of La substituted barium ferrites synthesized by the oxide one pot synthesis (OOPS) process. pp. 2250-2253.